The Pennsylvania State University
The J. Jeffrey and Ann Marie Fox Graduate School

THE GEOMETRY OF RELATIVISTIC QUANTUM CLOCKS: A STUDY IN QUANTUM PROPER TIME

A Dissertation in
Physics
by
Joseph A. Balsells

Submitted in Partial Fulfillment
of the Requirements
for the Degree of

Doctor of Philosophy

August 2025

The dissertation of Joseph A. Balsells was reviewed and approved by the following:

Martin Bojowald
Professor of Physics
Dissertation Advisor
Chair of Committee

Eugenio Bianchi
Professor of Physics

Mikael Rechtsman
Professor of Physics

Ping Xu
Professor of Mathematics

Irina Mocioiu
Professor of Physics
Director of Graduate Studies in Physics

Abstract

This dissertation develops a geometric framework for analyzing the dynamics of relativistic quantum systems, with particular emphasis on the notion of quantum proper time. Motivated by the need to reconcile the distinct formal roles that time plays in general relativity and quantum theory, the work reformulates quantum theory using phase space variables composed of expectation values and higher-order statistical moments. These variables define a symplectic structure on quantum state space, enabling a Hamiltonian formulation of quantum dynamics that parallels classical mechanics while encoding quantum corrections perturbatively.

Within this framework, the evolution of semiclassical quantum states—including delocalized or entangled systems—is governed by a quantum Hamilton function constructed as an expansion in statistical moments. This expansion retains the geometric homogeneity properties of the classical Hamiltonian, extending the dynamics into the quantum regime while preserving a Finsler-like structure. The approach clarifies how quantum fluctuations, correlations, and entanglement influence effective trajectories and time evolution, and it enables a consistent treatment of constrained systems such as the relativistic point particle.

Several physical applications are explored. These include corrections to gravitational time dilation due to finite wave packet spread, a phase space characterization of entanglement entropy, and a modified dispersion relation arising from quantum fluctuations. These corrections lead to experimentally testable predictions, including potential violations of the equivalence principle in freely falling quantum systems, shifts in atomic clock frequencies, and modifications to arrival times in atom interferometers. The formalism thus establishes a foundation for near-term experimental tests probing the quantum structure of spacetime.

Finally, the work motivates a broader view in which spacetime geometry itself may be understood as emerging from the quantum degrees of freedom it governs. The results provide a platform for extending effective quantum theories into gravitational regimes and lay the groundwork for future efforts to incorporate backreaction and fully dynamical quantum geometry.

Table of Contents

List of Figures

List of Tables

List of Symbols

$E_{\mathcal{N}}$	Logarithmic negativity
e	einbein field
f'	derivative with respect to coordinate time. Also derivative of a single-variable function.
$\dot{f}$	derivative with respect to a worldline parameter
γ	Lorentz factor
γ_{ij}	spatial metric
$\mathcal{H}$	a Hilbert space
η, ϕ, ψ	Hilbert space elements
$\eta(1,2)$	Eötvös parameter, Definition Eq. (6.13)
ι	insertion operator
$\mu(\rho)$	purity of the state with density operator ρ
m	parameter with units of mass
$\nu_{\pm}$	larger and smaller symplectic eigenvalues
ν_{-}^{PT}	smaller symplectic eigenvalue after partial transposition
N	lapse function
N^i	shift vector
Π	Poisson tensor
$\mathbb{P}_{ij}$	components of the Poisson tensor in a basis
ρ	density matrix. Also Lemaître radial coordinate.

S	action functional
$S_V(\rho)$	von Neumann entropy of the state with density operator ρ
σ	arbitrary worldline parameter. Also the covariance matrix.
τ	proper time
Tr	trace
X_F	Hamiltonian vector field associated with the function F
Ω	symplectic form

Notation particular to this dissertation

$\alpha!$	factorial of the multi-index α, Definition Eq. (2.33)
$\lvert\alpha\rvert$	order of the multi-index α, Definition Eq. (2.34)
$A_{\mathcal{Q}}$	extension of A over quantum degrees of freedom
$\bar{a}, \bar{b}$	index variables over quantum and spacetime variables
$\Delta^{B_1 B_2}_{A_1 A_2}$	uncertainty product of A_1, A_2, B_1, and B_2, Definition Eq. (2.84)
$\Delta\left(x^\alpha p^\beta\right)$	a centralized and symmetrized moment, Definition Eq. (2.31)
$\Delta^2(\cdot)$	any expression of homogeneity degree two in quantum variables, Eq. (4.9)
H	unconstrained Hamilton function
H	Hamiltonian constraint function
I, J	indices over quantum variables
$\bar{i}, \bar{j}$	indices over quantum and space variables
L	nonsingular Lagrange function
L	singular Lagrange function
$\sqrt{P}$	Finsler root, Definition Eq. (2.69)
s	fluctuation coordinate
ω	linear functional

Standard and semi-standard notation

$\propto$	proportional to

$\sim$	equivalence relation
$:=$	is defined as
$\equiv$	an identity or alternative notation
$\cong$	isomorphic
$\mapsto$	maps to
$\oplus$	direct sum
$\otimes$	tensor product
$\bar{\phi}$	complex conjugate of ϕ
$\|A\|$	norm of A
$\hat{A}$	an operator
$\left\langle \hat{A} \right\rangle$	expectation value of the operator $\hat{A}$
$\|\Psi\rangle$	Dirac notation for a Hilbert space element
$\mathbb{I}_n$	identity matrix in n dimensions
$\mathcal{A}$	operator algebra
$\mathbb{C}$	the field of complex numbers
c	speed of light
g_{ab}	spacetime metric
Γ^a_{bc}	connection coefficients of a pseudo-Riemannian connection (Christoffel symbols)
$\hbar$	reduced Planck constant
i	imaginary unit
$\hat{\mathbb{I}}$	unit operator
k_B	Boltzmann constant
M_P	Planck mass
p_q	momentum conjugate to q
$\mathbb{R}$	the field of real numbers
v^i	spatial velocity coordinates
x^i	spatial position coordinates

Acknowledgments

I would like first to acknowledge my advisor, Martin Bojowald. Meeting with Martin could feel like visiting the oracle at Delphi—awe-inspiring and mysterious. If I came to him with a problem, I generally would not get a detailed manual for its solution. Instead, he often would provide a picture of how the solution must appear. And then, like a devout disciple, I would work to understand.

Even though it sometimes took me weeks to learn the basic definitions to converse better, Martin is nothing if not patient. And if it took months more to work through the details, he was still there. When eventually I would step out of the cave of shadows and see the meaning in his intuition, I would marvel how lucky I was to study with him.

I am indebted to the friends I made along the way. To Ding, to Jackson, and to Källan, who came before me, who laughed, and who showed me how to navigate this path. To Dennis, who shared in a happy lunch routine, and without whom the office always felt a little less full. To Stephen and Yeonhye, whose pizza and company nourished both body and soul. To Daniel, Erick, Monica, and all of Eugenio's students, who provided essential counterpoints to my experience. To Samarth, whose tenacity reminded me that anything can be done. And to Mauricio, for countless productive discussions, for being a delightful conference companion, and for a Chilean education in pisco sour.

The science that I have completed could in principle have been done by anyone else. But as things worked out, it took me to do it. The me that I am is due to my family. I acknowledge the role they played in molding my clay and supporting me while I set through many years to arrive at and finally complete this dissertation.

My grandparents, Joe and Ella, showed me the rich experience of life, taking me around the world. They fostered my intellectual development from my first bowl of folate-enriched Malt-o-Meal, to cold mornings looking through the telescope at Jupiter.

I am grateful to my twin brother, Cito. Born a minute ahead of me, and twenty-eight years later defending his dissertation weeks before me, you have motivated my efforts.

Of my mother, Julie, I acknowledge the long phone calls we had where she provided, and continues to provide, sound advice. Her concern for my finishing of this dissertation propelled me through many hours of writing. Mother, this is for you.

Paige. I have the great pleasure of acknowledging your support both as my wife and as a keen scholar. We sometimes joke that we are not two individuals, but in fact the same person. I've seen you do it, so I know that I can too. Thank you for working with me so that I might reach my potential.

I acknowledge partial funding support by NSF Grant No. PHY-2206591.

Any opinions, findings, and conclusions or recommendations expressed in this publication are those of the author and do not necessarily reflect the views of the NSF.

Zeit ist das, was man an der Uhr abliest.

[Time is what you read on the clock.]

—Albert Einstein (1879–1955)

Chapter 1
Introduction

1.1 Motivation and overview

Time is a central concept in both general relativity and quantum mechanics, yet the two theories offer fundamentally different notions of its role and measurement. In general relativity, time is geometric—woven into the fabric of spacetime and experienced differently depending on an object's motion and gravitational environment. Proper time, the physical time measured along a worldline, is central to relativistic predictions and precision timekeeping. In quantum mechanics, by contrast, time appears as an external parameter: it drives evolution but is not itself an observable or a dynamical quantity. The tension between these frameworks becomes apparent when attempting to describe the behavior of quantum systems in relativistic or gravitational settings—such as clocks in superpositions of spacetime trajectories.

This dissertation investigates the question:

> *Can we define a notion of quantum proper time that respects the principles of both general relativity and quantum mechanics, and remains meaningful for clocks in delocalized or superposed states?*

To address this, I explore the dynamics of quantum clocks within a geometric framework that generalizes the concept of proper time to the quantum regime. The central idea is that a quantum system's evolution can be understood as a geodesic in a suitably defined geometric space of quantum states—one that reflects both its informational and physical properties. Within this perspective, *quantum proper time* emerges not from the coordinate structure of spacetime alone, but also from the internal state space geometry of the clock itself.

The results presented here point toward a unified, geometrically grounded under-

standing of time for quantum systems under relativistic conditions. They contribute both to the foundations of quantum theory and to efforts aimed at bridging the gap between quantum mechanics and gravity.

The remainder of this chapter sets the stage for the developments that follow. We begin in Sec. 1.2 by reviewing the role of clocks in general relativity and provide the variational definition of classical proper time as Eq. (1.3). From there, in Sec. 1.3 we examine existing approaches to modeling quantum clocks and highlight conceptual and technical challenges that arise—particularly in scenarios involving nonflat backgrounds. These motivate the need for a new framework capable of incorporating both the geometric nature of time in relativity and the nonlocal structure of quantum mechanics. We conclude the chapter with a summary of the dissertation's main contributions (Sec. 1.4) and an overview of its organization (Sec. 1.5).

1.2 Clocks in general relativity and classical proper time

The notion of time is inseparable from the devices we use to measure it.

Historically, clocks exhibited a subset of degrees of freedom that were accessible to observation—first under the Newtonian conception of absolute time, which flows uniformly and independently of any physical processes, and later through their behavior in a gravitational context. These accessible degrees of freedom—the clock's position and momentum relative to a chosen inertial frame—correspond to what we now recognize as classical degrees of freedom. Quantum degrees of freedom, although present, remained inaccessible to observation and played no role in the classical modeling of spacetime.

In Newtonian theory, an idealized clock is characterized by its Euclidean degrees of freedom: position components x^i and velocity components v^i for $i = 1, 2, 3$, with the time it measures assumed to be independent of these coordinates. However, careful observation reveals that real clocks experience velocity-dependent time dilation [1], as well as time dilation due to presence in a gravitational field [2].

Time dilation is a relational effect, implying the relevant degrees of freedom for one clock—including the time it shows—cannot be specified without reference to those of another. This may be illustrated by considering a pair of clocks, A and B, in different classical states (x_A, v_A) and (x_B, v_B). The difference in their ticking rates can be quantified by a Lorentz-like factor which depends on their positions and velocities,

$$\frac{\mathrm{d}\tau_A}{\mathrm{d}\tau_B} = \gamma(x_A, x_B, v_A, v_B). \tag{1.1}$$

Although this relationship distinguishes neither clock in principle, practical situations in general relativity typically single out one clock as an observer or local frame. In such a situation, the degrees of freedom of one clock are fixed and the differential relation (1.1) provides a description of the degrees of freedom of the other clock relative to the first. This perspective promotes the time-coordinate of the second clock to a dynamical degree of freedom—on equal footing with its spatial position—and allows these quantities to evolve with respect to a new parameter, interpreted as the proper time shown by the reference clock.

By rewriting the proper time intervals of the observed and reference clocks as $\mathrm{d}\tau$ and $\mathrm{d}\sigma$, respectively, and specifying the degrees of freedom of the observed clock in coordinates of the reference clock frame as $x^a(\sigma)$, general relativity provides an explicit expression for the time dilation factor $\gamma(x_A, x_B, v_A, v_B)$ in the form

$$\mathrm{d}\tau = \sqrt{-\frac{1}{c^2} g_{ab}(x) \frac{\mathrm{dx^a}}{\mathrm{d}\sigma} \frac{\mathrm{dx^b}}{\mathrm{d}\sigma}}\mathrm{d}\sigma\,, \tag{1.2}$$

which matches the schematic structure of Eq. (1.1). The function γ depends on the position and velocity of the observed clock relative to the (implied) position and velocity of the reference clock. It also depends on the spacetime metric g_{ab}, assumed to have signature $(-,+,+,+)$. While the form of Eq. (1.2) may not appear natural *a priori*, it is sufficiently general to accommodate all experimentally verified relationships between clock rates to date [3].

The left-hand-side of Eq. (1.2) is explicitly independent of the choice of reference clock, and the right-hand-side is invariant under reparametrization $\sigma \to \sigma' = f(\sigma)$. This reflects the physical fact that no observer or parametrization is fundamentally preferred; σ may be any smooth parameter.

The differential relationship (1.2) can be integrated to give the total proper time τ accumulated by a clock travelling along a parameterized worldline $x^a(\sigma)$ between two spacetime points $x^a(0)$ and $x^a(1)$ as

$$\tau[x^a, \dot{x}^a] = \int_0^1 \sqrt{-\frac{1}{c^2} g_{ab}(x) \frac{\mathrm{dx^a}}{\mathrm{d}\sigma} \frac{\mathrm{dx^b}}{\mathrm{d}\sigma}}\mathrm{d}\sigma. \tag{1.3}$$

Among all the different possible paths between these two points, freely falling ideal clocks measure proper time along geodesics of the spacetime manifold. These geodesics

extremize the proper time functional (1.3) and are solutions to the geodesic equation

$$\frac{d^2x^a}{d\tau^2} + \Gamma^a_{bc}\frac{dx^b}{d\tau}\frac{dx^c}{d\tau} = 0, \tag{1.4}$$

where Γ^a_{bc} are the Christoffel symbols of the Levi-Civita connection associated with the metric.

This general relativistic clock model successfully accommodates velocity-dependent time dilation by the dependence on the velocities, and interprets gravitational time-dilation geometrically as a consequence of spacetime curvature. In this sense, the geometry of spacetime directly governs the ticking of clocks and proper time becomes a geometric quantity.

1.3 Time in quantum theory

Standard nonrelativistic quantum theory treats time as a classical background parameter—it governs the evolution of states via the Schrödinger equation but is not itself subject to quantization or measurement. As a result, time does not correspond to an operator in the same way that position or momentum does. This asymmetry mirrors the Newtonian framework in classical physics and becomes problematic from the relativistic perspective. Quantum field theory on curved spacetime achieves a formal unification of quantum mechanics with general relativity, but spacetime in this setting remains a fixed classical background that merely provides a new stage for standard quantum processes such as scattering and particle production. Defining time from within the quantum framework, rather than treating it as an external parameter, remains subtle and unresolved [4, 5].

The standard approach to quantizing a continuous degree of freedom proceeds by promoting the classical observables to operators obeying the canonical commutation relation

$$[\hat{x}^a, \hat{p}_b] = i\hbar\delta^a_b\hat{\mathbb{I}}\,. \tag{1.5}$$

To realize canonical quantization of time in this way, the singular Lagrangian action (1.3) can be reformulated as a first-order constrained Hamiltonian action. This procedure is reviewed in Chapter 3. The resulting first-order action is

$$S[x^a, e, p_a, p_e] = \int \mathrm{d}\sigma \left[p_a\dot{x}^a + \frac{e}{2}\left(g^{ab}(x)p_ap_b + m^2c^2\right)\right], \tag{1.6}$$

where the einbein $e(\sigma)$, defined on the worldline, acts as a Lagrange multiplier. Its

variation enforces the Hamiltonian constraint

$$\mathrm{H} = g^{ab}(x)p_a p_b + m^2c^2 = 0\,, \tag{1.7}$$

which is valid for both massive and massless particles. This constraint restricts classical evolution to the subspace of phase space where the Hamiltonian vanishes.

In canonical quantization, the constraint is imposed at the level of states, selecting the physical Hilbert space $\mathcal{H}_{\mathrm{phys}}$ as the Cauchy completion of states which are annihilated by the constraint operator,

$$\hat{\mathrm{H}}|\Psi\rangle = 0. \tag{1.8}$$

A consequence of this constraint is that the Schrödinger equation appears to generate no time evolution,

$$i\hbar\partial_t|\Psi\rangle = \hat{\mathrm{H}}|\Psi\rangle = 0. \tag{1.9}$$

The quantum state $|\Psi\rangle$ thus appears "frozen," exhibiting no explicit dependence on an external time parameter. This manifestation of timelessness is a central aspect of the problem of time in canonical quantum gravity, which is also governed dynamically by a constraint [6–8].

One promising approach to the problem of time lies in the study of composite systems, where one subsystem serves as a clock for the other and time emerges from correlations between them. This approach, known as the Page–Wootters mechanism [9], aims to replace the external time parameter with relational dynamics.

When the metric g^{ab} is flat, the Hamiltonian (1.7) may be promoted without ambiguity to a quantum operator,

$$\hat{\mathrm{H}} = -\hat{p}_t^2 + \hat{p}_x^2. \tag{1.10}$$

(Here, we temporarily disregard the constant term proportional to mc^2, which would contribute only an overall phase to the quantum state and is therefore physically unobservable.) In this simplified setting, the Page–Wootters mechanism provides a viable framework for defining relational dynamics.

The choice of a time coordinate corresponds to a factorization of the total Hilbert space into a tensor product of a clock subsystem and a system of interest:

$$\mathcal{H} \cong \mathcal{H}_C \otimes \mathcal{H}_S\,. \tag{1.11}$$

Within this structure, the constraint operator $\hat{\mathrm{H}}$ has the factored form

$$\hat{\mathrm{H}} = \hat{H}_C \otimes \mathbf{1} + \mathbf{1} \otimes \hat{H}_S \,, \tag{1.12}$$

governing the joint dynamics of clock and system. Due to the simple structure of (1.10), a natural factorization places $\hat{H}_C = -\hat{p}_t^2$ and $\hat{H}_S = \hat{p}_x^2$.

Physical states of the joint system, denoted $|\Psi\rangle\rangle$, satisfy the constraint $\hat{\mathrm{H}}|\Psi\rangle\rangle = 0$. Covariant time observables $[\hat{T}, \hat{H}_c] \propto 1$ with eigenvectors $|t\rangle$ (or, more generally, POVMs) decompose states as

$$|\Psi\rangle\rangle = \int \mathrm{d}t |t\rangle_C \otimes |\psi(t)\rangle_S \tag{1.13}$$

where $|\psi(t)\rangle_S = \langle t|\Psi\rangle\rangle$. The constraint operator acting on this decomposition leads to a Schrödinger equation for the system state evolving by the system Hamiltonian,

$$i\hbar \frac{\mathrm{d}}{\mathrm{d}t} |\psi(t)\rangle_S = H_S |\psi(t)\rangle_S. \tag{1.14}$$

In this way, the clock degrees of freedom in $\mathcal{H}_C$ define an internal time with respect to which the state in $\mathcal{H}_S$ evolves.

However, when such models are embedded in curved spacetime they encounter significant conceptual and technical difficulties. The decomposition in Eq. (1.12), based on the flat metric Eq. (1.10) is generally not possible for a metric which depends on position coordinates. Instead, in such cases factorization of the Hilbert space will lead to a constraint operator with an additional clock-system interaction term, H_{int}. Application of the Page–Wootters mechanism now leads to a Schrödinger equation in which the effective Hamiltonian is not Hermitian and the dynamics not unitary [10]:

$$i\hbar \frac{\mathrm{d}}{\mathrm{d}t} |\psi(t)\rangle_S = H_S |\psi(t)\rangle_S + \int \mathrm{d}t' \langle t|H_{\mathrm{int}}|t'\rangle |\psi(t')\rangle_S. \tag{1.15}$$

Formally, this nonunitarity reflects the fact that the system is not closed, but interacting with the clock. Open quantum system approaches may offer a path forward, but they also underscore the limitations of treating time relationally in curved spacetime within the original Page–Wootters framework.

These difficulties may also point to a deeper issue: the classical background structure of spacetime itself may need to be reexamined. Classical observations of clocks and test particles led to the formulation of spacetime as a smooth manifold equipped with a Lorentzian metric. But quantum effects inevitably induce backreaction on classical

degrees of freedom, even in principle. Since matter responds to geometry, and geometry is inferred from the behavior of matter, a more complete quantum understanding of matter naturally calls for a corresponding refinement of our conception of spacetime. Fortunately, much is already known about the quantum degrees of freedom of matter, providing a solid foundation for exploring such extensions.

In what follows, we present our phase space quantization as an alternative to the Page–Wootters construction for relativistic systems governed by a Hamiltonian constraint, outline its physical consequences, and explore its implications for the behavior of quantum clocks in curved spacetime.

1.4 Summary of main contributions

This dissertation is based largely on material from three journal articles written jointly with my advisor, Martin Bojowald.

In my preprint on *Quantum Proper Time: A Finsler Space from Entropy and Purity* [11], I show that new nonclassical degrees of freedom—specifically those associated with the entropy and purity of quantum states—give rise to a family of Finsler geometries on quantum state space. This framework unifies quantum state evolution and dynamical evolution of expectation values within a single variational principle, allowing one to associate a proper time to quantum trajectories, including those corresponding to entangled or mixed states. The resulting formalism reduces to classical proper time in the semiclassical limit but exhibits nontrivial corrections for delocalized, entangled, or nonpure systems. This work provides a novel characterization of logarithmic negativity for two-mode systems and identifies new quantum information parameters which may be broadly useful.

In a complementary line of investigation on *Geometry and Proper Time of a Relativistic Quantum Clock* [12], I examined how the phase space framework applies to clocks in Schwarzschild spacetime, including the emergence corrections to the gravitational redshift arising from purely quantum features. These corrections are, in principle, testable with next-generation atomic clocks [13]. Additionally, I analyzed the role of the observer by computing proper time for a quantum clock initialized in both the standard Schwarzschild slicing and the Painlevé–Gullstrand slicing. While proper time is gauge-invariant in the classical theory, our results suggest that this invariance may be violated at the first semiclassical order.

In *Adherence and violation of the equivalence principle from classical to quantum*

mechanics [14], I provided a detailed analysis of a quantum particle in free fall, modeled as a wave packet characterized by its center of mass and quantum fluctuations. These fluctuations, which determine the wave packet's width and spreading, obey an uncertainty relation that depends on the particle's mass, thereby introducing mass dependence into the system's dynamics. The presence of tidal gravitational fields leads to a coupling between the center of mass motion and internal quantum degrees of freedom. The analysis shows that quantum effects can lead to violations of certain formulations of the weak equivalence principle (WEP), with magnitudes potentially observable by experimental platforms such as Eötvös-type tests and clock-based return time measurements.

Together, these works support a view of proper time in relativistic quantum systems as a state-dependent, geometrically grounded quantity—one that encodes both the system's motion and its quantum information content. This perspective has implications not only for the interpretation of time in foundational physics but also for the design and analysis of quantum experiments in gravitational fields, where coherence and localization increasingly play a central role.

1.5 Structure of the dissertation

This dissertation aims to construct a manifest embedding of quantum particle mechanics within general spacetimes. While the physics of classical matter in curved spacetime and nonrelativistic quantum mechanics are each well understood, they are typically treated as separate frameworks. Yet, because quantum experiments are always performed within a spacetime setting, a unified formulation is both natural and necessary.

Chapter 2 begins with a review of the geometric formulation of quantum particle mechanics, emphasizing a phase-space approach based on expectation values and moments. Chapter 3 introduces the canonical formulation of classical spacetime physics. A key strength of the canonical approach is its ability to disentangle physical degrees of freedom from gauge artifacts. In this framework, observer frames are associated with choices of spacetime slicing, which provide a concrete setting for realizing the unconstrained quantum dynamics developed in Chapter 2.

In Chapter 4, we extend the quantum theory back to the full spacetime by reintroducing gauge freedom and analyze the resulting geometric structure. In particular, we investigate how quantum features are described by a Finsler geometry and identify the conditions under which this geometry reduces to a pseudo-Riemannian form. This analysis is guided by, and contributes to, a novel phase space characterization of quantum

entanglement, offering new insight into the interplay between geometry and informational structure in quantum systems.

Chapter 5 applies the formalism to a concrete physical scenario: a quantum clock in radial free fall toward a Schwarzschild black hole. This example illustrates, within a well-trodden relativistic setting, how classical notions such as proper time and geodesic motion are generalized or modified by quantum effects.

Finally, Chapter 6 presents detailed calculations demonstrating several observable consequences of the formalism. These include modifications to particle dispersion relations, a nonzero Eötvös parameter signaling violations of universal free fall, corrected return times in gravitational scattering scenarios, and the reconstruction of quantum, mass-dependent wave packet effects on the propagation phase in atom interferometry.

Chapter 2
Quantum mechanics in phase space

Only by taking into account the quantum properties of the bodies that form the reference frames, physical quantum operators can be defined in quantum gravity.

—Carlo Rovelli
Classical and Quantum Gravity **8** 317 (1991)

The work builds on recent developments in the geometrization of quantum mechanics [15–20]. The identification of Kähler structures presented in Sec. 2.2 is included for completeness and self-containment, and closely follows the derivations in [18, 20], to which the reader is referred for further details. Sec. 2.3 introduces moment coordinates on quantum phase space. The Poisson structure on this space defined in Eq. (2.18) enables the reformulation of quantum dynamics in terms of Poisson brackets, as discussed in Sec. 2.4. However, this Poisson structure is not canonical when expressed in terms of moment variables. To address this, Sec. 2.5 reviews a canonical transformations to Casimir–Darboux coordinates originally developed in [21]. We further relate these canonical parametrizations to standard representations used in the continuous-variable quantum information literature for one- and two-mode systems, and identify a new quantum information parameter that distinguishes the genuinely Finslerian geometry of the two-mode case from the Riemannian structure of simpler systems.

2.1 Quantum mechanics in Hilbert space

In canonical quantization, the quantum system is specified by an operator algebra $\mathcal{A}$, whose commutation relations are derived from the Poisson brackets of the classical theory. In a nonrelativistic system with a finite number n of continuous degrees of freedom,

the nonvanishing commutators among the generators of $\mathcal{A}$ are given by the canonical commutation relations (CCRs)

$$[\hat{x}^i, \hat{p}_j] = i\hbar\delta^i_j\hat{\mathbb{I}}\,, \qquad i, j = 1, \ldots, n\,. \tag{2.1}$$

Here, $\hat{x}^i$ and $\hat{p}_i$ may correspond to the classical phase space variables of a particle system, or alternatively, to the quadrature operators of an n-mode bosonic field. In the latter case, they are related to the creation and annihilation operators by

$$\hat{x}_k = \frac{1}{\sqrt{2}}\left(\hat{a}_k + \hat{a}_k^\dagger\right) \qquad \hat{p}_k = \frac{1}{i\sqrt{2}}\left(\hat{a}_k - \hat{a}_k^\dagger\right)\,. \tag{2.2}$$

These definitions ensure that the quadrature operators satisfy the same canonical commutation relations as the position and momentum operators, up to dimensionful scaling by $\hbar$.

In stark contrast to the classical theory, the quantum theory is: (i) linear, and (ii) infinite-dimensional. The latter refers to the fact that any representation of the canonical commutation relation (CCR) algebra $\mathcal{A}$ must act on an infinite-dimensional Hilbert space. This can be seen by taking the trace of both sides of Eq. (2.1). In a finite-dimensional representation, the trace of a commutator always vanishes, so applying this to Eq. (2.1) yields the contradiction $\mathrm{Tr}\left(\hat{\mathbb{I}}\right) = 0$.

A representation of the canonical commutation relations can be realized on the infinite-dimensional Hilbert space[1] $\mathcal{H} = (L^2(\mathbb{R}^n), \langle\cdot,\cdot\rangle)$, equipped with the inner product

$$\langle\phi, \psi\rangle := \int \overline{\phi(x)}\psi(x)d^n x\,. \tag{2.3}$$

In this representation, the position and momentum operators act as

$$\hat{x}^i \to x^i \qquad \hat{p}_j \to \frac{\hbar}{i}\frac{\partial}{\partial x^j}. \tag{2.4}$$

By the Stone–von Neumann theorem, all irreducible representations of the canonical commutation relation algebra on a finite number of degrees of freedom are unitarily equivalent to this one.

Within this framework, a central role is played by orthonormal bases of the Hilbert space, which may be constructed, for example, from the eigenfunctions of a self-adjoint

[1] In what follows, we adopt the convention of using the same symbol to denote both the Hilbert space and its underlying vector space.

operator. These eigenfunctions form a Schauder basis, allowing any state in the Hilbert space to be expressed as a (possibly infinite) linear combination of them. While this formalism is powerful and well-suited to many problems, it renders quantum theory structurally quite distinct from classical mechanics.

2.2 Geometric quantum mechanics via Kähler structures

We now develop a geometric reformulation of quantum theory by introducing an alternative characterization of a quantum state's degrees of freedom—one that emphasizes physically meaningful quantities such as expectation values and moments, and which bridges more naturally with classical phase space structures. Since we have at our disposal the unique (up to unitary equivalence) Hilbert space representation, this reformulation is naturally introduced through the Kähler structure of a Hilbert space.

When the complex Hilbert space $\mathcal{H}$ is viewed as a real-vector space equipped with a complex structure J, its sesquilinear (or Hermitian) inner product naturally decomposes into real and imaginary parts as

$$\langle \phi, \psi \rangle = \frac{1}{2\hbar} G(\phi, \psi) + \frac{i}{2\hbar} \Omega(\phi, \psi) \,, \tag{2.5}$$

where G and Ω are bilinear forms on the tangent bundle of $\mathcal{H}$, with each fiber canonically identified with $\mathcal{H}$ itself. The prefactor $(2\hbar)^{-1}$ is conventional and added for latter convenience.

It follows from properties of the sesquilinear inner product that G defines a Riemannian metric, while Ω defines a symplectic form. These are related through the complex structure $J(\psi) = i\psi$, satisfying

$$G(\phi, \psi) = \Omega(\phi, J\psi) \,. \tag{2.6}$$

The triple (G, Ω, J) thus defines a Kähler structure on $\mathcal{H}$.

The symplectic form Ω, arising from the imaginary part of the inner product, endows the Hilbert space with a geometric structure analogous to classical phase space. This motivates interpreting the Hilbert space as a quantum phase space, where dynamics can be described in terms of Hamiltonian flows.

On the symplectic manifold $(\mathcal{H}, \Omega)$, the symplectic form Ω provides a bundle isomor-

phism between the tangent bundle $\mathcal{H}$ and the cotangent bundle $\mathcal{H}^*$ given by

$$\psi \mapsto \Omega(\psi, \cdot)\,. \tag{2.7}$$

The nondegeneracy of Ω guarantees that this map is an isomorphism at each point, allowing one to associate Hamiltonian vector fields with differential 1-forms via contraction with Ω.

Any self-adjoint operator $\hat{F} \in \mathcal{A}$ determines a real-valued function on $\mathcal{H}$, defined by

$$F(\psi) \coloneqq \left\langle \psi, \hat{F}\psi \right\rangle\,. \tag{2.8}$$

This function generates a Hamiltonian vector field X_F via the symplectic form Ω, satisfying

$$\iota_{X_F}\Omega = \mathrm{d}F\,. \tag{2.9}$$

To compute the Hamiltonian vector field explicitly, consider a tangent vector η at the point ψ. The directional derivative of F in the direction η is

$$\begin{aligned}(\mathrm{d}F)(\eta) &= \frac{\mathrm{d}}{\mathrm{d}t}F(\psi + t\eta)\bigg|_{t=0} \\ &= \frac{\mathrm{d}}{\mathrm{d}t}\left\langle \psi + t\eta, \hat{F}(\psi + t\eta)\right\rangle\bigg|_{t=0} \\ &= \left\langle \psi, \hat{F}\eta\right\rangle + \left\langle \eta, \hat{F}\psi\right\rangle\,.\end{aligned} \tag{2.10}$$

Using the self-adjointness of $\hat{F}$, the second term is the complex conjugate of the first, yielding

$$(\mathrm{d}F)(\eta) = 2\mathrm{Re}\left\langle \hat{F}\psi, \eta\right\rangle\,. \tag{2.11}$$

Recalling the Kähler structure, the symplectic form Ω and the inner product G are related by

$$\Omega(\phi, \chi) = 2\hbar\mathrm{Im}\langle\phi, \chi\rangle, \quad G(\phi, \chi) = 2\hbar\mathrm{Re}\langle\phi, \chi\rangle, \tag{2.12}$$

so we may rewrite the derivative as

$$(\mathrm{d}F)(\eta) = \frac{1}{\hbar}G(\hat{F}\psi, \eta) = \Omega\left(\frac{1}{i\hbar}\hat{F}\psi, \eta\right)\,. \tag{2.13}$$

Therefore, comparing with Eq. (2.9), we conclude that the Hamiltonian vector field

associated with F is

$$X_F(\psi) = \frac{1}{i\hbar}\hat{F}\psi. \tag{2.14}$$

Such vector fields are called Schrödinger vector fields as their integral curves correspond to solutions of a Schrödinger equation

$$\frac{\mathrm{d}}{\mathrm{d}t}\psi = \frac{1}{i\hbar}\hat{F}\psi\,. \tag{2.15}$$

In this geometric formulation, time evolution appears as a Hamiltonian flow on the Hilbert space, generated by the symplectic structure Ω and the Hamilton function $H(\psi) = \left\langle \psi, \hat{H}\psi \right\rangle$, given by the expectation value of the Hamilton operator.

For two real-valued functions F and G on a symplectic manifold, the Poisson bracket is defined using the symplectic form Ω as

$$\{F, G\} \coloneqq \Omega\left(X_F, X_G\right)\,, \tag{2.16}$$

where X_F and X_G are the Hamiltonian vector fields associated with F and G, respectively.

Since the symplectic form is nondegenerate, it admits an inverse Ω^{-1}, which defines a bivector field Π that maps pairs of 1-forms to scalars. In terms of $\Pi = \Omega^{-1}$, the Poisson bracket of two smooth functions F and G can also be written as

$$\{F, G\} = \Pi\left(\mathrm{d}F, \mathrm{d}G\right). \tag{2.17}$$

When the symplectic form is nondegenerate, the definitions (2.16) and (2.17) are entirely equivalent. However, in truncations defined later, we typically encounter degenerate Poisson structures—that is, bivector fields Π that fail to arise from an invertible symplectic form. In such cases, the Poisson bracket is taken as primary, and the Poisson bivector Π is defined through its action on differentials.

The degeneracy of Π defines a foliation of the phase space into symplectic leaves, each of which inherits a nondegenerate symplectic structure. Dynamics then takes place on these leaves, and the geometry becomes locally—but not globally—symplectic.

In the geometric formulation of quantum mechanics, let F and G be the expectation values of self-adjoint operators $\hat{F}$ and $\hat{G}$. The corresponding Hamiltonian vector fields X_F and X_G are given by Eq. (2.15). Substituting these into the Poisson bracket definition (2.16), the Poisson bracket evaluated at a point $\psi \in \mathcal{H}$ is

$$\{F, G\}(\psi) = \frac{1}{i\hbar}\left\langle \psi, \left[\hat{F}, \hat{G}\right]\psi \right\rangle\,. \tag{2.18}$$

In this geometric formulation, the Poisson bracket of expectation value functions reproduces the commutator of the corresponding operators.

The Poisson structure defined by Eq. (2.18) extends to arbitrary smooth functions on the Hilbert space, not necessarily arising from operator expectation values, by requiring bilinearity, antisymmetry, and the Leibniz rule.

2.2.1 Pure states and projective geometry

Pure states play an important role in the theory because they represent the most precise specification of a quantum state. A quantum state is defined abstractly as a positive linear functional $\omega\colon \mathcal{A} \to \mathbb{C}$ on the operator algebra $\mathcal{A}$ satisfying normalization $\omega\left(\hat{\mathbb{I}}\right) = 1$. In the Hilbert space formulation, where $\mathcal{H}$ carries an irreducible representation of $\mathcal{A}$ as specified in (2.4), a state is realized concretely as a positive, trace-class, trace-one, linear operator ρ on $\mathcal{H}$.

A pure state operator ρ_ψ is represented by a rank-one projection operator constructed from a representative $\psi \in \mathcal{H}$

$$\rho_\psi = \frac{|\psi\rangle\langle\psi|}{\langle\psi|\psi\rangle}\,. \tag{2.19}$$

Such states are invariant under nonzero complex rescalings of the representative ψ, including time-dependent ones. This motivates the definition of an equivalence relation $\sim$ on $\mathcal{H}$,

$$\psi \sim \lambda(\tau)\psi \quad :\Longleftrightarrow \quad \lambda(\tau) \in \mathbb{C} \setminus \{0\} \text{ at fixed } \tau. \tag{2.20}$$

The quotient space $P(\mathcal{H}) := \mathcal{H}/\sim$ is the projective Hilbert space, whose elements correspond uniquely to pure states.

The geometric structure of projective Hilbert spaces has been extensively studied [20, 22–24], and provides a useful language for analyzing the properties and dynamics of pure quantum states.

For finite dimensional systems, the projective Hilbert space is isomorphic to a complex projective space of corresponding dimension. For example, for the two-dimensional spin–1/2 system, the space of pure states form the Bloch sphere $S^2 \cong \mathbb{C}P^1$. However, whenever $\mathcal{H}$ is infinite-dimensional, the projective Hilbert space is also infinite dimensional.

Although the symplectic form Ω, the Riemannian metric G, and the complex structure J were originally defined on $\mathcal{H}$, they all descend to the projective Hilbert space $P(\mathcal{H})$ under the equivalence relation $\psi \sim \lambda\psi$, making it into a Kähler manifold. More precisely, one works with the unit sphere $S(\mathcal{H}) = \{\psi \in \mathcal{H} \,|\, \langle\psi,\psi\rangle = 1\}$ and views $P(\mathcal{H})$ as the

quotient $S(\mathcal{H})/U(1)$, identifying states that differ by a phase. Since purity is conserved by Hamiltonian evolution, this allows one to describe pure state quantum dynamics geometrically as Hamiltonian flow on $P(\mathcal{H})$, where the generator of time evolution corresponds to the expectation value function of the Hamiltonian operator.

The resulting manifold $P(\mathcal{H})$ carries an induced metric, called the Fubini–Study metric, which encodes the Riemannian component of the Kähler structure. It can be shown that the geodesic distance between two states ϕ and ψ is computed by [19]

$$d_{\mathrm{FS}}(\phi,\psi) = \arccos\sqrt{\frac{\langle\phi,\psi\rangle\langle\psi,\phi\rangle}{\langle\phi,\phi\rangle\langle\psi,\psi\rangle}}\,, \tag{2.21}$$

which is invariant under both global phase shifts and reparametrizations of the state vector. This metric defines a distance between pure states and underlies many results in quantum information theory, in particular, in the distinguishability of states.

It is possible to rewrite the Poisson bracket (2.18) explicitly as an expression between expectations values of pure states as

$$\left\{\mathrm{Tr}(\rho_\psi \hat{F}), \mathrm{Tr}(\rho_\psi \hat{G})\right\} = \frac{1}{i\hbar}\mathrm{Tr}(\rho_\psi[\hat{F},\hat{G}]). \tag{2.22}$$

However, the relationship with (2.18) breaks down when ρ_ψ is replaced by a general mixed state ρ, for which the geometry of the projective Hilbert space no longer suffices.

The inclusion of mixed states therefore requires a generalization of the constructions given in [20, 22–24], which can still be formulated by means of a Poisson bracket [18] on the space of states, but in general not with a Kähler structure. In this vein, we also note that generalizations of the CCRs in Eq. (2.1), such as those involving nonassociative algebras [25], can lead to operator algebras that do not admit a representation on a Hilbert space.

In the fully general setting, one works with the algebraic definition of the Poisson bracket [26], defined for an algebraic state $\omega : \mathcal{A} \to \mathbb{C}$ as

$$\left\{\omega\left(\hat{A}\right), \omega\left(\hat{B}\right)\right\} = \frac{1}{i\hbar}\,\omega\left([\hat{A},\hat{B}]\right). \tag{2.23}$$

This expression satisfies all formal properties of a Poisson bracket, including bilinearity, antisymmetry, and the Jacobi identity. It can be extended to polynomials in $\hat{x}^i$ and $\hat{p}_i$ using the Leibniz rule.

The purely algebraic formulation is more general than the Hilbert space approach, as

it does not require a choice of representation, provided the algebra $\mathcal{A}$ is equipped with a star-structure that generalizes adjointness relations of operators. Throughout this text, we adopt the shorthand

$$\left\langle \hat{A} \right\rangle \coloneqq \omega\left(\hat{A}\right) \tag{2.24}$$

so that the algebraic and Hilbert space formulations coincide whenever $\mathcal{A}$ is associative and admits a Hilbert space representation.

2.3 Moments as coordinates on quantum phase space

In the quantum theory, each classical degree of freedom gives rise to a tower of countably infinitely many new degrees of freedom. For instance, in general the powers $\langle \hat{x}^n \rangle \neq \langle \hat{x} \rangle^n$, reflecting the presence of fluctuations and higher-order quantum correlations.

Instead of representing states as wave functions or density matrices with respect to a Schauder basis, an alternative and often more insightful approach is to characterize states by their moments. Alternative coordinate systems will be introduced in Sec. 2.5, where we discuss canonical structures on the quantum phase-space.

In the Hilbert space representation, the set of fundamental operators $(\hat{x}^i, \hat{p}_j)$ induces a bundle structure on $\mathcal{H}$ [18], where the bundle projection identifies all points ϕ, $\psi \in \mathcal{H}$ that have the same expectation value for the canonical observables

$$\langle \phi, \hat{x}^i \phi \rangle = \langle \psi, \hat{x}^i \psi \rangle \,, \quad \langle \phi, \hat{p}_i \phi \rangle = \langle \psi, \hat{p}_i \psi \rangle \quad \text{for all } i = 1, \ldots, n \,. \tag{2.25}$$

The base manifold of this bundle is identified with the classical phase space, parametrized by the basic expectation values

$$x^i \coloneqq \langle \hat{x}^i \rangle \,, \tag{2.26}$$

$$p_i \coloneqq \langle \hat{p}_i \rangle \,. \tag{2.27}$$

This defines a natural projection from the quantum state space to the classical phase space, with the fiber over each point consisting of all quantum states sharing the same classical position and momentum expectations.

We complete the coordinate system by selecting the remaining variables to be the centralized and symmetrized higher-order moments, which encode fluctuations and

correlations beyond the basic expectation values.[2] These are defined by

$$\Delta\Big((x^1)^{\alpha_1}\cdots(x^n)^{\alpha_n}p_1^{\beta_1}\cdots p_n^{\beta_n}\Big) \coloneqq \Big\langle(\hat{x}^1-x^1)^{(\alpha_1}\cdots(\hat{x}^n-x^n)^{(\alpha_n}(\hat{p}_1-p_1)^{\beta_1)}\cdots(\hat{p}_n-p_n)^{\beta_n)}\Big\rangle \tag{2.28}$$

where the parentheses around the multi-indices indicate total symmetrization over the enclosed operators. These moments serve as fiber coordinates in the bundle structure over classical phase space and characterize the quantum corrections to classical behavior.

As shown in [18], these functions generate Hamiltonian vector fields that are symplectically orthogonal to the classical directions $\partial/\partial x^i$ and $\partial/\partial p_i$, ensuring a clean separation between classical and genuinely quantum degrees of freedom in the extended phase space.

The higher-order moments can be written more compactly by introducing multi-indices $\alpha = (\alpha_1, \ldots, \alpha_n)$ and $\beta = (\beta_1, \ldots, \beta_n)$, which encode powers of the basic phase-space variables. We define the corresponding monomials as

$$x^\alpha = (x^1)^{\alpha_1}\cdots(x^n)^{\alpha_n} \tag{2.29}$$

$$p^\beta = (p_1)^{\beta_1}\cdots(p_n)^{\beta_n}. \tag{2.30}$$

With this notation, a general higher-order quantum moment takes the form

$$\Delta\Big((x^1)^{\alpha_1}\cdots(x^n)^{\alpha_n}p_1^{\beta_1}\cdots p_n^{\beta_n}\Big) \equiv \Delta\Big(x^\alpha p^\beta\Big). \tag{2.31}$$

The coordinates $(x^a, p_a, \Delta(x^\alpha p^\beta))$, for all multi-indices α and β, form a complete set in the sense that they uniquely determine the state. A proof of existence and uniqueness in the classical case is contained in [27]. Generalization of the proof to existence and uniqueness of wave function and density matrix states is discussed in [18] and [14]. A self-contained exposition of wave function reconstruction is provided in Appendix B.

As part of the proof, one must assume that the moments are finite and satisfy positivity conditions. These conditions are identified in [18] as uncertainty relations specifying the boundary component of the quantum phase space. For example, for a single canonical pair (x, p), second-order moments must have

$$\Delta(x^2)\Delta(p^2) - \Delta(xp)^2 \geq \frac{\hbar^2}{4}. \tag{2.32}$$

[2]The choice to use centralized and symmetrized moments is motivated by their natural appearance in noncommutative series expansions around classical trajectories, as in Eq. (2.41). Noncentral, nonsymmetric moments could be used, and in fact are more natural in the context of state reconstruction explored in Appendix B.

Such a relation is in general poorly defined if any moment is infinite. Higher-order relations are developed for quantum states in [28], although we will not need them here. We remark that the existence of such conditions is a restriction on the kinematical phase space to the space of physical states only and does not imply relations between the moments of a given state which remain independent. An intuitive description of these variables in one and two space dimensions is elaborated in [29].

In future equations, we will use further arithmetic rules for the multi-indices, including the factorial

$$\alpha! \coloneqq \alpha_1! \cdots \alpha_n! \tag{2.33}$$

and order

$$|\alpha| \coloneqq \alpha_1 + \cdots + \alpha_n \,. \tag{2.34}$$

We define the order of a moment as the value of the sum $|\alpha + \beta| = \sum_i (\alpha_i + \beta_i)$. A quantum state is called semiclassical if its moments satisfy the scaling condition

$$\Delta(x^\alpha p^\beta) = O(\hbar^{|\alpha+\beta|/2}). \tag{2.35}$$

This condition permits a systematic $\hbar$-expansion about the classical limit.

Each term in the moment hierarchy carries different physical units, which can complicate the interpretation of expansions like Eq. (2.35). In applications where characteristic length and momentum (or energy) scales are available—denoted x_c and p_c, respectively—these can be used to rescale the moments and formulate the hierarchy in terms of dimensionless quantities. Under such a rescaling, the semiclassical hierarchy is well defined when the dimensionless ratio $\hbar/(x_c p_c)$ is small, i.e., $\hbar/(x_c p_c) \ll 1$. This condition reflects the physical intuition that the minimum quantum of action $\hbar$ is small compared to the typical phase space volume occupied by the system.

Conversely, when the ratio $\hbar/(x_c p_c)$ is approximately unity, quantum effects become dominant and the system is highly nonclassical. In this regime, higher-order moments are no longer suppressed, and the expansion cannot be truncated reliably.

Even in the absence of external length or momentum scales, the spirit of the expansion (2.35) can still be applied to control the moment expansion. In practice, it is sufficient to check the relative magnitudes of higher-order moments relative to lower-order ones. For instance, semiclassical behavior is supported when dimensionless ratios such as

$$(\Delta(x^4)/\Delta(x^2)^2 < 1 \quad \text{or} \quad \Delta(x^2p^2)/\Delta(xp)^2 < 1 \tag{2.36}$$

are satisfied. These conditions ensure that the contribution of higher moments remains perturbative, even in systems without fixed characteristic scales, however they are generally hard to check.

As a concrete example, the unsqueezed single-mode Gaussian state with fluctuation parameter σ has moments given for a and b positive integers by

$$\Delta(x^a p^b) = 2^{-(a+b)} \hbar^b \sigma^{a-b} \frac{a!b!}{(a/2)!(b/2)!} \quad \text{if } a \text{ and } b \text{ are even} \tag{2.37}$$

and $\Delta(x^a p^b) = 0$ otherwise. The semiclassicality condition for such a state depends on the preparation of the state. This state is semiclassical provided that the fluctuation obeys $\sigma^2 = \kappa\hbar$ for some fixed scaling coefficient κ.

The class of states satisfying the semiclassical hierarchy (2.35) is much larger than the Gaussian family. The scaling condition constrains the $\hbar$-dependence but leaves the numerical coefficients of the moments unspecified, allowing a wide variety of physically distinct states—differing in correlations, entropy, and purity—to qualify as semiclassical.

2.4 Poisson dynamics

The Poisson structure defined in Eq. (2.18) allows us to associate a Hamiltonian vector field to each observable, generating a Hamiltonian flow on the (quantum) phase space. Of particular interest is the flow generated by the quantum Hamilton function, defined as

$$H_{\mathcal{Q}}(\psi) \coloneqq \left\langle \hat{H} \right\rangle . \tag{2.38}$$

According to Eq. (2.15), the Hamiltonian flow generated by this function is equivalent to the Schrödinger evolution

$$\frac{\mathrm{d}}{\mathrm{d}t}\psi = \frac{1}{i\hbar}\hat{H}\psi . \tag{2.39}$$

However, it is not necessary to evolve wave functions and then extract physically meaningful quantities via inner product evaluations in Hilbert space. Instead, in the phase space formulation, one works directly with observable quantities such as expectation values and moments. If $A(x, p, \Delta(x^\alpha p^\beta))$ is a dynamical variable (explicitly t-independent), then its evolution is determined by the Poisson structure

$$\frac{\mathrm{d}}{\mathrm{d}t}A = \{A, H_{\mathcal{Q}}\}. \tag{2.40}$$

When states are parameterized by their basic expectation values, $x = \langle \hat{x} \rangle$ and $p = \langle \hat{p} \rangle$, along with central moments $\Delta(x^\alpha p^\beta)$, the quantum Hamilton function $H_\mathcal{Q}$ becomes a function of these variables. It is useful to develop a general expression for $H_\mathcal{Q}$ showing its dependence on these phase space variables.

Such an expression can be obtained through a series expansion centered around the basic expectation values:

$$\begin{aligned} H_\mathcal{Q}\Big(x^a, p_a, \Delta(x^\alpha p^\beta)\Big) &\coloneqq \Big\langle \hat{H}\Big(x^a + (\hat{x}^a - x^a), p_a + (\hat{p}_a - p_a)\Big)\Big\rangle \\ &= \sum_{\alpha=0}^{\infty} \sum_{\beta=0}^{\infty} \frac{1}{\alpha!\beta!} \frac{\partial^{|\alpha+\beta|} H(x,p)}{\partial^\alpha x \partial^\beta p}\, \Delta(x^\alpha p^\beta) \end{aligned} \tag{2.41}$$

where the sums range over all multi-indices beginning from the zero multi-index $0 = (0,0,0,0)$. In differential geometric terms, Eq. (2.41) is the coordinate representation of the quantum Hamilton function as a function on the infinite-dimensional quantum phase space.

Terms in this representation of $H_\mathcal{Q}$ are distinguished by the order of the quantum moment they contain. The zeroth-order term always reproduces exactly the classical Hamilton function. This implies that quantum dynamics reduce to their underlying classical analog when H can be expressed as a quadratic function of x and p. This characteristic contributes to the prevalence of quadratic potentials in modeling quantum systems and explains the extensive research devoted to systems governed by quadratic potentials in the literature, for example in that of [30], where the Newtonian gravitational potential is approximated by its second order series expansion. Second, when dealing with nonquadratic potentials, the remaining terms in this expansion reveal the emergence of quantum effects. States whose fluctuations are nonzero are extended. In the higher-order terms, quantum fluctuations of the state couple to the external field through a derivative expansion of the potential.

In the nonquadratic setting, the quantum effects can dominate or act as perturbations depending on the relative magnitude of higher-order terms. If the Hamiltonian is polynomial in the basic operators, the expansion of $H_\mathcal{Q}$ terminates at finite order, and perturbation theory may not be necessary. Otherwise for Hamiltonians involving non-polynomial interactions, one must consider the convergence properties of the series (2.41). In this case, systems satisfying the moment hierarchy condition in Eq. (2.35) are well behaved as higher-order terms are suppressed by powers of $\hbar$.

Truncating the expansion at a finite order yields a closed semiclassical dynamics

with controlled errors. At leading order, the dynamics reproduces the classical equations of motion, while higher-order terms introduce perturbative corrections from quantum fluctuations and correlations. These perturbative effects can capture interesting quantum features of the system, such as tunneling phenomena, as demonstrated in [31].

2.5 Canonical variables

The quantum phase space variables $\Delta\big(x^\alpha p^\beta\big)$ do not form a set of canonical coordinates, as they have nontrivial Poisson brackets with one another. These brackets, derived in [18], are given for the moments of a single canonical pair x, p by

$$\begin{aligned}\Big\{\Delta(x^a p^b), \Delta(x^c p^d)\Big\} \;=\; & \sum_{r,s=0}^{\infty} \Big(-\frac{1}{4}\hbar^2\Big)^{r+s} \sum_{j,k} \binom{a}{j}\binom{b}{k}\binom{c}{k}\binom{d}{j} \\ & \times \Delta(x^{a+c-j-k} p^{b+d-j-k})(\delta_{j,2r+1}\delta_{k,2s} - \delta_{j,2r}\delta_{k,2s+1}) \\ & + ad\,\Delta(x^{a-1}p^b)\Delta(x^c p^{d-1}) - bc\,\Delta(x^a p^{b-1})\Delta(x^{c-1}p^d) \quad (2.42)\end{aligned}$$

where the inner sums run over $0 \le j \le \min(b, c)$ and $0 \le k \le \min(a, d)$, respectively.[3] The Poisson tensor implied by this relation has a complicated structure.

While the quantum moments $\Delta\big(x^\alpha p^\beta\big)$ provide a physically meaningful and complete description of the quantum state, their noncanonical Poisson structure (2.42) complicates the formulation of dynamics. For instance, the quantum Hamilton function for a nonrelativistic free particle is

$$H_{\mathcal{Q}} = \frac{p^2}{2m} + \frac{\Delta(p^2)}{2m}\,. \tag{2.43}$$

Although $\Delta(p^2)$ arises from quantum fluctuations, it appears additively alongside the classical kinetic energy term, raising the question of how to interpret its physical contribution. Does it modify the particle's kinetic energy, or should it be viewed as part of an effective potential? The lack of a canonical structure for the moments obscures such distinctions. And while the equation of motion for x retains the canonical form $\dot{x} = \partial H_{\mathcal{Q}}/\partial p$, the moment equations are not in Hamiltonian form. To clarify the underlying geometry and enable a more transparent formulation of quantum dynamics, it is useful to introduce canonical coordinates on the truncated quantum phase space. The Casimir–Darboux theorem [32] guarantees the local existence of such coordinates.

[3] For low-order moments, it is often more practical to compute Poisson brackets directly from the definition (2.18), rather than using the expression above.

In what follows, we construct canonical variables for second-order moments. First, we address the case of a single canonical pair (x, p) in Sec. 2.5.1, and then extend this construction to two canonical pairs (x, p_x, y, p_y) in Sec. 2.5.2. The two-pair construction is more involved than simply taking two copies of a single pair due to the presence of inter-mode correlations. The results presented here build on the constructions introduced in [21] and are informed by foundational treatments of quantum optics in phase space [33]. A key component of our derivation of Finsler structures in quantum theory in Chapter 4 is a new parameterization of quantum-information properties related to the second-order moments of a state, which may also have broader applications. We construct this and other new inverse formulas relating the canonical variables to the original quantum moments in Sec. 2.5.3.

2.5.1 Single-mode canonical realization

The x-coordinates at second order, $(\Delta(x^2), \Delta(xp_x), \Delta(p_x^2))$, have the brackets

$$\begin{aligned} \left\{\Delta(x^2), \Delta(p_x^2)\right\} &= 4\Delta(xp_x)\,, \\ \left\{\Delta(x^2), \Delta(xp_x)\right\} &= 2\Delta(x^2)\,, \\ \left\{\Delta(xp_x), \Delta(p_x^2)\right\} &= 2\Delta(p_x^2). \end{aligned} \tag{2.44}$$

In this case, it is known [34–36] that the transformation

$$\Delta\left(x^2\right) = s^2 \qquad \Delta(xp_x) = sp_s \qquad \Delta\left(p_x^2\right) = p_s^2 + \frac{U}{s^2} \tag{2.45}$$

to new variables (s, p_s, U) implies the canonical Poisson bracket $\{s, p_s\} = 1$ making (s, p_s) a canonical pair. The third variable, U, Poisson commutes with all second-order moments, making U an element of the center of the Poisson algebra generated by (2.44). In a Poisson algebra, central elements are known as Casimir functions, in analogy with the corresponding concept in Lie algebras. Casimir functions represent conserved quantities as they are invariant under any Hamiltonian flow. These Casimir functions can be systematically identified for any algebra.

The Poisson algebra for a single-mode system, given by Eqs. (2.44), is isomorphic to the $\mathrm{sp}(2, \mathbb{R})$ Lie algebra. The single-mode covariance matrix

$$\sigma = \begin{pmatrix} \Delta(x^2) & \Delta(xp_x) \\ \Delta(xp_x) & \Delta(p_x^2) \end{pmatrix} \tag{2.46}$$

together with the symplectic form $\Omega_{ij} = \{x_i, x_j\}$ (with $\mathbf{x} = (x, p_x)$ has components x_i) allow the Casimir of $\mathrm{sp}(2, \mathbb{R})$ to be constructed equivalently either as the sum of squared eigenvalues of $\Omega\sigma$ or as the value of the trace of $(\Omega\sigma)^2$. More generally, the algebra $\mathrm{sp}(2n, \mathbb{R})$ has n Casimirs which are constructed as

$$U^{(2k)} \propto \mathrm{Tr}\left[(\Omega\sigma)^{2k}\right], \quad k = 1, \ldots n. \tag{2.47}$$

By construction, these quantities are invariant under symplectic transformations. Inverting the mapping (2.45) identifies the single-mode Casimir as the uncertainty product

$$U = \Delta(x^2)\Delta(p_x^2) - \Delta(xp_x)^2 \tag{2.48}$$

which is, by Eq. (2.47), a quadratic Casimir.

As a direct consequence of the uncertainty relation, U is bounded from below by $\hbar^2/4$. We may therefore write U as

$$U = p_q^2 \frac{\hbar^2}{4} \tag{2.49}$$

with a momentum $p_q \geq 1$, canonically conjugate to a coordinate q that does not appear in the Hamiltonian. (It is convenient to separate p_q and $\hbar$ in (2.49) such that $\hbar$ can be used to characterize semiclassical orders. As a consequence, both p_q and q are unitless.)

2.5.2 Two-mode canonical realization

In a quantum system with two continuous degrees of freedom, there are ten second-order moments: six describing the individual modes and four capturing cross-mode correlations. The second moments are naturally organized into the two-mode covariance matrix, which in mode-ordering takes the block form

$$\sigma = \begin{pmatrix} \sigma_x & \sigma_{xy} \\ \sigma_{xy}^\top & \sigma_y \end{pmatrix}, \tag{2.50}$$

where σ_x and σ_y are the single-mode covariance matrices, and σ_{xy} encodes intermode correlations:

$$\sigma_x = \begin{pmatrix} \Delta(x^2) & \Delta(xp_x) \\ \Delta(xp_x) & \Delta(p_x^2) \end{pmatrix}, \quad \sigma_y = \begin{pmatrix} \Delta(y^2) & \Delta(yp_y) \\ \Delta(yp_y) & \Delta(p_y^2) \end{pmatrix}, \quad \sigma_{xy} = \begin{pmatrix} \Delta(xy) & \Delta(xp_y) \\ \Delta(p_x y) & \Delta(p_x p_y) \end{pmatrix}. \tag{2.51}$$

Although there are ten independent second-order moments, constraints reduce the

number of physically relevant degrees of freedom. This reduction is typically realized through unitary transformations of the quantum state, $\rho \mapsto U\rho U^\dagger$, which induce symplectic transformations on the covariance matrix, $\sigma \mapsto S\sigma S^\top$, with $S \in \mathrm{sp}(4,\mathbb{R})$.

In particular, transformations $S'_x, S'_y \in \mathrm{sp}(2,\mathbb{R})$ diagonalizing the single-mode covariance matrices,

$$S'_x \sigma_x S'^\top_x = U_x \mathbb{I}_2 \tag{2.52}$$
$$S'_y \sigma_y S'^\top_y = U_y \mathbb{I}_2, \tag{2.53}$$

can be extended to $\mathrm{sp}(4,\mathbb{R})$ as

$$S_x = S'_x \oplus \mathbb{I}_2 \tag{2.54}$$
$$S_y = \mathbb{I}_2 \oplus S'_y\,. \tag{2.55}$$

These transformations commute and act in either order on the two-mode covariance matrix to diagonalize the single-mode blocks,

$$S_y S_x \sigma S_x^\top S_y^\top = \begin{pmatrix} U_x \mathbb{I}_2 & S'_x \sigma_{xy} S'^\top_y \\ S'_y \sigma_{xy}^\top S'^\top_x & U_y \mathbb{I}_2 \end{pmatrix}. \tag{2.56}$$

The remaining off-diagonal blocks can be diagonalized according to their singular-value decomposition via an orthogonal symplectic transformation $O = O_x \oplus O_y$ with $O_x, O_y \in \mathrm{sp}(2,\mathbb{R})$. This brings the covariance matrix into its so-called Simon normal form [37],

$$\sigma_{\mathrm{sf}} = S\sigma S^\top = \begin{pmatrix} U_x & 0 & c_+ & 0 \\ 0 & U_x & 0 & c_- \\ c_+ & 0 & U_y & 0 \\ 0 & c_- & 0 & U_y \end{pmatrix} \tag{2.57}$$

where $S = O S_y S_x \in \mathrm{sp}(4,\mathbb{R})$.

The single-mode quantities U_x and U_y, together with the cross-mode correlators c_+ and c_-, are invariant under local symplectic transformations and play a central role in the characterization of two-mode quantum states. These invariants underpin many entanglement criteria and have been widely used in foundational and applied analyses (e.g., [33, 38–40]).

In contrast to this invariant-based viewpoint, we offer an alternative perspective

grounded in the intrinsic Poisson structure of the quantum moments themselves. This approach reveals the true dynamical degrees of freedom of the state directly through the structure of the moment algebra. The relevant second-order moments are organized into the vector

$$\begin{aligned}\Delta_i \;=\; \Big(&\Delta(x^2), \Delta(xp_x), \Delta(p_x^2), \Delta(y^2), \Delta(yp_y), \Delta(p_y^2), \\ &\Delta(xy), \Delta(xp_y), \Delta(p_x y), \Delta(p_x p_y)\Big).\end{aligned} \tag{2.58}$$

The Poisson structure defined in Eq. (2.18) determines the Poisson tensor $\mathbb{P}_{ij} = \{\Delta_i, \Delta_j\}$. This antisymmetric tensor has rank eight, indicating that among the ten second-order moments Δ_i, there exist four canonical pairs: (s_x, p_{s_x}), (s_y, p_{s_y}), (α, p_α), and (β, p_β). These canonical coordinates provide a complete and dynamically meaningful parametrization of the physical degrees of freedom, superseding the commonly used local invariants (U_x, U_y, c_+, c_-).

In addition, a faithful mapping must include two Casimir functions—quantities that Poisson-commute with all observables and remain conserved under any Hamiltonian evolution. These are identified as the quadratic and quartic Casimirs C_1 and C_2, which arise naturally from the the $\mathrm{sp}(4, \mathbb{R})$ Lie algebra structure, as given by Eq. (2.47). In the canonical picture, the Casimirs C_1 and C_2 can be understood as the conjugate momenta of cyclic configuration variables φ and ψ, which do not appear explicitly in the Hamiltonian and thus remain dynamically frozen. (We notate these cyclic coordinates as angles because C_1 and C_2 both have units of angular momentum. The angle φ appears in the dual-spherical coordinates illustrated by Figure 4.1.)

The canonical mapping introduced in [21, 41] extends the mapping for a single degree of freedom by defining fluctuation coordinates as

$$\Delta(x^2) = s_x^2 \quad , \quad \Delta(y^2) = s_y^2 \quad , \quad \Delta(xp_x) = s_x p_{s_x} \quad , \quad \Delta(yp_y) = s_y p_{s_y}. \tag{2.59}$$

However, owing to cross-mode correlations, an extension of the single-mode mapping requires additional ingredients of the $\mathrm{sp}(4, \mathbb{R})$ structure not contained in two copies of $\mathrm{sp}(2, \mathbb{R})$. The position-position covariance $\Delta(xy)$ introduces correlation as an independent phase-space degree of freedom, β, through the definition

$$\Delta(xy) = s_x s_y \cos(\beta). \tag{2.60}$$

The momentum conjugate to β, denoted p_β, appears in the angular-momentum-like

cor- relation moments

$$\Delta(xp_y) = s_x p_{s_y} \cos(\beta) - \sin(\beta)\frac{s_x}{s_y}\left(p_\alpha + p_\beta\right) \tag{2.61}$$

and

$$\Delta(p_x y) = s_y p_{s_x} \cos(\beta) + \sin(\beta)\frac{s_y}{s_x}\left(p_\alpha - p_\beta\right). \tag{2.62}$$

These expressions also depend on the fourth quantum momentum, p_α.

The single-mode invariants

$$U_x = \Delta(x^2)\Delta(p_x^2) - \Delta(xp_x)^2 \quad , \quad U_y = \Delta(y^2)\Delta(p_y^2) - \Delta(yp_y)^2 \tag{2.63}$$

are no longer global constants, but rather given by the phase-space functions

$$\begin{aligned} U_x &= (p_\alpha - p_\beta)^2 \\ &+\frac{1}{2\sin^2(\beta)}\left((C_1^2 - 4p_\alpha^2) - \sqrt{(C_1^2 - 4p_\alpha^2)^2 - (C_1^4 - C_2^4)}\sin(\alpha+\beta)\right) \end{aligned} \tag{2.64}$$

and

$$\begin{aligned} U_y &= (p_\alpha + p_\beta)^2 \\ &+\frac{1}{2\sin^2(\beta)}\left((C_1^2 - 4p_\alpha^2) - \sqrt{(C_1^2 - 4p_\alpha^2)^2 - (C_1^4 - C_2^4)}\sin(\alpha-\beta)\right). \end{aligned} \tag{2.65}$$

These depend on the angular canonical pairs (α, p_α) and (β, p_β) and the two Casimir variables, C_1 and C_2.

The canonical mapping for the three momentum-momentum correlations then has

$$\Delta(p_x^2) = p_{s_x}^2 + \frac{(p_\alpha - p_\beta)^2}{s_x^2} + \frac{1}{2s_x^2\sin^2(\beta)}\left(C_1^2 - 4p_\alpha^2 - \sqrt{P}\sin(\alpha+\beta)\right), \tag{2.66}$$

$$\Delta(p_y^2) = p_{s_y}^2 + \frac{(p_\alpha + p_\beta)^2}{s_y^2} + \frac{1}{2s_y^2\sin^2(\beta)}\left(C_1^2 - 4p_\alpha^2 - \sqrt{P}\sin(\alpha-\beta)\right), \tag{2.67}$$

and

$$\Delta(p_x p_y) = \left(p_{s_x}p_{s_y} + \frac{p_\alpha^2 - p_\beta^2}{s_x s_y}\right)\cos(\beta) + \left(\frac{p_{s_y}}{s_x}(p_\alpha - p_\beta) - \frac{p_{s_x}}{s_y}(p_\beta + p_\alpha)\right)\sin(\beta)$$

$$-\frac{1}{2s_x s_y \sin^2(\beta)}\left((C_1^2 - 4p_\alpha^2)\cos(\beta) - \sqrt{P}\sin(\alpha)\right). \tag{2.68}$$

Each of these involves the square root

$$\sqrt{P(p_\alpha, C_1, C_2)} = \sqrt{(C_1^2 - 4p_\alpha^2)^2 - (C_1^4 - C_2^4)}. \tag{2.69}$$

We refer to $\sqrt{P}$ as the Finsler root, and to the quartic polynomial under the square root as the Finsler discriminant. This polynomial, $P(p_\alpha, C_1, C_2)$, generally cannot be factored over the real numbers, except under specific conditions on the momenta. For this reason, it controls the qualitative structure of the geometry, distinguishing between Riemannian and genuinely Finslerian behavior. The full structure of the Finsler geometry is developed in Sec. 4.2, while Sec. 4.4 explores special cases where this quartic decomposes into the sum of two Riemannian structures.

Before applying this transformation to the geodesic Hamiltonian, we develop the inverse mapping.

2.5.3 Inverse formulas for two-mode canonical variables

The inverse mapping from covariance data to canonical variables is given by

$$s_x = \sqrt{\Delta(x^2)} \quad , \quad p_{s_x} = \frac{\Delta(xp_x)}{\sqrt{\Delta(x^2)}} \tag{2.70}$$

$$s_y = \sqrt{\Delta(y^2)} \quad , \quad p_{s_y} = \frac{\Delta(yp_y)}{\sqrt{\Delta(y^2)}} \tag{2.71}$$

$$\cos(\beta) = \frac{\Delta(xy)}{\sqrt{\Delta(x^2)\Delta(y^2)}} \tag{2.72}$$

$$p_\alpha = \frac{\Delta(xy)(\Delta(yp_y) - \Delta(xp_x)) + \Delta(x^2)\Delta(p_x y) - \Delta(y^2)\Delta(xp_y)}{2\sqrt{\Delta(x^2)\Delta(y^2) - \Delta(xy)^2}} \tag{2.73}$$

$$p_\beta = \frac{\Delta(xy)(\Delta(yp_y) + \Delta(xp_x)) - \Delta(x^2)\Delta(p_x y) - \Delta(y^2)\Delta(xp_y)}{2\sqrt{\Delta(x^2)\Delta(y^2) - \Delta(xy)^2}} \tag{2.74}$$

together with expressions for C_1 and C_2, and then α. The expressions for C_1 and C_2 can be identified from expressions for the symplectic eigenvalues and we develop these first. Then we identify an expression for α which is the canonical variable with the most complicated relationship to moments.

Unlike a classical state, a quantum state cannot be sharply localized at a single point

$\mathbf{x} = (x, p_x, y, p_y)$ in phase space due to the uncertainty principle. This nonlocality is captured at first order in $\hbar$ by the covariance matrix σ, which defines an uncertainty ellipsoid centered at $\mathbf{x}$ whether or not the state is Gaussian. The shape of this ellipsoid is determined by the symplectic eigenvalues ν_+ and ν_-, which specify the lengths of its semi-principal axes. These eigenvalues generalize singular values to symplectic geometry, remaining invariant under $\mathrm{sp}(4, \mathbb{R})$ transformations. As such, they encode intrinsic, observer-independent features of the two-mode quantum state, including its total uncertainty and entropic content. They are obtained from the spectrum of the matrix $i\Omega\sigma$, where $\Omega_{ij} = \{x_i, x_j\}$ is the canonical symplectic form, with x_i the components of $\mathbf{x}$.

The quadratic and quartic Casimirs of our canonical mapping can be expressed in terms of ν_+ and ν_- as

$$C_1^2 = \nu_+^2 + \nu_-^2 \tag{2.75}$$

$$C_2^2 = \nu_+^2 - \nu_-^2, \tag{2.76}$$

or, explicitly in terms of second-order moments, as

$$\begin{aligned} C_1^2 = {} & \Delta(x^2)\Delta(p_x^2) - \Delta(xp_x)^2 \\ & + \Delta(y^2)\Delta(p_y^2) - \Delta(yp_y)^2 \\ & + 2\Delta(xy)\Delta(p_xp_y) - 2\Delta(xp_y)\Delta(p_xy) \end{aligned} \tag{2.77}$$

and

$$\begin{aligned} & C_2^4 = \\ & 4\Big(\Delta(p_xp_y)(\Delta(xp_x) - \Delta(yp_y)) - \Delta(p_x^2)\Delta(xp_y) + \Delta(p_y^2)\Delta(p_xy)\Big) \\ & \times\Big(\Delta(xy)(\Delta(yp_y) - \Delta(xp_x)) + \Delta(x^2)\Delta(p_xy) - \Delta(y^2)\Delta(xp_y)\Big) \\ & +4\Big(\Delta(p_xy)(\Delta(xp_x) + \Delta(yp_y)) - \Delta(p_x^2)\Delta(xy) - \Delta(y^2)\Delta(p_xp_y)\Big) \\ & \times\Big(\Delta(xp_y)(\Delta(xp_x) + \Delta(yp_y)) - \Delta(p_xp_y)\Delta(x^2) - \Delta(p_y^2)\Delta(xy)\Big) \\ & +2\left(\Delta(x^2)\Delta(p_x^2) - \Delta(xp_x)^2 + \Delta(p_xp_y)\Delta(xy) - \Delta(p_xy)\Delta(xp_y)\right)^2 \\ & +2\left(\Delta(p_xp_y)\Delta(xy) - \Delta(p_xy)\Delta(xp_y) + \Delta(y^2)\Delta(p_y^2) - \Delta(yp_y)^2\right)^2 \\ & +C_1^4\,. \end{aligned} \tag{2.78}$$

The lengthy expression for C_2 is a consequence of its relation to the determinant of the

covariance matrix according to

$$\det(\sigma) = \frac{1}{4}(C_1^4 - C_2^4). \tag{2.79}$$

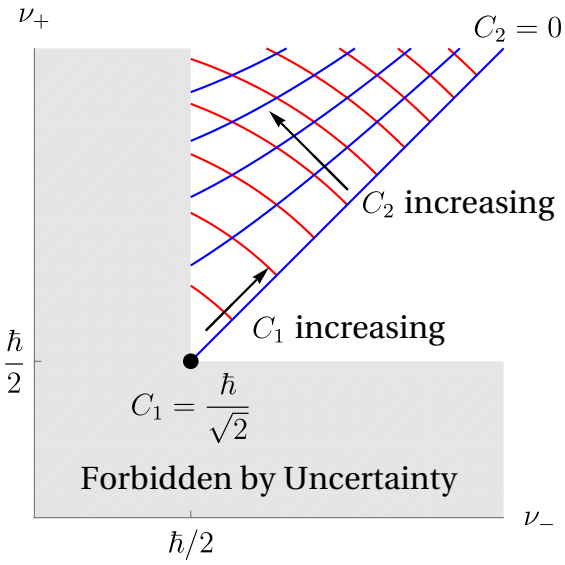

Figure 2.1: The allowed region for symplectic eigenvalues (ν_-^2, ν_+^2) of a two-mode quantum state, constrained by the uncertainty principle. The shaded area is forbidden due to the lower bound $\nu_\pm^2 \geq \hbar^2/4$. The curves of constant $C_1^2 = \nu_+^2 + \nu_-^2$ (red) and constant $C_2^2 = \nu_+^2 - \nu_-^2$ (blue) define a grid over the permitted region. The corner point $\nu_+^2 = \nu_-^2 = \hbar^2/4$ corresponds to a pure, unentangled vacuum state. Arrows indicate directions of increasing total uncertainty C_1^2 and increasing asymmetry C_2^2 between the modes.

From the Robertson-Schrödinger uncertainty relation

$$\sigma + \frac{i\hbar}{2}\Omega \geq 0 \tag{2.80}$$

it follows that $\nu_+ \geq \nu_- \geq \hbar/2$. These imply the uncertainty bounds

$$C_1^2 \geq \frac{\hbar^2}{2} \tag{2.81}$$

$$C_2 \geq 0. \tag{2.82}$$

Together, C_1^2 and C_2^2 define orthogonal directions in the space of symplectic eigenval-

ues, as illustrated in Fig. 2.1. The first Casimir, C_1, sets the overall scale of quantum fluctuations. For pure states C_1 reaches its limiting value, $\hbar/\sqrt{2}$, and increases under mixedness. In contrast, the second Casimir, C_2, captures anisotropy in the symplectic spectrum. When $C_2 = 0$, the eigenvalues are equal ($\nu_+ = \nu_-$), and the state is symplectically isotropic—it is circular in an appropriate canonical basis. As C_2 increases, the ellipsoid becomes increasingly distorted and one canonical mode dominates the uncertainty. This asymmetry, like C_1, is invariant under symplectic transformations.

An explicit expression for α in terms of moments is too long to be displayed here, but it can be obtained by computing $U_x - U_y$ in two different ways, first from (2.63) and then from (2.64) and (2.65), such that

$$\Delta(x^2)\Delta(p_x^2) - \Delta(y^2)\Delta(p_y^2) - \Delta(xp_x)^2 + \Delta(yp_y)^2 = -4p_\alpha p_\beta - \sqrt{P}\frac{\cos\alpha}{\sin\beta}\,. \tag{2.83}$$

The remaining equations in (2.70)–(2.74) as well as (2.77) and (6.14) then provide a complete expression for $\cos\alpha$ in terms of second-order moments. In particular, the terms on the left-hand side of (2.83) as well as the product $p_\alpha p_\beta$ on the right can all be written in terms of different uncertainty products, for which we use the general definition

$$\Delta^{B_1 B_2}_{A_1 A_2} = \Delta(A_1 B_1)\Delta(A_2 B_2) - \Delta(A_1 B_2)\Delta(A_2 B_1)\,. \tag{2.84}$$

With this notation, we can write

$$\cos\alpha = -\frac{\sin\beta}{\sqrt{P}}\frac{(\Delta^{xy}_{yp_y})^2 - (\Delta^{xy}_{xp_y})^2 + \Delta^{xy}_{xy}\Delta^{xp_x}_{xp_x} - \Delta^{xy}_{xy}\Delta^{yp_y}_{yp_y}}{\Delta^{xy}_{xy}}\,. \tag{2.85}$$

We return to provide additional characterization of α when we discuss its role in shaping the Finsler geometry experienced by two-mode states in Chapter 4.

Application of the canonical realizations identified here for one- and two-mode systems toward efficient quantum state sampling is introduced and discussed in Appendix C.

Chapter 3
Constraints and the problem of time

> *"I wish it need not have happened in* my time*," said Frodo.*
>
> *"So do I," said Gandalf, "and so do all who live to see such times. But that is not for them to decide. All we have to decide is what to do with the time that is given us."*
>
> —J.R.R. Tolkien,
> *The Fellowship of the Ring*

The previous chapter introduced a geometric formulation of quantum mechanics. Before applying these techniques to the quantum description of relativistic clocks, we must first establish a classical model of clocks that admits a consistent quantization. This chapter presents a pedagogical derivation of the Hamiltonian formulation and subsequent quantization of the relativistic point particle, which serves as the foundational model for relativistic clock systems.

Starting in Sec. 3.2 from the classical reparametrization-invariant Lagrangian action, Eq. (3.1), we construct a first-order Hamiltonian action, Eq. (3.17), and identify the associated Hamiltonian constraint, Eq. (3.15). Having settled on the canonical approach, two routes to the quantum theory remain: one may either fix the gauge at the classical level and then quantize the resulting unconstrained theory, or quantize first and then implement quantum gauge fixing.

In Sec. 3.3, we take the first approach and carry out classical phase space reduction. Using the ADM formalism, we relate reparametrization invariance to the slicing ambiguity in spacetime, allowing the evolution parameter to be interpreted as the proper time of an ADM inertial observer. By imposing gauge conditions adapted to the frame of this observer, we identify physical degrees of freedom—thereby completing phase space

reduction to the physical phase space. The resulting unconstrained evolution Hamiltonian, Eq. (3.43), governs the clock's dynamics relative to this frame and admits quantization via conventional canonical methods.

We compare the classical reduction approach with the corresponding reduction on the quantum phase space in Sec. 3.4, where we argue that both procedures yield a consistent quantization—i.e., the system is anomaly-free. In Sec. 3.5, we present the resulting quantum theory using the effective Hamiltonian formalism developed in Chapter 2. Since this formulation describes dynamics in the local frame of an observer and is therefore noncovariant, we reverse the reduction procedure in Sec. 3.6, reintroducing constraints to define a spacetime-covariant quantum theory.

This approach to quantization of the relativistic point particle provides a concrete example of how classical gauge symmetry, constraint dynamics, and semiclassical quantum evolution interrelate in a simple system and paves the way to further questions regarding geodesic motion of massive or massless quantum states in curved spacetime and observer-dependence at the intersection of quantum theory and general relativity.

3.1 Reparametrization-invariant actions for free particles

The classical theory of particle motion in general curved spacetimes is extraordinarily well-tested [3]. We adopt the mathematical structures developed in this regime as our starting point. Quantization of these structures should then yield a (hopefully unique) extension into the quantum regime that remains compatible with the classical limit.

The spacetime trajectory $\gamma : [0, 1] \to M$, given in coordinates by $x^a(\sigma) = x^a \circ \gamma(\sigma)$, of a free relativistic particle is determined classically by the stationary solutions of the proper time functional

$$\tau[\gamma] = \int_0^1 \sqrt{-\frac{1}{c^2} g_{ab}(x) \frac{\mathrm{d}x^a}{\mathrm{d}\sigma} \frac{\mathrm{d}x^b}{\mathrm{d}\sigma}} \mathrm{d}\sigma \,, \tag{3.1}$$

where g_{ab} is the spacetime metric with signature $(-, +, +, +)$.

The equations of motion of (3.1) are independent of mass and valid even in the massless case, however in the massless case the integrand vanishes and $\tau = 0$. The parameter σ is a real evolution parameter and plays the role of time. The theory defined by (3.1) is invariant under arbitrary smooth reparametrization of the worldline parameter, $\sigma \mapsto \sigma' = f(\sigma)$. In this sense, the theory admits no preferred or absolute notion of external time.

A notable feature of classical relativity is that the action $\tau[\gamma]$ for a freely falling test particle is independent of the particle's internal properties—an observation elevated to the status of a physical principle through the equivalence principle [42]. Despite this unique feature, other actions typically encountered in physics have dimensions of $\mathrm{M} \cdot \mathrm{L}^2 \cdot \mathrm{T}^{-1}$. This choice of units is not arbitrary but dictated by the existence of a fundamental constant of nature: the reduced Planck constant $\hbar$, which appears in the path integral formulation of quantum mechanics. In particular, the propagator for a quantum particle is given by

$$\langle x_1^a; \sigma_1 | x_0^a; \sigma_0 \rangle = \int_{x_0^a}^{x_1^a} \mathcal{D}[x(\sigma)] \exp\left[i \frac{S[x(\sigma)]}{\hbar} \right] \tag{3.2}$$

where the action $S[x(\sigma)]$ must have the same dimensions as $\hbar$ to ensure the exponent is dimensionless. To obtain an action with these physical dimensions, we multiply the proper time by an overall constant and define the free particle action as

$$S[\gamma] = -mc^2 \tau[\gamma] \,, \tag{3.3}$$

where m is a parameter with units of mass, c is the speed of light, and $\tau[\gamma]$ denotes the proper time functional defined in Eq. (3.1). The minus sign ensures that physical trajectories minimize the action. The identification of m with the Newtonian inertial mass depends on taking the nonrelativistic limit, which is only possible for massive particles. For massless particles, m does not admit this interpretation.

Although we do not follow the path-integral approach to quantization in this dissertation, it nonetheless highlights certain features more transparently. For instance, substituting Eq. (3.3) into the propagator expression reveals that the exponent scales as the ratio of proper distance to the particle's Compton wavelength

$$\frac{S}{\hbar} = \frac{c\tau}{\hbar/(mc)} \,. \tag{3.4}$$

In the classical, tree-level limit, an overall multiplicative factor in the action does not change the variational equations of motion. However, as shown in the loop corrections analyzed later in this work, such quantum effects typically violate the weak equivalence principle [14].

The proper-time functional (3.1) defines the square-root Lagrangian

$$\mathrm{L}(x^a, \dot{x}^a) = \sqrt{-\frac{1}{c^2} g_{ab}(x) \frac{\mathrm{d}x^a}{\mathrm{d}\sigma} \frac{\mathrm{d}x^b}{\mathrm{d}\sigma}} \,. \tag{3.5}$$

However, the velocity Hessian of this Lagrangian, $\partial^2 L / \partial \dot{x}^a \partial \dot{x}^b$, is singular, complicating the construction of the canonical theory. To address this, we now turn to an equivalent classical formulation that is better suited for canonical analysis.

3.2 The einbein action and proper time normalization

The einbein action for a relativistic clock moving between spacetime events $x^a(0)$ and $x^a(0)$ is given by

$$S[x, e] = \int_0^1 \mathrm{d}\sigma \left(-\frac{1}{2e} g_{ab} \frac{\mathrm{d}x^a}{\mathrm{d}\sigma} \frac{\mathrm{d}x^b}{\mathrm{d}\sigma} + \frac{e(mc)^2}{2} \right) , \tag{3.6}$$

where $e(\sigma)$ is a worldline scalar field (the einbein), and m is a parameter with units of mass. This action has the singular Lagrangian

$$\mathrm{L}(x, e, \dot{x}, \dot{e}) = -\frac{1}{2e} g_{ab} \frac{\mathrm{d}x^a}{\mathrm{d}\sigma} \frac{\mathrm{d}x^b}{\mathrm{d}\sigma} + \frac{e(mc)^2}{2} \,. \tag{3.7}$$

Varying the action (3.6) with respect to e gives the constraint

$$e^2 = -\frac{1}{m^2 c^2} g_{ab} \frac{\mathrm{d}x^a}{\mathrm{d}\sigma} \frac{\mathrm{d}x^b}{\mathrm{d}\sigma} \,. \tag{3.8}$$

Substituting this result back into the einbein action (i.e., resolving the constraint) reproduces the square-root form (3.3). The einbein and square-root actions thus define equivalent variational problems.

Equation (3.8) provides the general relation between the einbein and the spacetime metric prior to any gauge fixing. In the massive case, the gauge choice

$$e = \frac{1}{m} \tag{3.9}$$

enforces proper time normalization of the worldline

$$g_{ab} \frac{\mathrm{d}x^a}{\mathrm{d}\sigma} \frac{\mathrm{d}x^b}{\mathrm{d}\sigma} = -c^2 \,. \tag{3.10}$$

In the massless case, the einbein appears as a Lagrange multiplier, and its variation imposes the null condition on the worldline

$$g_{ab}\frac{\mathrm{d}x^a}{\mathrm{d}\sigma}\frac{\mathrm{d}x^b}{\mathrm{d}\sigma} = 0\,. \tag{3.11}$$

Thus, e remains unconstrained and reflects the freedom to rescale the affine parameter along the null geodesic.

We can translate the Lagrangian action (3.6) into a Hamiltonian one. The momenta conjugate to the x^a are

$$p_a = \frac{\partial \mathrm{L}}{\partial \dot{x}^a} = -\frac{1}{e}g_{ab}\dot{x}^b \tag{3.12}$$

and the velocities are expressed as

$$\dot{x}^a = -e g^{ab} p_b. \tag{3.13}$$

Since the einbein $e(\sigma)$ appears in the action without a time derivative, its conjugate momentum vanishes identically

$$p_e = \frac{\partial \mathrm{L}}{\partial \dot{e}} = 0\,, \tag{3.14}$$

indicating that p_e is a primary constraint. Formally, p_e generates gauge transformations associated with the reparametrization invariance of the worldline.

In both the massive and massless cases, the system exhibits a secondary constraint

$$g^{ab}(x), p_a p_b + m^2c^2 = 0,\,. \tag{3.15}$$

Verifying this condition requires invoking the Lagrangian equation of motion for the einbein, Eq. (3.8); hence, the constraint is classified as secondary.

The first-class Hamilton function for the action (3.6) constructed via a singular Legendre transform is

$$\begin{aligned} \mathrm{H} &= p_e\dot{e} + p_a\dot{x}^a(x,p) - \mathrm{L}(e,x,\dot{x}(x,p)) \\ &= p_e\dot{e} - \frac{e}{2}\left(g^{ab}(x)p_a p_b + m^2c^2\right) \end{aligned} \tag{3.16}$$

and implies the first-order action

$$\begin{aligned} S[x^a,e,p_a,p_e] &= \int \mathrm{d}\sigma\,(p_a\dot{x}^a + p_e\dot{e} - \mathrm{H}) \\ &= \int \mathrm{d}\sigma\left[p_a\dot{x}^a + \frac{e}{2}\left(g^{ab}(x)p_a p_b + m^2c^2\right)\right]. \end{aligned} \tag{3.17}$$

Equation (3.17) is the first-order relativistic action in parametrized form. The einbein field appears as a Lagrange multiplier for the Hamiltonian constraint. The equations of motion obtained from the requirement $\delta S = 0$ for arbitrary variations of its arguments are[1]

$$\frac{\delta S}{\delta x^a} = -\dot{p}_a + \frac{e}{2}\frac{\partial g^{bc}}{\partial x^a}p_b p_c = 0 \tag{3.18}$$

$$\frac{\delta S}{\delta p_a} = \dot{x}^a + e g^{ab} p_b = 0 \tag{3.19}$$

$$\frac{\delta S}{\delta e} = \frac{1}{2}(g^{ab}p_a p_b + m^2 c^2) = 0 \tag{3.20}$$

The constrained Hamiltonian dynamics represented by these equations are equivalent to the Lagrangian equations and make sense in both the massive and massless cases.

The Lagrange multiplier e can be related to the evolution parameter. Consider the equations of motion

$$\frac{1}{e}\frac{\mathrm{d}x^a}{\mathrm{d}\sigma} = -g^{ab}p_b \tag{3.21}$$

$$\frac{1}{e}\frac{\mathrm{d}p_a}{\mathrm{d}\sigma} = \frac{1}{2}\frac{\partial g^{bc}}{\partial x^a}p_b p_c \tag{3.22}$$

These are equivalent to the second-order equation

$$\ddot{x}^a + \Gamma^a_{bc}\dot{x}^b\dot{x}^c = \dot{x}^a\frac{\dot{e}}{e} \tag{3.23}$$

where Γ^a_{bc} are the usual Christoffel symbols for the metric g_{ab}. Reparametrization from σ to an affine parameter, $\tau(\sigma)$, requires the einbein field $e(\sigma)$ to satisfy the first-order inhomogeneous differential equation

$$\frac{\mathrm{d}e/\mathrm{d}\sigma}{e(\sigma)} = -\left(\frac{\mathrm{d}^2\sigma}{\mathrm{d}\tau^2}\right)\left(\frac{\mathrm{d}\sigma}{\mathrm{d}\tau}\right)^{-2}. \tag{3.24}$$

In particular, Eq. (3.24) admits a solution with constant $e(\sigma)$ along the worldline, i.e., $de/\mathrm{d}\sigma = 0$, provided that σ is proportional to τ. In this case, the parameter σ is affine.

For a massive particle, the proper-time gauge $e = 1/m$ implies the Hamilton function

$$\mathrm{H}_{\mathrm{massive}} = -\frac{1}{2m}\left(g^{ab}(x)p_a p_b + m^2 c^2\right). \tag{3.25}$$

[1]The minus sign on $\dot{p}_a$ in the first equation comes from integrating by parts

For a massless particle we impose any gauge condition on e and obtain

$$\mathrm{H}_{\text{massless}} = -\frac{1}{2} g^{ab}(x) k_a k_b \,. \tag{3.26}$$

Both expressions define Hamiltonian constraints, and we denote them with the roman letter H. In the massless case, the momentum is written as k_a to emphasize that it is defined only up to arbitrary rescaling.

In the massive case, the proper-time normalization gives the singular Lagrangian

$$\mathrm{L} = -\frac{1}{2} m g_{ab} \dot{x}^a \dot{x}^b + \frac{1}{2} m c^2 \,. \tag{3.27}$$

The classical proper-time functional can therefore be expressed as

$$\tau[\gamma] = \int \sqrt{\frac{2\mathrm{L}}{mc^2} - 1}\, \mathrm{d}\tau \,. \tag{3.28}$$

This expression can be interpreted in two ways. (i) If we insert the Lagrangian (3.27), we rewrite the integral (3.28) in the form (3.1). (ii) If the constraint $\mathrm{H} = 0$ is used, it implies $\mathrm{L} = -mc^2$, such that (3.28) equals $\int \mathrm{d}\tau$ and indeed represents proper time.

On the cotangent bundle the classical pathlength functional can be rewritten as

$$\tau[x(\tau), p(\tau)] = \int \sqrt{1 + \frac{2\mathrm{H}}{mc^2}}\, \mathrm{d}\tau \,. \tag{3.29}$$

On the one hand, inserting the Hamiltonian constraint $\mathrm{H}_{\text{massive}}$ gives the path integral

$$\tau = \int \sqrt{-\frac{g^{ab}(x) p_a p_b}{m^2 c^2}}\, \mathrm{d}\tau \,. \tag{3.30}$$

And on the other, when we maintain the constraint that the Hamiltonian vanish, we ensure that the theory remains reparameterizable and the expression still measures proper time.

Canonical quantization, undertaken in Sec. 3.5, will ultimately yield a quantum-effective expression that corrects the classical constraint $\mathrm{H} \to \mathrm{H}_{\mathcal{Q}} = \mathrm{H} + O(\hbar)$. The proper-time formula (3.29), using the quantum effective Hamiltonian constraint will then serve as our definition of quantum proper time.

However, the Hamiltonians introduced in this section are constraint functions. Rather than quantizing the constrained system directly—i.e., promoting H to a quantum operator $\hat{\mathrm{H}}$ and working with quantum constraints—we simplify the analysis by first performing

classical phase space reduction. This reduction can be carried out starting from either Eq.(3.25) or Eq.(3.26).

3.3 Classical constraint reduction and the problem of time

Due to the Hamiltonian constraint, not all phase space variables correspond to independent physical degrees of freedom. The constraint can be used to eliminate one variable—usually p_0. This elimination procedure is called "resolving the constraint." Resolving the constraint in the parametrized action (3.17) yields the first-order action

$$S[x^0, x^i, p_j] = \int \mathrm{d}\sigma \left(p_i \dot{x}^i + p_0 \dot{x}^0 \right) \tag{3.31}$$

where p_0 is understood to be the function obtained by solving the Hamiltonian constraint, defined as

$$p_0 = -H(x^i, p_j, x^0)/c\,. \tag{3.32}$$

This expresses the time component of the momentum as a function of the spatial coordinates, momenta, and coordinate time.

Even after resolving the Hamiltonian constraint, the Hamilton function H may still carry explicit dependence on the coordinate x^0 (for example in cosmological spacetimes, or inside a black hole horizon where the metric is no longer static). Since its conjugate momentum p_0 is unphysical, the variable x^0 itself is pure gauge. To complete the reduction of phase space, we must therefore eliminate all reference to x^0.

As a gauge variable, x^0 may be fixed by any convenient gauge condition. A possible choice is

$$x^0(\sigma) = c\sigma\,, \tag{3.33}$$

which identifies the worldline parameter σ with the coordinate time. However, in general, other gauge choices may be more insightful.

To illustrate this, we describe an alternative gauge choice to deparametrize the action. To identify the gauge, we rewrite the resolved action (3.31) in the form

$$S[t, x^i, p_j] = \int \mathrm{d}\sigma \, \frac{\mathrm{d}t}{\mathrm{d}\sigma} \left(p_i \frac{\mathrm{d}x^i/\mathrm{d}\sigma}{\mathrm{d}t/\mathrm{d}\sigma} - H(x^i, p_j, t) \right), \tag{3.34}$$

where, for convenience, we have written $x^0 = ct$ to absorb the dependence on the speed of light c.

The multiplicative factor $\frac{\mathrm{d}t}{\mathrm{d}\sigma}$ acts as a local dilation, relating the worldline parameter

σ to the coordinate time t. The underlying worldline gauge theory permits arbitrary reparametrizations of σ, reflecting this freedom. If $t = f(\sigma)$ is locally invertible (which we will always assume it is), we can perform a change of variables in the integral (3.34) and write $\sigma = f^{-1}(t)$. The chain rule then implies the deparameterized action

$$S[x^i, p_j] = \int \mathrm{d}t \, \left(p_i \frac{\mathrm{d}x^i}{\mathrm{d}t} - H(x^i, p_i, t) \right) , \tag{3.35}$$

expressed in terms of the deparametrized velocities

$$\frac{\mathrm{d}x^i}{\mathrm{d}t} \coloneqq \frac{\mathrm{d}x^i/\mathrm{d}\sigma}{\mathrm{d}t/\mathrm{d}\sigma} \tag{3.36}$$

This procedure has the same effect as assigning $\sigma \mapsto t$, however the relationship between them may more complicated than simple equality and depends on the solution to the differential equation $dt/d\sigma = f(\sigma)$.

The integrand of Eq. (3.35) is the deparametrized Lagrange function,

$$L(x^i, x^{i\prime}) \coloneqq p_i \frac{\mathrm{d}x^i}{\mathrm{d}t} - H(x^i, p_i, t) \, , \tag{3.37}$$

where we define the apostrophe (prime) derivative with respect to coordinate time t. This defines the Lagrangian action on the spatial hypersurface

$$S[x^i, x^{i\prime}] = \int \mathrm{d}t \, L(x^i, x^{i\prime}) \, . \tag{3.38}$$

In the case of the mass-shell constraint (3.15), the above-described procedure requires solving a quadratic equation in p_0. The roots of this equation are naturally interpreted using the ADM decomposition of the inverse spacetime metric,

$$g^{ab} = \begin{pmatrix} -\frac{1}{N^2} & \frac{N^i}{N^2} \\ \frac{N^i}{N^2} & \gamma^{ij} - \frac{N^i N^j}{N^2} \end{pmatrix} . \tag{3.39}$$

In these variables, the two roots of the Hamiltonian constraint following immediately from the quadratic formula are

$$p_0 = N^i p_i \pm |N| \sqrt{\gamma^{ij} p_i p_j + m^2 c^2} \, . \tag{3.40}$$

This expression represents a linearized form of the constraint (3.15), and its two roots correspond, in a precise sense, to separate constraints for particles and antiparticles [43]. In what follows, we do not pursue this distinction and simply select the positive root. Moreover, we will assume a positive lapse function, $N > 0$, so that the time-orientation of the ADM observer (Box 3.1) aligns with the direction of increasing worldline parameter.

The lapse and shift functions, N and N^i, represent gauge degrees of freedom of the spacetime metric. In a particular foliation of spacetime with $N^i = 0$ and $N = 1$, the fully-reduced Hamiltonian governing evolution relative to the chosen observer frame is, for a massive particle,

$$H(x^i, p_i; t) = c\sqrt{\gamma^{ij}(x^i, t)p_i p_j + m^2c^2}\,, \tag{3.41}$$

and for a massless particle

$$H(x^i, k_i; t) = c\sqrt{\gamma^{ij}(x^i, t)k_i k_j}\,. \tag{3.42}$$

Ref. [44] identifies synchronous coordinates that realize such a slicing for the Kerr metric.

From the role of reference frame theory, if we wanted to keep the role of the observer explicit, we could work in the general spacetime gauge where the Hamiltonian takes the (possibly time-dependent) form

$$H(\vec{x}, \vec{p}; t) = N(\vec{x}, t)\sqrt{\gamma^{ij}(\vec{x}, t)p_i p_j c^2 + m^2c^4} - N^i(\vec{x}, t)p_i c\,. \tag{3.43}$$

This function is not manifestly covariant—it is defined on the spatial hypersurface Σ_t. Nonetheless, at the classical level, the resulting *spacetime* trajectory implied by this Hamilton function,

$$x^a(\sigma) \coloneqq \Big(ct(\sigma),\, x^i(t(\sigma))\Big)\,, \tag{3.44}$$

(for arbitrary σ) *is* covariant. If the local Lorentz transformation laws for t and x^i are assumed, then the covariance of (3.44) follows trivially. However, from the perspective adopted here, covariance is not taken as a fundamental principles, but rather as an empirical feature that the theory is constructed to reproduce. Our interest lies in examining how covariance might persist—or break down—at the quantum level. In particular, the specific form of covariance under the Lorentz group $SO(1,3)$ is not imposed a priori and may, in fact, be modified by quantum effects (the group—or its representation at the very least—must be enlarged to cover new nonclassical degrees of freedom).

Covariance, as a physical principle, relates the observations of a system made by different observers. However, in the quantum regime, the noncommutativity of measurements implies that such covariance is not automatically preserved ([45]). Preliminary results originally published in [12] and revisited in Sec. 5.6 of this dissertation, compare quantum proper time in Schwarzschild spacetime using both the standard foliation and the Painlevé-Gullstrand slicing. These results suggest a potential violation of covariance in the quantum theory, highlighting the frame-dependence of quantum-corrected geometric quantities.

Box 3.1 ADM Observer

We can make the identity of the observer precise. Let $x^i = (x^1, x^2, x^3)$ denote the coordinates on each hypersurface Σ_t of the foliation $\{\Sigma_t\}_{t\in\mathbb{R}}$, and let (t, x^1, x^2, x^3) denote the corresponding smooth extension to a coordinate system on the full spacetime.

Definition: An ADM observer is defined as one whose worldline remains at fixed spatial coordinates $x^i =$ const.. The coordinate basis vectors $(\partial_t, \partial_1, \partial_2, \partial_3)$ define the ADM observer frame, and the vector ∂_t is tangent to the wordline of such an observer.

Proposition: The Hamiltonian (3.43) corresponds to the particle energy as measured in the ADM observer frame.

Proof: In general, ∂_t is not orthogonal to the hypersurfaces Σ_t. Let n denote the future-directed unit normal to the hypersurface Σ_t. We assume for simplicity that the basis $\partial_i \in T(\Sigma_t)$ is already orthonormal (if it is not, then we additionally must construct normal coordinates in the hypersurface). We have, by construction $g(n, n) = -1$ and $g(\partial_i, \partial_j) = \delta_{ij}$. The ADM decomposition of the coordinate vector field ∂_t in terms of this orthonormal basis is

$$\partial_t = Nn + N^i\partial_i\,, \tag{3.45}$$

an expression which defines the lapse N, and shift N^i. Let $p^a = (E/c, p^i)$ denote the components a particle's 4-momentum, relative to the orthonormal frame (n, ∂_i).

The energy measured by the ADM observer is

$$-g(\partial_t, p) = NE - N^i p_i c\,. \tag{3.46}$$

Corollary: The expression

$$E(\vec{x}, \vec{p}) := \sqrt{\gamma^{ij}(\vec{x}) p_i p_j c^2 + m^2 c^4}\,. \tag{3.47}$$

represents the energy of the particle as measured in the frame of an observer whose worldline is orthogonal to the ADM foliation. For an ADM observer, the lapse N corrects for time dilation and the shift term $-N^i p_i$ is a projection of the momentum onto the spatial flow of the coordinates themselves.

Example: In flat spacetime with $N = 1$, $N^i = 0$, and $\gamma^{ij} = \delta^{ij}$, the ADM particle energy reduces to the standard relativistic energy:

$$H(\vec{x}, \vec{p}) = \sqrt{\vec{p}^2 c^2 + m^2 c^4}\,. \tag{3.48}$$

Since the Hamiltonian in Eq. (3.43) is unconstrained, we may proceed with conventional canonical quantization to obtain the quantum theory. However, before doing so, we consider an alternative route: quantization followed by quantum-level gauge fixing.

3.4 Quantum constraint reduction and the problem of time

In the classical theory, we have seen that the Hamiltonian constraint eliminates an entire canonical pair, such as (x^0, p_0), resolving the redundancy associated with time reparametrization invariance. An alternative approach, following Dirac, is to first quantize the constrained classical system and then impose the constraint at the quantum level.

In this setting, one might expect to encounter moments associated with the time coordinate $t = x^0$ and its conjugate momentum $p_0 = -E/c$. However, this raises the question of how to interpret the time and energy operators $\hat{t}$ and $\hat{E}$. While one can assign a formal representation of these operators on a Hilbert space such as $L^2(\mathrm{R}^4)$ via $\hat{t} = t$ and $\hat{p}_0 = i\hbar\partial/\partial t$, the well-known Pauli theorem presents an obstruction. Specifically, the theorem asserts that if a self-adjoint time operator conjugate to the energy exists, then both operators must have continuous spectra spanning the entire real line. As a corollary, no self-adjoint time operator can be conjugate to a semibounded Hamiltonian—that is,

one that possesses a ground state.

In Dirac quantization, the classical constraint $\mathrm{H} = 0$ is promoted to a quantum constraint $\hat{\mathrm{H}} = 0$. Then, just as each classical observable x gives rise in the quantum theory to an infinite tower of expectation values $\langle \hat{x}^n \rangle$, the formalism developed in [16, 17] shows that each classical constraint gives rise to an infinite tower of quantum constraints, involving moments of all orders.

In addition to the expectation value of the Hamiltonian operator, any expression of the form $\langle \hat{O}\hat{\mathrm{H}} \rangle$, where $\hat{O}$ is a generic polynomial in $\hat{x}$ and $\hat{p}$, must also vanish on physical states. These constitute higher-order constraints involving quantum moments. As phase-space functions on nonphysical states, $\langle \hat{\mathrm{H}} \rangle$ and $\langle \hat{O}\hat{\mathrm{H}} \rangle$ are in general independent functions in the sense that $\langle \hat{\mathrm{H}} \rangle = 0$ does not imply $\langle \hat{O}\hat{\mathrm{H}} \rangle = 0$. Moments of physical states are therefore obtained only if we impose the primary constraint $H_{\mathcal{Q}} = 0$ as well as the infinite tower of higher-order constraints $\langle \hat{O}\hat{\mathrm{H}} \rangle = 0$ for suitable $\hat{O}$, such as all polynomials up to a certain degree (if we use a truncation) in the basic operators.

A detailed analysis of such gauge systems, given in [16, 17], shows that the resulting constraints are mutually consistent in the sense that all gauge transformations respect the joint constraint surface on which all the constraints up to a given order are zero. Moreover, at least for Hamiltonians that do not depend explicitly on time, a consistent gauge fixing can be chosen that sets moments involving a time variable, given here by coordinate time t, equal to zero. The resulting reduced phase space on which constraints are solved with this gauge fixing is then equivalent to a semiclassical quantization of the classically reduced system discussed in the previous section.

This step, which amounts to a choice of gauge fixing in the underlying gauge theory depends on the spacetime coordinate system used to express the background metric g^{ab} as specific functions of the coordinates. In physical language, this step represents the choice of a reference frame, which does not affect observables classically because of general covariance. By introducing moment variables, our methods allow us to determine possible implications of reference frames in a quantum setting.

Classical phase space transformations induce corresponding transformations on the quantum phase space, ensuring that classical frame changes are mirrored by well-defined quantum frame transformations. The structure of these symmetries and their correspondence is discussed in Appendix A.

3.5 Quantization

The analyses of Secs. 3.3 and 3.4 show that ADM energy (3.43) of a point particle in a spacetime with spatial metric γ^{ij} and lapse and shift functions $N(\vec{x})$, $N^i(\vec{x})$, can be robustly interpreted as the value of the Hamiltonian generating time evolution in a chosen spacetime foliation. In particular, the physical degrees of freedom of the relativistic point particle, when described in an arbitrary frame, are governed by the Hamilton function

$$H(\vec{x},\vec{p}) = N(\vec{x})\sqrt{\gamma^{ij}(\vec{x})p_i p_j c^2 + m^2c^4} - N^i(\vec{x})p_i c\,. \tag{3.49}$$

This Hamilton function is unconstrained and may be quantized via conventional canonical quantization.

In Chapter 2, we reformulated quantum evolution as Hamiltonian evolution of the expectation values x^i, p_j and moments $\Delta(x^\alpha p^\beta)$ of phase space variables, generated by the effective Hamilton function

$$\begin{aligned} H_{\mathcal{Q}}\Big(\vec{x},\vec{p},\Delta(x^\alpha p^\beta)\Big) &= \Big\langle H\Big(x+(\hat{x}-x),p+(\hat{p}-p)\Big)\Big\rangle \\ &= \sum_{\alpha=0}^{\infty}\sum_{\beta=0}^{\infty}\frac{1}{\alpha!\beta!}\frac{\partial^{|\alpha+\beta|}H(x,p)}{\partial^\alpha x\partial^\beta p}\,\Delta(x^\alpha p^\beta)\,. \end{aligned} \tag{3.50}$$

Expanding to second order gives the Hamilton function the form[2]

$$H_{\mathcal{Q}} = H + \frac{1}{2}\frac{\partial^2 H}{\partial x^i\partial x^j}\Delta(x^i x^j) + \frac{\partial^2 H}{\partial x^i\partial p_j}\Delta(x^i p_j) + \frac{1}{2}\frac{\partial^2 H}{\partial p_i\partial p_j}\Delta(p_i p_j) + \text{ h.o.t.}\,. \tag{3.51}$$

The first derivatives of the Hamilton function (3.43) (incidentally giving the classical equations of motion) are:

$$\frac{\partial H}{\partial x^i} = E\left(\frac{\partial N}{\partial x^i} + \frac{1}{2}N\frac{\partial\gamma^{kl}}{\partial x^i}\frac{p_k p_l c^2}{E^2} - \frac{\partial N^k}{\partial x^i}\frac{p_k c}{E}\right) \tag{3.52}$$

$$\frac{1}{c}\frac{\partial H}{\partial p_i} = N\gamma^{ik}\frac{p_k c}{E} - N^i \tag{3.53}$$

[2]The sum extends over $i,j=1,2,3$. The factors of $1/2$ appearing in front of the pure spatial and the pure momentum derivatives account for the symmetry of the corresponding moments, while the mixed position-momentum moments are not symmetric under exchange of indices and therefore do not require such a numerical factor.

The second derivatives are:

$$\frac{\partial^2 H}{\partial x^i \partial x^j} = E\left[\frac{\partial^2 N}{\partial x^i \partial x^j} + \frac{1}{2}\left(\frac{\partial N}{\partial x^i}\frac{\partial \gamma^{kl}}{\partial x^j} + \frac{\partial N}{\partial x^j}\frac{\partial \gamma^{kl}}{\partial x^i}\right)\frac{p_k p_l c^2}{E^2} - \frac{N}{4}\frac{\partial \gamma^{kl}}{\partial x^i}\frac{\partial \gamma^{mn}}{\partial x^j}\frac{p_k p_l p_m p_n c^4}{E^4} + \frac{N}{2}\frac{\partial^2 \gamma^{kl}}{\partial x^i \partial x^j}\frac{p_k p_l c^2}{E^2} - \frac{\partial^2 N^k}{\partial x^i \partial x^j}\frac{p_k c}{E}\right] \quad (3.54)$$

$$\frac{1}{c}\frac{\partial^2 H}{\partial x^i \partial p_j} = \frac{\partial N}{\partial x^i}\gamma^{jk}\frac{p_k c}{E} - \frac{N}{2}\gamma^{jk}\frac{\partial \gamma^{mn}}{\partial x^i}\frac{p_k p_m p_n c^3}{E^3} + N\frac{\partial \gamma^{jk}}{\partial x^i}\frac{p_k c}{E} - \frac{\partial N^j}{\partial x^i}\,, \quad (3.55)$$

and

$$\frac{1}{c^2}\frac{\partial^2 H}{\partial p_i \partial p_j} = \frac{1}{E}\left(\gamma^{ij} - N\gamma^{il}\gamma^{jk}\frac{p_l p_k c^2}{E^2}\right). \quad (3.56)$$

Putting these together,

$$\begin{aligned} H_{\mathcal{Q}} = {} & NE - N^i p_i c \\ & + \frac{1}{2}E\left[\frac{\partial^2 N}{\partial x^i \partial x^j} + \frac{1}{2}\left(\frac{\partial N}{\partial x^i}\frac{\partial \gamma^{kl}}{\partial x^j} + \frac{\partial N}{\partial x^j}\frac{\partial \gamma^{kl}}{\partial x^i}\right)\frac{p_k p_l c^2}{E^2} - \frac{N}{4}\frac{\partial \gamma^{kl}}{\partial x^i}\frac{\partial \gamma^{mn}}{\partial x^j}\frac{p_k p_l p_m p_n c^4}{E^4} + \frac{N}{2}\frac{\partial^2 \gamma^{kl}}{\partial x^i \partial x^j}\frac{p_k p_l c^2}{E^2} - \frac{\partial^2 N^k}{\partial x^i \partial x^j}\frac{p_k c}{E}\right]\Delta(x^i x^j) \\ & + \left(\frac{\partial N}{\partial x^i}\gamma^{jk}\frac{p_k c}{E} - \frac{N}{2}\gamma^{jk}\frac{\partial \gamma^{mn}}{\partial x^i}\frac{p_k p_m p_n c^3}{E^3} + N\frac{\partial \gamma^{jk}}{\partial x^i}\frac{p_k c}{E} - \frac{\partial N^j}{\partial x^i}\right)\Delta(x^i p_j)c \\ & + \frac{1}{2}\frac{1}{E}\left(\gamma^{ij} - N\gamma^{il}\gamma^{jk}\frac{p_l p_k c^2}{E^2}\right)\Delta(p_i p_j)c^2\,, \end{aligned} \quad (3.57)$$

where $E(\vec{x}, \vec{p})$ is the function given by Eq. (3.47).

This Hamilton function generates evolution for the basic expectation values $\vec{x}, \vec{p}$ and for the second moments $\Delta^2()$ of a delocalized semiclassical state. The classical term $NE - N^i p_i c$ corresponds to the energy measured by an idealized observer at a sharply localized spacetime event, as in the case of a point particle interacting with a perfectly localized detector. Once quantum corrections are included, however, the measurement becomes intrinsically nonlocal—the particle's spatial profile is no longer sharply defined, and the effective energy includes contributions that depend on the state's spread. When the lapse and shift functions depend explicitly on position, $N = N(\vec{x})$ and $N^i = N^i(\vec{x})$, this nonlocality introduces ambiguity: one can no longer cleanly separate effects due to the observer's frame from those arising from the delocalization of the particle itself.

This ambiguity is closely related to the notion of proper time uncertainty: in the presence of quantum delocalization, the particle no longer follows a single classical trajectory, and the proper time accumulated along its worldline becomes state-dependent. Since the lapse function $N(\vec{x})$ weights the rate of proper time flow relative to coordinate time, variations in $N(\vec{x})$ across the spatial support of the quantum state lead to fluctuations in the accumulated proper time. As a result, the energy measured by the ADM observer, which classically corresponds to the rate of change of proper time along the worldline, now acquires quantum corrections sensitive to the geometry of the slicing and the spread of the state. In this sense, quantum corrections to the energy functional encode an observer-dependent uncertainty in proper time.

As written, the expression (3.57) is organized by moments. It is possible to compress the expression a little bit. The whole expression is a multivariable Taylor series. Individual parts of it have the series expansions

$$\langle N(\hat{\vec{x}})\rangle = N + \frac{1}{2}\Delta\left(x^i x^j\right)\frac{\partial^2 N}{\partial x^i \partial x^j} + O\left(\hbar^{3/2}\right) \tag{3.58}$$

and

$$\langle N^k(\hat{\vec{x}})\rangle = N^k + \frac{1}{2}\Delta\left(x^i x^j\right)\frac{\partial^2 N^k}{\partial x^i \partial x^j} + O\left(\hbar^{3/2}\right) . \tag{3.59}$$

Using this and grouping by inverse powers of E gives

$$\begin{aligned}
\frac{H_{\mathcal{Q}}}{E} &= \langle N(\hat{\vec{x}})\rangle - \langle N^k(\hat{\vec{x}})\rangle\frac{p_k c}{E} - \frac{\partial N^j}{\partial x^i}\frac{\Delta(x^i p_j)c}{E} \\
&\quad + \left[\frac{1}{4}\Delta(x^i x^j)\left(\frac{\partial N}{\partial x^i}\frac{\partial \gamma^{kl}}{\partial x^j} + \frac{\partial N}{\partial x^j}\frac{\partial \gamma^{kl}}{\partial x^i} + N\frac{\partial^2 \gamma^{kl}}{\partial x^i \partial x^j}\right)p_k p_l\right. \\
&\qquad + \frac{\partial}{\partial x^i}\left(N\gamma^{jk}\right)p_k\Delta(x^i p_j) \\
&\qquad\quad \left. + \frac{1}{2}\gamma^{ij}\Delta(p_i p_j)\right]\frac{c^2}{E^2} \\
&\quad - \frac{N}{2}\left[\frac{1}{4}\Delta(x^m x^n)\frac{\partial \gamma^{ij}}{\partial x^m}\frac{\partial \gamma^{kl}}{\partial x^n}p_i p_j p_k p_l\right. \\
&\qquad + \gamma^{kl}\frac{\partial \gamma^{ij}}{\partial x^m}p_i p_j p_k \Delta(x^m p_l) \\
&\qquad\quad \left. + \gamma^{il}\gamma^{jk}p_i p_j \Delta(p_k p_l)\right]\frac{c^4}{E^4}
\end{aligned} \tag{3.60}$$

which is now degree-zero homogeneous in momenta.

This exact effective Hamiltonian for a second-order truncation simplifies in the synchronous gauge, $N = 1$, $N^i = 0$, to

$$\frac{H_{\mathcal{Q}}}{E} = 1 + \left[\frac{1}{4}\Delta(x^i x^j)\frac{\partial^2\gamma^{kl}}{\partial x^i \partial x^j}p_k p_l + \frac{\partial\gamma^{jk}}{\partial x^i}p_k\Delta(x^i p_j) + \frac{1}{2}\gamma^{ij}\Delta(p_i p_j)\right]\frac{c^2}{E^2}$$
$$-\frac{1}{2}\left[\frac{1}{4}\Delta(x^m x^n)\frac{\partial\gamma^{ij}}{\partial x^m}\frac{\partial\gamma^{kl}}{\partial x^n}p_i p_j p_k p_l + \gamma^{kl}\frac{\partial\gamma^{ij}}{\partial x^m}p_i p_j p_k\Delta(x^m p_l) + \gamma^{il}\gamma^{jk}p_i p_j\Delta(p_k p_l)\right]\frac{c^4}{E^4}\,. \tag{3.61}$$

This expression, or its general gauge counterpart, expression (3.57), could be used to study quantum effects on massless particles.

In the nonrelativistic limit, where $\gamma^{ij}p_i p_j \ll (mc)^2$, we can derive approximate expressions for the effective Hamilton function. The energy expands as

$$E \approx mc^2 + \frac{\gamma^{ij}p_i p_j}{2m}\,, \tag{3.62}$$
$$\frac{1}{E} \approx \frac{1}{mc^2} - \frac{\gamma^{ij}p_i p_j c^2}{2m^3c^6} \approx \frac{1}{mc^2}\,, \tag{3.63}$$
$$\frac{1}{E^2} \approx \frac{1}{(mc^2)^2} - \frac{\gamma^{ij}p_i p_j}{m^4c^6} \approx \frac{1}{(mc^2)^2}\,, \tag{3.64}$$
$$\frac{1}{E^3} \approx \frac{1}{(mc^2)^3} - \frac{3\gamma^{ij}p_i p_j}{2m^5c^8} \approx \frac{1}{(mc^2)^3}\,. \tag{3.65}$$

Relativistic corrections to inverse powers of E are suppressed by increasing powers of $1/c^2$. In particular, the term in (3.60) proportional to c^4/E^4 contributes no corrections at leading order in the nonrelativistic expansion. Therefore we find,

$$\begin{aligned} H_{\mathcal{Q}}^{\text{nonrelativistic}} \approx\ & \langle N(\hat{\vec{x}})\rangle\left(mc^2 + \frac{\gamma^{ij}p_i p_j}{2m}\right) - \langle N^k(\hat{\vec{x}})\rangle p_k c - \frac{\partial N^j}{\partial x^i}\Delta(x^i p_j)c \\ &+ \left[\frac{1}{4}\Delta(x^i x^j)\left(\frac{\partial N}{\partial x^i}\frac{\partial\gamma^{kl}}{\partial x^j} + \frac{\partial N}{\partial x^j}\frac{\partial\gamma^{kl}}{\partial x^i} + N\frac{\partial^2\gamma^{kl}}{\partial x^i\partial x^j}\right)p_k p_l \right. \\ &\quad + \frac{\partial}{\partial x^i}\left(N\gamma^{jk}\right)p_k\Delta(x^i p_j) \\ &\quad \left. + \frac{1}{2}\gamma^{ij}\Delta(p_i p_j)\right]\frac{1}{m}\,. \end{aligned} \tag{3.66}$$

In the synchronous gauge $N = 1, N^i = 0$ this simplifies further to

$$H_{\mathcal{Q}}^{\substack{\text{synchronous,}\\ \text{nonrelativistic}}} \approx mc^2 + \frac{\gamma^{ij}p_i p_j}{2m} + \frac{1}{2m}\left(\frac{\Delta(x^k x^l)}{2}\frac{\partial^2\gamma^{ij}}{\partial x^k \partial x^l}p_i p_j + 2\frac{\partial\gamma^{ij}}{\partial x^k}p_i\Delta(x^k p_j) + \gamma^{ij}\Delta(p_i p_j)\right). \tag{3.67}$$

This simplified expression and its implications will be the focus of the remaining studies of this dissertation, in Chapters 4, 5, and 6.

3.6 Extending dynamics to spacetime via gauge embedding

After the considerations of the last sections, we are now in a position where an arbitrary spacetime observer with the worldline (3.45) can, in their local frame Σ_t, use one of the Hamiltonians from Sec. 3.5 to evolve both physical classical degrees of freedom and the semiclassical statistics of a quantum state, with dynamics expressed in their proper time.

The Hamiltonians from Sec. 3.5 have additional terms beyond those of the classical theory. As a result, quantum backreaction on the classical degrees of freedom x^i implies that the spacetime trajectory $(t, x^i(t))$ will generally deviate from the classical prediction. However, while these deviations can be predicted using the theory laid out so far, we cannot yet determine the proper time experienced by the quantum state itself. In the language of Sec. 3.3, doing so requires reversing the phase space reduction—moving from the unconstrained theory governed by the hypersurface Hamiltonian $H_{\mathcal{Q}}$ to the constrained spacetime theory governed by $\mathrm{H}_{\mathcal{Q}}$. We construct $\mathrm{H}_{\mathcal{Q}}$ in Eq. (3.84).

For clarity, we begin by demonstrating this lifting procedure in the classical setting where we are familiar with all of the ingredients and the result.

3.6.1 Parametrization of the classical theory

When starting from the reduced theory governed by an unconstrained Hamiltonian $H(\vec{x}, \vec{p})$, a specific time coordinate t—typically the proper time of a chosen observer—has already been selected. As a result, the theory is no longer reparametrization-invariant: evolution $x^i(0) \mapsto x^i(t)$ is explicitly tied to a particular foliation or reference frame. To restore reparametrization invariance, we enlarge the phase space by reintroducing the canonical pair (x^0, p_0), which had been fixed in the reduced formulation, and then reinstate gauge symmetry.

Since H generates time translations with respect to a fixed observer frame, we promote

this evolution to a gauge symmetry by imposing the first-class constraint

$$\phi(x^a, p_a) = p_0 + \frac{1}{c} H(\vec{x}, \vec{p}) = 0\,. \tag{3.68}$$

This constraint generates gauge transformations in the extended phase space, with the gauge parameter identified as the worldline parameter σ. The resulting reparametrizations transform the initial data

$$\left(x^0(0), x^i\left(x^0(0)\right)\right) \mapsto \left(x^0(\sigma), x^i\left(x^0(\sigma)\right)\right) = \left(x^0(\sigma), x^i(\sigma)\right) =: x^a(\sigma)\,. \tag{3.69}$$

On the constraint surface $\phi = 0$, the gauge flow generated by ϕ coincides—by definition—with (minus) the physical evolution generated by H. Since rescaling the constraint ϕ does not alter the constraint surface itself, the associated gauge parameter can be freely reparameterized. This reparametrization freedom is made explicit by introducing the einbein $e(\sigma)$, leading to the rescaled constraint

$$\phi(x^a, p_a; e, p_e) = -e\left(p_0 + \frac{1}{c} H(\vec{x}, \vec{p})\right) = 0\,. \tag{3.70}$$

By imposing this constraint $\phi = 0$, rather than fixing the time coordinate x^0, we recover a reparametrization-invariant formulation in which physical trajectories lie on the constraint surface and correspond to gauge orbits under the Hamiltonian flow generated by ϕ.

3.6.2 Regaining covariance of the classical theory

Although the constraint $\phi = 0$ restores reparametrization invariance, it does not recover the full observer covariance of the original relativistic theory. In particular, the original theory possessed an additional symmetry under the exchange of particle and antiparticle sectors—or equivalently, under time reversal. To recover the fully covariant, quadratic Hamiltonian constraint, this symmetry must be reinstated by explicitly including the negative-energy (antiparticle) branch. Specifically, the two linear constraints,

$$\phi_- \coloneqq p_0 - N\sqrt{\gamma^{ij} p_i p_j + m^2 c^2} - N^i p_i \;=\; 0 \tag{3.71}$$

$$\phi_+ \coloneqq p_0 + N\sqrt{\gamma^{ij} p_i p_j + m^2 c^2} - N^i p_i \;=\; 0 \tag{3.72}$$

are multiplied, resulting (after division by $-N^2$) in the familiar quadratic Hamiltonian constraint of the covariant theory

$$\mathrm{H} \coloneqq \phi_-\phi_+ = -\frac{p_0^2}{N^2} + 2\frac{N^i}{N^2}p_0p_i + \left(\gamma^{ij} - \frac{N^iN^j}{N^2}\right)p_ip_j + m^2c^2 = 0\,. \tag{3.73}$$

This constraint is quadratic in the momenta and admits a pseudo-Riemannian interpretation, typically expressed by introducing the bilinear form g^{ab}, defined in Eq. (3.39), so that

$$\mathrm{H}(x^a, p_b) = g^{ab}(x)p_ap_b + m^2c^2 = 0\,. \tag{3.74}$$

This puts the theory back into the fully covariant (spacetime) form, where time evolution is a gauge redundancy, and physical observables must be reparametrization-invariant.

Analogous to the rescaled linear constraint in Eq. (3.70), we may introduce the einbein to explicitly control reparametrization freedom, yielding the constraint

$$\mathrm{H}(x^a, p_b) = -\frac{e}{2}\left(g^{ab}(x)p_ap_b + m^2c^2\right) = 0\,, \tag{3.75}$$

which is the exact form of the constraint from the first-order action in Eq. (3.17). Fixing the new gauge by setting $e = 1/m$, we obtain the proper-time gauge form

$$\mathrm{H}(x^a, p_b) = -\frac{1}{2m}\left(g^{ab}(x)p_ap_b + m^2c^2\right) = 0\,. \tag{3.76}$$

This expression satisfies the identity

$$1 + \frac{2\mathrm{H}}{mc^2} = -\frac{1}{c^2}\frac{g^{ab}(x)p_ap_b}{m^2}\,, \tag{3.77}$$

which allows us to recover the original form of the proper-time functional

$$\tau = \int\sqrt{1 + \frac{2\mathrm{H}}{mc^2}}\,\mathrm{d}\tau = \int\sqrt{-\frac{1}{c^2}\frac{g^{ab}(x)p_ap_b}{m^2}}\,\mathrm{d}\tau\,. \tag{3.78}$$

That the parameter τ on the right-hand-side indeed measures proper time follows by substituting the constraint $\mathrm{H} = 0$ into the first form of the expression.

The proper-time functional Eq. (3.78) defines a norm on the cotangent space at each

spacetime point, given by

$$\tilde{F}\left(x, \frac{p}{m}\right) \coloneqq \sqrt{-\frac{1}{c^2}\frac{g^{ab}(x)p_a p_b}{m^2}}\,. \tag{3.79}$$

The subgroup of general linear transformations on the cotangent space $\mathbb{R}^4$ that preserve this norm consists precisely of Lorentz transformations. These act on covectors as $p_a \mapsto (\Lambda^{-1})^b{}_a\, p_b$, preserving the quadratic form defined by the metric $g^{ab}(x)$.

3.6.3 Parametrization of the semiclassical quantum theory

Reparametrization invariance can be recovered in the quantum theory by enlarging the quantum phase space using the same procedure as in the classical case. However, the resulting expressions contain additional terms that make the formalism considerably more involved.

In place of the unconstrained Hamilton function $H(\vec{x}, \vec{p})$, canonical quantization formulated in terms of moments on quantum phase space gave $H_{\mathcal{Q}}(\vec{x}, \vec{p}, \Delta^2())$ as Eq. (3.57). Keeping track of the sign of the energy, we can introduce the gauge variable $p_0 = -H_{\mathcal{Q}}/c$ and write the first-class particle and antiparticle constraints

$$p_0 - \langle N(\hat{\vec{x}})\rangle\frac{E}{c} - \langle N^i(\hat{\vec{x}})\rangle p_i - \frac{\partial N^i}{\partial x^j}\Delta(x^j p_i) - A\frac{c}{E} + B\frac{N}{2}\frac{c^3}{E^3} = 0 \tag{3.80}$$

$$p_0 + \langle N(\hat{\vec{x}})\rangle\frac{E}{c} - \langle N^i(\hat{\vec{x}})\rangle p_i - \frac{\partial N^i}{\partial x^j}\Delta(x^j p_i) + A\frac{c}{E} - B\frac{N}{2}\frac{c^3}{E^3} = 0 \tag{3.81}$$

where

$$\begin{aligned} A &= \frac{1}{4}\Delta(x^k x^l)\left(\frac{\partial N}{\partial x^k}\frac{\partial \gamma^{ij}}{\partial x^l} + \frac{\partial N}{\partial x^l}\frac{\partial \gamma^{ij}}{\partial x^k} + N\frac{\partial^2 \gamma^{ij}}{\partial x^k \partial x^l}\right)p_i p_j \\ &\quad + \frac{\partial}{\partial x^k}\left(N\gamma^{ij}\right)p_i\Delta(x^k p_j) + \frac{1}{2}\gamma^{ij}\Delta(p_i p_j)\,, \end{aligned} \tag{3.82}$$

and

$$B = \frac{1}{4}\Delta(x^m x^n)\frac{\partial \gamma^{ij}}{\partial x^m}\frac{\partial \gamma^{kl}}{\partial x^n}p_i p_j p_k p_l + \gamma^{kl}\frac{\partial \gamma^{ij}}{\partial x^m}p_i p_j p_k \Delta(x^m p_l) + \gamma^{il}\gamma^{jk}p_i p_j \Delta(p_k p_l). \tag{3.83}$$

Multiplying the two linear constraints (and dividing by $-\langle N(\hat{\vec{x}})\rangle^2$) gives the Hamiltonian

constraint

$$\begin{aligned}\mathrm{H}_{\mathcal{Q}}(x^0,\vec{x},p_0,\vec{p},\Delta^2()) &= -\frac{p_0^2}{\langle N\rangle^2}+2\frac{1}{\langle N\rangle^2}\left(\langle N^i\rangle p_i+\frac{\partial N^i}{\partial x^j}\Delta(x^j p_i)\right)p_0 \\ &+ \gamma^{ij}p_ip_j-\left(\frac{\langle N^i\rangle}{\langle N\rangle}p_i+\frac{1}{\langle N\rangle}\frac{\partial N^i}{\partial x^j}\Delta(x^j p_i)\right)^2+m^2c^2 \\ &+ 2\frac{A}{\langle N\rangle}-\frac{N}{\langle N\rangle}\frac{c^2B}{E^2}+\frac{c^2A^2}{\langle N\rangle^2E^2}-\frac{N}{\langle N\rangle}\frac{c^4AB}{\langle N\rangle E^4}+\frac{N^2}{\langle N\rangle^2}\frac{c^6B^2}{4E^6}=0\,.\end{aligned} \tag{3.84}$$

However, this constraint involves products of second-order moments $\Delta^2()\Delta^2()$. To the order of our truncation these terms should be set to zero. The resulting expression, though lengthy, can be written explicitly as

$$\begin{aligned}\mathrm{H}_{\mathcal{Q}}(x^0,\vec{x},p_0,\vec{p},\Delta^2()) &= -\frac{p_0^2}{N^2}+2\frac{N^i}{N^2}p_ip_0+\left(\gamma^{ij}-\frac{N^iN^j}{N^2}\right)p_ip_j+m^2c^2 \\ &+\frac{\Delta(x^kx^l)}{N^3}\frac{\partial^2N}{\partial x^k\partial x^l}\,p_0^2 \\ &+\frac{\Delta(x^kx^l)}{N^2}\left(\frac{\partial^2N^i}{\partial x^k\partial x^l}-2\frac{\partial^2N}{\partial x^k\partial x^l}\frac{N^i}{N}\right)p_ip_0+\frac{2}{N^2}\frac{\partial N^i}{\partial x^j}\Delta(x^jp_i)p_0 \\ &+\frac{\Delta(x^kx^l)}{N}\left(\frac{\partial^2N}{\partial x^k\partial x^l}\frac{N^iN^j}{N^2}-\frac{\partial^2N^i}{\partial x^k\partial x^l}\frac{N^j}{N}\right)p_ip_j-\frac{2}{N}\frac{\partial N^i}{\partial x^j}\frac{N^j}{N}\Delta(x^jp_i)p_j \\ &+\frac{\Delta(x^kx^l)}{2N}\left(\frac{\partial N}{\partial x^k}\frac{\partial\gamma^{ij}}{\partial x^l}+\frac{\partial N}{\partial x^l}\frac{\partial\gamma^{ij}}{\partial x^k}+N\frac{\partial^2\gamma^{ij}}{\partial x^k\partial x^l}\right)p_ip_j+\frac{2}{N}\frac{\partial}{\partial x^k}\left(N\gamma^{ij}\right)p_i\Delta(x^kp_j)+\frac{\gamma^{ij}}{N}\Delta(p_ip_j) \\ &-\frac{1}{\gamma^{ij}(\vec{x})p_ip_j+m^2c^2}\left(\frac{1}{4}\Delta(x^mx^n)\frac{\partial\gamma^{ij}}{\partial x^m}\frac{\partial\gamma^{kl}}{\partial x^n}p_ip_jp_kp_l+\gamma^{kl}\frac{\partial\gamma^{ij}}{\partial x^m}p_ip_jp_k\Delta(x^mp_l)+\gamma^{il}\gamma^{jk}p_ip_j\Delta(p_kp_l)\right).\end{aligned} \tag{3.85}$$

This expression is remarkably general: it governs simultaneously the evolution of classical expectation values and second-order statistical moments of a quantum state in an arbitrary spacetime. Its derivation rests on a sequence of well-motivated steps: we begin with the classical Hamiltonian governing the evolution of expectation values, apply conventional canonical quantization to the unconstrained physical degrees of freedom, reformulate the resulting quantum theory using an exact—though unfamiliar—set of alternative variables, truncate this formulation at second order for practical tractability, and finally lift the theory back into a covariant spacetime framework.

As a second-order derivative expansion of the classical constraint, and owing to the nature of derivatives under the Leibniz rule, the quantum constraint naturally contains a multiplication of terms. And although this constraint remains homogeneous of degree-two in the momenta, it is no longer quadratic. As a result, it cannot be expressed in terms of

a bilinear form, and the extension of the particle theory to include quantum degrees of freedom appears to lack a pseudo-Riemannian structure. Nonetheless, $\mathrm{H}_{\mathcal{Q}}$ still defines a reparametrization-invariant theory—only now the familiar quadratic geometry must be replaced by a generalized degree-two structure: Finsler geometry.

The norm defined by $\mathrm{H}_{\mathcal{Q}}$ acts on an enlarged cotangent space that includes additional quantum coordinates. The identity of this tangent space is obscured by our use so far of noncanonical coordinates. In particular, it is not immediately clear whether momentum (co)variances $\Delta(p_i p_j)$ can be considered quadratic in a new momentum, or whether the mixed covariances $\Delta(x^k p_j)$ correspond to linear quantum momenta. Canonical quantum coordinates can be identified through canonical transformations of the moments, such as those constructed in Sec. 2.5. The linear symmetry group acting on this extended cotangent space and preserving the quantum-corrected norm is not currently known. An initial exploration of the symmetries associated with the quantum moments is presented in Appendix A.

Special cases—such as restricting the number of quantized degrees of freedom, working in a synchronous classical frame, or taking the nonrelativistic limit—can simplify the analysis significantly. These cases lead to tractable models that still capture essential features of the quantum-corrected geometry. The resulting structures define new types of Finsler geometry, which will be the focus of the next chapter.

Chapter 4
Finsler geometry of quantum phase space

"Where is the library?"

"Turn right, proceed thirty-four paces, turn right again, twelve paces, then through door on the right, thirty-five paces, through archway on right another eleven paces, turn right one last time, fifteen paces, enter the door on the right."

Mappo stared at Iskaral Pust.

The High Priest shifted nervously.

"Or," the Trell said, eyes narrowed, "turn left, nineteen paces."

"Aye," Iskaral muttered.

—Steven Erikson
Deadhouse Gates

A quantum clock cannot be modeled as a point mass moving along a single spacetime geodesic if it is in a state with nonzero position fluctuations. Instead, it is an extended object subject to tidal forces and a superposition of time dilations at different altitudes. Here, a geometrical formulation of quantum mechanics is used to show that additional quantum properties representing correlations between different directions can be introduced to realize generalized notion of geodesic motion. This motion takes place in an enlarged spacetime carrying a non-Riemannian geometrical structure. A specific version of Finsler geometry parameterized by entropy and purity of the state provides a novel setting for a combination of quantum and gravitational effects.

4.1 Pseudo-Riemannian structure for a single degree of freedom

In a synchronous gauge of the metric—where the lapse and shift are fixed to $N = 1$, $N^i = 0$—and in the nonrelativistic limit, the quantum Hamiltonian constraint $\mathrm{H}_{\mathcal{Q}}$ defined in Eq. (3.85), truncated to leading order in $\hbar$, takes the form

$$\begin{aligned}\mathrm{H}_{\mathcal{Q}}(x^0, \vec{x}, p_0, \vec{p}, \Delta^2()) &= -\frac{1}{2m}\Big(- p_0^2 + \gamma^{ij} p_i p_j + m^2 c^2 \\ &\quad + \frac{\Delta(x^k x^l)}{2} \frac{\partial^2 \gamma^{ij}}{\partial x^k \partial x^l} p_i p_j + 2 \frac{\partial \gamma^{ij}}{\partial x^k} p_i \Delta(x^k p_j) + \gamma^{ij} \Delta(p_i p_j) \Big) . \end{aligned} \tag{4.1}$$

If we consider only quantized motion along the x-direction (or the radial direction in a spherical coordinate system), we can apply the one-dimensional canonical mapping (2.44) to express the (massive-particle, nonrelativistic, synchronous-frame) geodesic quantum Hamiltonian defined in Eq. (3.67) in terms of momenta as

$$\begin{aligned}\mathrm{H}_{\mathcal{Q}}(x^0, \vec{x}, p_0, \vec{p}, \Delta^2()) &= -\frac{1}{2m}\Big(- p_0^2 + \gamma^{ij} p_i p_j + m^2 c^2 \\ &\quad + \frac{s^2}{2} \frac{\partial^2 \gamma^{ij}}{\partial x^2} p_i p_j + 2 \frac{\partial \gamma^{ix}}{\partial x} s p_i p_s + \gamma^{xx} \left(p_s^2 + \frac{\hbar^2}{4 s^2} p_q^2 \right) \Big) . \end{aligned} \tag{4.2}$$

This expression is strictly quadratic in momentum components, which now include p_s and p_q. Quantum corrections can therefore be expressed by a six-dimensional metric

$$g_{\mathcal{Q}}^{\bar{i}\bar{j}} := \begin{pmatrix} -1 & 0 & 0 & 0 & 0 & 0 \\ 0 & \gamma^{xx} + \frac{1}{2} s^2 \partial_x^2 \gamma^{xx} & \gamma^{yx} + \frac{1}{2} s^2 \partial_x^2 \gamma^{yx} & \gamma^{zx} + \frac{1}{2} s^2 \partial_x^2 \gamma^{zx} & s \partial_x \gamma^{xx} & 0 \\ 0 & \gamma^{xy} + \frac{1}{2} s^2 \partial_x^2 \gamma^{xy} & \gamma^{yy} + \frac{1}{2} s^2 \partial_x^2 \gamma^{yy} & \gamma^{zy} + \frac{1}{2} s^2 \partial_x^2 \gamma^{zy} & s \partial_x \gamma^{yx} & 0 \\ 0 & \gamma^{xz} + \frac{1}{2} s^2 \partial_x^2 \gamma^{xz} & \gamma^{yz} + \frac{1}{2} s^2 \partial_x^2 \gamma^{yz} & \gamma^{zz} + \frac{1}{2} s^2 \partial_x^2 \gamma^{zz} & s \partial_x \gamma^{zx} & 0 \\ 0 & s \partial_x \gamma^{xx} & s \partial_x \gamma^{yx} & s \partial_x \gamma^{zx} & \gamma^{xx} & 0 \\ 0 & 0 & 0 & 0 & 0 & \frac{1}{4} \hbar^2 \gamma^{xx} / s^2 \end{pmatrix} . \tag{4.3}$$

such that

$$H_{\mathcal{Q}}(x, y, z, s, q, p_x, p_y, p_z, p_s, p_q) = -\frac{1}{2m} \left(g_{\mathcal{Q}}^{\bar{i}\bar{j}} p_{\bar{i}} p_{\bar{j}} + m^2 c^2 \right) . \tag{4.4}$$

with an extended $p_{\bar{i}} = (p_t, p_x, p_y, p_z, p_s, p_q)$.

The block structure of the metric arises from our choice of synchronous gauge. The modified spatial Riemannian metric appearing in this formulation corresponds to a truncated Taylor expansion of the underlying classical metric coefficients, evaluated in

the quantum state

$$\langle\gamma^{ij}(\hat{x})\rangle = \left\langle \exp\left[(\hat{x}-\langle\hat{x}\rangle)\,\frac{\mathrm{d}}{\mathrm{d}\hat{x}}\right]\right\rangle \gamma^{ij}(\langle\hat{x}\rangle) = \left(1+\frac{1}{2}\Delta(x^2)\partial_x^2\right)\gamma^{ij}(x)+O(\hbar^{3/2}). \quad (4.5)$$

This series expansion of the metric is analogous to the expansion (3.50) for $H(\hat{x})$. With this consideration we have

$$\gamma_{\mathcal{Q}}^{\bar{i}\bar{j}} = \begin{pmatrix} \langle\gamma^{ij}(\hat{x})\rangle & s\partial_x\gamma^{ix} & 0 \\ s\partial_x\gamma^{xj} & \gamma^{xx} & 0 \\ 0 & 0 & \frac{1}{4}\hbar^2\gamma^{xx}/s^2 \end{pmatrix}. \quad (4.6)$$

This formula defines an effective metric $\gamma_{\mathcal{Q}}^{\bar{i}\bar{j}}$ governing the free motion of a quantum test particle on a curved background. The block corresponding to the classical physical degrees of freedom consists of the expectation values of the components of the classical inverse spatial metric, evaluated in the quantum state of the particle. As a result, rather than interacting directly with the classical background, the quantum particle experiences a smoothed, state-dependent effective geometry. Furthermore, unlike a classical point particle, a quantum object possesses additional internal structure. In the present formulation, Eq. (4.6) incorporates these features by introducing a spatial fluctuation coordinate s, representing the width of the wave packet, along with its uncertainty coordinate q, which encodes residual quantum information beyond leading-order expectation values.

For the purposes of computing proper time, because this simplified case remains quadratic, we may immediately generalize the Riemannian expression in Eq. (3.78). Moreover, for a quadratic Hamiltonian, the inverse Legendre transform is well defined and in fact yields a quadratic quantum Lagrangian which can be organized by defining the quantum-effective metric as the inverse of the Hamilton quadratic form

$$g^{\mathcal{Q}}_{\bar{a}\bar{b}} := \left(g_{\mathcal{Q}}^{\bar{a}\bar{b}}\right)^{-1}. \quad (4.7)$$

Thus we would obtain

$$\mathrm{L}_{\mathcal{Q}} = -\frac{1}{2}mg^{\mathcal{Q}}_{\bar{a}\bar{b}}\dot{x}^{\bar{a}}\dot{x}^{\bar{b}} + \frac{mc^2}{2}. \quad (4.8)$$

For small moments in the semiclassical approximation, the quantum metric could be inverted perturbatively, such that

$$g^{\mathcal{Q}}_{\bar{a}\bar{b}}\dot{x}^{\bar{a}}\dot{x}^{\bar{b}} = g_{ab}\dot{x}^a\dot{x}^b + O(\Delta^2(\cdot)) \quad (4.9)$$

where $\Delta^2(\cdot)$ stands for any expression of homogeneity degree two in the quantum variables, s, $\dot{s}$, $\dot{q}$ as well as $\sqrt{\hbar}$.

The Lagrangian equations would then be obtained as the stationary solutions to a reparametrization-invariant quantum proper time path functional

$$\tau_{\mathcal{Q}} := \int \sqrt{-\frac{1}{c^2} g^{\mathcal{Q}}_{\bar{a}\bar{b}} \mathrm{d}x^{\bar{a}} \mathrm{d}x^{\bar{b}}} \,. \tag{4.10}$$

Here, the quantum-effective metric defines an effective line element[1]

$$\mathrm{d}s^2 = g^{\mathcal{Q}}_{\bar{a}\bar{b}}(x, s) \mathrm{d}x^{\bar{a}} \mathrm{d}x^{\bar{b}} \tag{4.11}$$

On the part of the quantum phase space where quantum states obey the semiclassical hierarchy condition, Eq. (2.35), the quantum Lagrange function splits into classical and nonclassical contributions. In such cases, the quantum proper time obtains dominant contributions from motion through the classical geometry with subdominant contributions from quantum effects

$$\begin{aligned} \tau_{\mathcal{Q}} &= \int - \left(\frac{2}{mc^2} \mathrm{L}_{\mathcal{Q}} + 1 \right) \mathrm{d}\sigma \\ &= \int \left(- \frac{2}{mc^2} \left(\mathrm{L}_{\text{classical}} + \mathrm{L}_{\text{nonclassical}} \right) - 1 \right) \mathrm{d}\sigma \\ &= \tau_{\text{classical}} + \tau_{\text{nonclassical}}. \end{aligned} \tag{4.12}$$

The additive nature of this expression is implied by the general semiclassical result (4.9) for the metric. This integral is evaluated over a quantum-corrected radial geodesic in the Schwarzschild geometry in Sec. 5.1.

4.2 The two-mode spacetime Finsler Hamiltonian

For single-mode dynamics, the canonical realization of the moment algebra, Eq. (2.45), yields a geodesic Hamiltonian that is quadratic in the newly-introduced momentum coordinates. In this case, the effective inverse metric Eq. (4.6) extends the Riemannian structure of the classical theory over the lowest semiclassical order of the effective spacetime theory.

[1]It is interesting to ask whether this quantum effective metric obeys an extended covariance condition with a higher-dimensional tensor transformation law that leaves the effective line element invariant. We leave this as an open question, but note that recent work on quantum reference frames, as mentioned in our Discussion section 6.5 suggests that this task may be challenging.

As shown in [21, 41], the quadratic dependence on momenta remains intact when extending moments of a single classical degree of freedom (x, p) up to at least fourth order, such as $\Delta(x^4)$. The pseudo-Riemannian structure of the classical theory then seems to be a generic feature of the effective theory of single-mode dynamics. However, according to the same papers, this property no longer holds when two independent classical degrees of freedom, (x, p_x) and (y, p_y), are quantized. In this section, we use a canonical realization of the Poisson algebra of two-mode second moments to address the canonical structure of an effective two-mode theory. Unlike single-mode systems, two-mode (or more generally, bipartite) systems inherently involve entanglement entropy, making entropy measures an essential aspect of their description.

The canonical mapping defined by Eqs. (2.59)–(2.68) enlarges the cotangent space from the three-dimensional space spanned by the momentum covector $p_i = (p_x, p_y, p_z)$ to the nine-dimensional space $V^* \cong \mathbb{R}^9$ spanned by the extended momentum covector

$$p_{\bar{a}} = (p_x, p_y, p_z, p_{s_x}, p_{s_y}, p_\alpha, p_\beta, C_1, C_2). \tag{4.13}$$

When needed, we denote the basis of the tangent space V by $e_{\bar{a}}$ and the dual basis of V^* by $\vartheta^{\bar{a}}$ where the $\bar{a}$ runs from 1 to 9 in both cases. As usual, these satisfy the duality condition

$$e_{\bar{a}}(\vartheta^{\bar{b}}) = \vartheta^{\bar{b}}(e_{\bar{a}}) = \delta^{\bar{b}}_{\bar{a}}\,. \tag{4.14}$$

Substituting the canonical mapping into the quantum geodesic Hamiltonian, Eq. (3.67), yields a function of canonical variables that is not quadratic in the momenta. Instead, due to the Finsler root $\sqrt{P}$, the Hamiltonian takes the form of a generalized 4-th root Finsler Hamiltonian

$$H_{\mathcal{Q}} = \frac{1}{2m}\left(\sqrt{A^{\bar{a}\bar{b}\bar{c}\bar{d}}p_{\bar{a}}p_{\bar{b}}p_{\bar{c}}p_{\bar{d}}} + B^{\bar{a}\bar{b}}p_{\bar{a}}p_{\bar{b}} + 2m^2c^2\right). \tag{4.15}$$

Even though this no longer induces a Riemannian structure on the quantum space, the degree-two homogeneity in the momenta implies that geometric notions including connection, parallel transport, and geodesic still exist; see for instance [46, 47]. We can provide explicit expressions for both $A^{\bar{a}\bar{b}\bar{c}\bar{d}}$ and $B^{\bar{a}\bar{b}}$ using the canonical mapping.

4.2.1 The covariant rank-four tensor $A^{\bar{a}\bar{b}\bar{c}\bar{d}}$

We begin with the covariant rank-four tensor $A^{\bar{a}\bar{b}\bar{c}\bar{d}}$, which is fully symmetric, and define its complete contraction with momentum covectors as[2]

$$A \coloneqq A^{\bar{a}\bar{b}\bar{c}\bar{d}} p_{\bar{a}} p_{\bar{b}} p_{\bar{c}} p_{\bar{d}}. \tag{4.18}$$

This nonquadratic contribution to $H_{\mathcal{Q}}$ arises from the term $\gamma^{ij}\Delta(p_i p_j)$, since the momentum-momentum covariance matrix $\Delta(p_i p_j)$ contains the square root $\sqrt{P}$. Isolating this contribution defines the kernel

$$K_{ij}(s_x, s_y, \alpha, \beta) = \csc^2(\beta) \begin{pmatrix} -\sin(\alpha+\beta)/s_x^2 & \sin(\alpha)/(s_x s_y) \\ \sin(\alpha)/(s_x s_y) & -\sin(\alpha-\beta)/s_y^2 \end{pmatrix}. \tag{4.19}$$

Using this kernel, the fully-contracted quartic part of the Finsler Hamiltonian takes the form

$$\sqrt{A} = \frac{1}{2} K_{ij}\gamma^{ij}\sqrt{P}\,. \tag{4.20}$$

The sign of this term is determined by the trace of the contraction of the kernel K_{ij} with the inverse metric,

$$\frac{1}{2} K_{ij}\gamma^{ij} = -\frac{\sin(\alpha+\beta)\gamma^{xx}}{2s_x^2} + \frac{\sin(\alpha)\gamma^{xy}}{s_x s_y} - \frac{\sin(\alpha-\beta)\gamma^{yy}}{2s_y^2}. \tag{4.21}$$

4.2.2 The bilinear form $B^{\bar{a}\bar{b}}$

The symmetric bilinear form $B^{\bar{a}\bar{b}}\colon V^* \times V^* \to \mathbb{R}$ is an extension of the single-variable expression (4.6). In the basis $e_{\bar{a}}$, the coefficients of $B^{\bar{a}\bar{b}}$ may be arranged in the block

[2]Similarly, we can define the complete momentum contraction of the symmetric rank-two tensor as

$$B \coloneqq B^{\bar{a}\bar{b}} p_{\bar{a}} p_{\bar{b}}. \tag{4.16}$$

In terms of these quantities, we have

$$H_{\mathcal{Q}} = \frac{1}{2m}\left(\sqrt{A} + B + 2m^2c^2\right), \tag{4.17}$$

which is the form seen in standard Finsler literature such as Ref. [48]'s eq. (2.1.9).

matrix[3]

$$B^{\bar{a}\bar{b}} = \begin{pmatrix} \langle\gamma^{ij}(\hat{x},\hat{y})\rangle & D[g^{iJ}] & E & 0 & 0 \\ D[g^{Ij}] & \tilde{g}^{IJ} & C & 0 & 0 \\ E^T & C^T & \Theta & 0 & 0 \\ 0 & 0 & 0 & \frac{1}{2}\mathrm{Tr}\,(\Sigma_x^{-1}\gamma^{-1}) & 0 \\ 0 & 0 & 0 & 0 & 0 \end{pmatrix}. \tag{4.22}$$

In this expression, i and j are ordinary spatial indices taking the values x, y, z, while I and J denote indices that correspond to the quantized modes, x or y. We expect that this somewhat awkward notation could be improved in a full quantum treatment of all three spatial directions where both indices range over $\{1, 2, 3\}$. However, since we are free to interpret the degrees of freedom as modes rather than strictly in terms of spatial directions, this type of index notation is likely unavoidable in general.

The component-wise expectation value of the metric is now a two-variable Taylor series with

$$\langle\gamma^{ij}(\hat{x},\hat{y})\rangle = \left(1 + \frac{1}{2}\left(s_x^2\partial_x^2 + 2s_x s_y\cos(\beta)\partial_{xy}^2 + s_y^2\partial_y^2\right)\right)\gamma^{ij}(x,y) + O(\hbar^{3/2}) \tag{4.23}$$

$$= \left(1 + \frac{1}{2}\left(\Delta(x^2)\partial_x^2 + 2\Delta(xy)\partial_{xy}^2 + \Delta(y^2)\partial_y^2\right)\right)\gamma^{ij}(x,y) + O(\hbar^{3/2}) \tag{4.24}$$

which represents the same state-averaging of spacetime as in the one degree of freedom case.

The 2×4 block $D[\gamma^{Ij}]$ defined for $I = 1, 2$ and $j = x, y, z$ is

$$D[\gamma^{Ij}] = \begin{pmatrix} (s_x\partial_x + s_y\cos(\beta)\partial_y)\gamma^{xj} \\ (s_y\partial_y + s_x\cos(\beta)\partial_x)\gamma^{yj} \end{pmatrix}. \tag{4.25}$$

This block is a generalization of the corresponding expression in one degree of freedom. When the inverse metric components γ^{ij} vary along a classical coordinate direction, this expression couples spatial momenta p_i to fluctuation momenta p_{s_I}. In other words, nonzero coefficients in $D[\gamma^{Ij}]$ indicate that the cotangent vectors associated with classical momenta and fluctuation momenta are not orthogonal.

The 2×2 block $\tilde{\gamma}^{IJ}$ defined for $I, J = 1, 2$ specifies the metric coupling of the

[3]Note that this expression does not define an invertible matrix and therefore does not constitute an inverse metric. As we will show below, the Finsler analog of γ^{ij} receives contributions from B as well as A and is invertible.

fluctuation momenta subspace

$$\tilde{\gamma}^{IJ} = \begin{pmatrix} \gamma^{xx} & \cos(\beta)\gamma^{xy} \\ \cos(\beta)\gamma^{xy} & \gamma^{yy} \end{pmatrix}. \tag{4.26}$$

The determinant of $\tilde{\gamma}^{IJ}$ is

$$\det(\tilde{\gamma}^{IJ}) = \gamma^{xx}\gamma^{yy} - \cos^2(\beta)(\gamma^{xy})^2, \tag{4.27}$$

indicating that the shape of the metric ellipsoid for the quantum correlations s_x, s_y differs from that of the classical coordinates x and y when $\Delta(xy) \neq 0$.

4.2.3 Fluctuation subspace trace terms

In the (xp) ordering defined by $\xi^i = (x, y, p_x, p_y)$, the covariance matrix $\Delta(\xi^i\xi^j)$ is rewritten as

$$\Sigma = \begin{pmatrix} \Sigma_x & \Sigma_{xp} \\ \Sigma_{xp}^\top & \Sigma_p \end{pmatrix} \tag{4.28}$$

so that we have position-position, position-momentum, and momentum-momentum covariance matrices

$$\Sigma_x = \begin{pmatrix} \Delta(x^2) & \Delta(xy) \\ \Delta(xy) & \Delta(y^2) \end{pmatrix}, \quad \Sigma_{xp} = \begin{pmatrix} \Delta(xp_x) & \Delta(xp_y) \\ \Delta(p_x y) & \Delta(yp_y) \end{pmatrix}, \quad \Sigma_p = \begin{pmatrix} \Delta(p_x^2) & \Delta(p_x p_y) \\ \Delta(p_x p_y) & \Delta(p_y^2) \end{pmatrix}. \tag{4.29}$$

The quadratic Casimir of the two-mode mapping, C_1^2, generalizes the quadratic Casimir of the single mode mapping, U. In Eq. (4.22), the inverse metric component acting in the $e_{C_1} \otimes e_{C_1}$ subspace equals half the trace of the inverse metric against the inverse position-covariance matrix

$$\mathrm{Tr}\left(\Sigma_x^{-1}\gamma^{-1}\right) = \csc^2(\beta)\left(\frac{\gamma^{xx}}{s_x^2} + \frac{\gamma^{yy}}{s_y^2} - \frac{2\cos(\beta)\gamma^{xy}}{s_x s_y}\right). \tag{4.30}$$

The matrix $B^{\bar{a}\bar{b}}$ is noninvertible because C_2 appears only in the quartic part. Physically however, it is the fundamental inverse tensor

$$\gamma_{\mathcal{Q}}^{\bar{a}\bar{b}}(x,p) := m\frac{\partial^2 H_{\mathcal{Q}}}{\partial p_{\bar{a}}\partial p_{\bar{b}}} \tag{4.31}$$

which determines meaningful geometric quantities. For the generalized quartic this is

$$\gamma_{\mathcal{Q}}^{\bar{a}\bar{b}} = B^{\bar{a}\bar{b}} + 3A^{\bar{a}\bar{b}} - 2A^{\bar{a}}A^{\bar{b}}, \tag{4.32}$$

where we have used normalized partial contractions $A^{\bar{a}}$, $A^{\bar{a}\bar{b}}$, and $A^{\bar{a}\bar{b}\bar{c}}$ defined through the relations

$$A^{3/4}A^{\bar{a}} = A^{\bar{a}\bar{b}\bar{c}\bar{d}}p_{\bar{b}}p_{\bar{c}}p_{\bar{d}}\,, \tag{4.33}$$

$$A^{1/2}A^{\bar{a}\bar{b}} = A^{\bar{a}\bar{b}\bar{c}\bar{d}}p_{\bar{c}}p_{\bar{d}}\,, \tag{4.34}$$

$$A^{1/4}A^{\bar{a}\bar{b}\bar{c}} = A^{\bar{a}\bar{b}\bar{c}\bar{d}}p_{\bar{d}}\,. \tag{4.35}$$

The expression $\gamma_{\mathcal{Q}}^{\bar{a}\bar{b}}$ computed this way is invertible.

4.2.4 The blocks E, C, and Θ

Analogs of the cross-mode momenta p_α and p_β did not appear in the one-dimensional restriction. Their role in the effective geometry described by (4.22) arises due to the blocks E, C, and Θ.

The term $(\partial\gamma^{iJ}/\partial x^k)p_i\Delta(x^k p_J)$ couples p_α and p_β to the classical momenta p_i through antisymmetric and symmetric derivatives of the metric

$$E^T = \sin(\beta)\begin{pmatrix} (s_y/s_x)\partial_y\gamma^{xb} - (s_x/s_y)\partial_x\gamma^{yb} \\ -\Big((s_y/s_x)\partial_y\gamma^{xb} + (s_x/s_y)\partial_x\gamma^{yb}\Big) \end{pmatrix}. \tag{4.36}$$

The components of $e_\beta \otimes e_b$ (the lower row) are symmetric gradients which capture how a quantum state interprets stretching or compression of the spacetime, without introducing rotation or shearing. That is, quantum correlations may affect how nearby geodesics converge or diverge. If the spacetime metric has vorticity, then components of $e_\alpha \otimes e_b$ are nonzero and couple the classical degrees of freedom directly to p_α.

The coefficients of $e_{s_I} \otimes e_\alpha$ and $e_{s_I} \otimes e_\beta$ arise entirely from the term $\gamma^{xy}\Delta(p_x p_y)$ and contribute the block

$$C = \sin(\beta)\frac{\gamma^{xy}}{s_x s_y}\begin{pmatrix} -s_x & -s_x \\ s_y & -s_y \end{pmatrix}. \tag{4.37}$$

Finally, the block containing the coefficients of the quantum angular momenta coordinates is

$$\Theta = \begin{pmatrix} \sin^2(\beta)\mathrm{Tr}\left(\sigma_3\Sigma_x^{-1}\sigma_3\gamma^{-1}\right) - 2\mathrm{Tr}\left(\Sigma_x^{-1}\gamma^{-1}\right) & -\gamma^{xx}/s_x^2 + \gamma^{yy}/s_y^2 \\ -\gamma^{xx}/s_x^2 + \gamma^{yy}/s_y^2 & \sin^2(\beta)\mathrm{Tr}\left(\Sigma_x^{-1}\gamma^{-1}\right) \end{pmatrix} \tag{4.38}$$

where

$$\sigma_3 = \begin{pmatrix} 1 & 0 \\ 0 & -1 \end{pmatrix}. \tag{4.39}$$

Similar to the one-variable case, the quadratic part of the generalized quartic Finsler metric depends explicitly on the correlation variables s_x and s_y. However, the two-variable quadratic metric (4.22) now depends also on the spatial correlation angle β, which introduces anisotropic behavior into the effective geometry. This anisotropy implies that the effective quantum geometry depends on the alignment (or misalignment) of x and y correlations.

The expression for the quadratic part of the effective quantum metric simplifies when the correlation structure of the quantum state aligns maximally with the slicing of the classical metric. In this case, $\beta = \pi/2$ (implying $\Delta(xy) = 0$, an isotropic state), the quadratic part of the effective quantum metric is

$$B^{\bar{a}\bar{b}} = \tag{4.40}$$

$$\begin{pmatrix}
\langle\gamma^{ij}(\hat{x},\hat{y})\rangle & s_x\partial_x\gamma^{ix} & s_y\partial_y\gamma^{iy} & \frac{s_y\partial_y\gamma^{ix}}{s_x} - \frac{s_x\partial_x\gamma^{iy}}{s_y} & -\frac{s_y\partial_y\gamma^{ix}}{s_x} - \frac{s_x\partial_x\gamma^{iy}}{s_y} & 0 & 0 \\
s_x\partial_x\gamma^{xj} & \gamma^{xx} & 0 & -\frac{\gamma^{xy}}{s_y} & -\frac{\gamma^{xy}}{s_y} & 0 & 0 \\
s_y\partial_y\gamma^{yj} & 0 & \gamma^{yy} & \frac{\gamma^{xy}}{s_x} & -\frac{\gamma^{xy}}{s_x} & 0 & 0 \\
\frac{s_y\partial_y\gamma^{xj}}{s_x} - \frac{s_x\partial_x\gamma^{yj}}{s_y} & -\frac{\gamma^{xy}}{s_y} & \frac{\gamma^{xy}}{s_x} & -\frac{\gamma^{xx}}{s_x^2} - \frac{\gamma^{yy}}{s_y^2} & \frac{\gamma^{yy}}{s_y^2} - \frac{\gamma^{xx}}{s_x^2} & 0 & 0 \\
-\frac{s_y\partial_y\gamma^{xj}}{s_x} - \frac{s_x\partial_x\gamma^{yj}}{s_y} & -\frac{\gamma^{xy}}{s_y} & -\frac{\gamma^{xy}}{s_x} & \frac{\gamma^{yy}}{s_y^2} - \frac{\gamma^{xx}}{s_x^2} & \frac{\gamma^{xx}}{s_x^2} + \frac{\gamma^{yy}}{s_y^2} & 0 & 0 \\
0 & 0 & 0 & 0 & 0 & \frac{1}{2}\left(\frac{\gamma^{xx}}{s_x^2} + \frac{\gamma^{yy}}{s_y^2}\right) & 0 \\
0 & 0 & 0 & 0 & 0 & 0 & 0
\end{pmatrix}$$

4.3 Quartic Finsler geometry

In the physics literature, non-Riemannian Finsler metrics have previously been considered in situations where spacetime geometry exhibits higher-order dependencies on direction, motivated for instance by modified dispersion relations [49, 50]. One example is the Randers metric [51],

$$\mathrm{d}s = k_a \mathrm{d}x^a + \sqrt{\pm g_{ab}(x)\mathrm{d}x^a\mathrm{d}x^b}, \tag{4.41}$$

where the field k_a parametrizes small Lorentz violations. Particle mechanics in the geometry (4.41) obey a dispersion relation different from the relativistic prediction. This mechanism has been applied in connection with the GZK threshold [52] and in

cosmological studies [53].

Finsler metrics based on higher-order polynomials have also been studied. In multi-metric geometry [54] one encounters the Finsler structure

$$F = \sum_{\mu} F^{(\mu)} \tag{4.42}$$

in which each $F^{(\mu)}$ is a Riemannian Finsler structure, $F^{(\mu)}(x,y) = \sqrt{g^{(\mu)}_{ij}(x)y^i y^j}$ where (x^i, y^i) are local coordinates on the tangent bundle of spacetime. In the bi-metric case with $F^{(1)} = \sqrt{g^{(1)}_{ij}(x)y^i y^j}$ and $F^{(2)} = \sqrt{g^{(2)}_{ij}(x)y^i y^j}$, the Finsler structure may be rewritten

$$F(x,y) = \sqrt{\sqrt{4g^{(1)}_{ij}g^{(2)}_{kl}y^i y^j y^k y^l} + \left(g^{(1)}_{ij} + g^{(2)}_{ij}\right) y^i y^j}\,, \tag{4.43}$$

a special case of the generalized 4th-root Finsler structure

$$F(x,y) = \sqrt{\sqrt{a_{ijkl}y^i y^j y^k y^l} + b_{ij}y^i y^j} \tag{4.44}$$

studied in [55, 56]. The Finsler geometry found here is precisely of this form, except that we have derived a Hamiltonian version.

On a Finsler manifold, the natural Lagrangian structure $L^F = F^2/2$ is complemented by the dual Finsler structure F^* which gives rise to the Hamiltonian $H^F = (F^*)^2/2$. Finsler Hamiltonians are discussed in [57]. When applied to (4.44), the result can be compared to our Hamiltonian construction. In our results, Finsler properties are not realized for the standard four spacetime dimensions. They are instead controlled by quantum entropy and purity through the conserved momenta C_1 and C_2. These quantum-information properties will be discussed in Sec. 4.5.

4.4 Riemannian special cases of the quartic geometry

The Finsler structure defined by the quantum-corrected geodesic Hamiltonian, Eq. (4.17), will define a Riemannian geometry if the quartic part of it, Eq. (4.20), is reducible.

4.4.1 Gaussian states

The statistical moments $\Delta(x^\alpha p^\beta)$ (for all multi-indices α and β) provide a complete parametrization of N-mode quantum states, pure or mixed. However, pure Gaussian states are uniquely characterized by a restricted subset of the second order moments. In

the position representation, Gaussian states are fully specified by their position-position statistics Σ_x and position-momentum statistics Σ_{xp}; see Eq. (4.29). The second-order momentum statistics, as well as all higher-order moments, are entirely determined by these two sets of parameters.

The N-mode pure Gaussian is parametrized explicitly by the position-space wavefunction

$$\psi_G(x, \Sigma_x, \Sigma_{xp}) = \left(\frac{1}{2\pi\sqrt{\det \Sigma_x}}\right)^{1/2} \exp\left(-\frac{1}{4}x^T\Sigma_x^{-1}\left(\mathbb{I} - i\frac{\Sigma_{xp}}{\hbar/2}\right)x\right) \tag{4.45}$$

where $x = (x_1, \ldots, x_N)$ is the position vector and matrix multiplication is assumed. The modulus of Eq. (4.46) recovers the standard Gaussian density

$$p_G(x, \Sigma_x) = \frac{1}{2\pi\sqrt{\det \Sigma_x}} \exp\left(-\frac{1}{2}x^T\Sigma_x^{-1}x\right). \tag{4.46}$$

The momentum-space wave function is obtained by Fourier transforming the position-space Gaussian wave function. This can be done analytically with the Gaussian integral formula

$$\int \exp\left(-\frac{1}{2}x^TAx + J^Tx\right) \mathrm{d}^n x = \sqrt{\frac{(2\pi)^n}{\det A}} \exp\left(\frac{1}{2}J^TA^{-1}J\right). \tag{4.47}$$

The momentum-space Gaussian wave function thus obtained is

$$\begin{aligned}\tilde{\psi}_G(p, \Sigma_x, \Sigma_{xp}) &= \left(\frac{\det(\Sigma_x)}{(2\pi)^2 \det\left(\frac{\hbar^2}{4}\mathbb{I} + \Sigma_{xp}^2\right)}\right)^{1/4} \\ &\times \exp\left(-\frac{1}{4}p^T\left(\frac{\hbar^2}{4}\mathbb{I} + \Sigma_{xp}^2\right)^{-1}\left(\mathbb{I} + i\frac{\Sigma_{xp}}{\hbar/2}\right)\Sigma_x p + \frac{i}{2}\arctan\left(\frac{\frac{\hbar}{2}\mathrm{Tr}(\Sigma_{xp})}{\frac{\hbar^2}{4} - \det(\Sigma_{xp})}\right)\right).\end{aligned} \tag{4.48}$$

This indicates that, in the Gaussian case, the momentum statistics are fully determined by the matrix equation

$$\Sigma_p = \Sigma_x^{-1}\left(\frac{\hbar^2}{4}\mathbb{I} + \Sigma_{xp}^2\right) \tag{4.49}$$

or equivalently, by the equations

$$\Sigma_x\Sigma_p - \Sigma_{xp}^2 = \frac{\hbar^2}{4}\mathbb{I}. \tag{4.50}$$

This result generalizes to multiple modes the statement that Gaussian states saturate the uncertainty relation.

Specializing to the two-mode case, either of the Eqs. (4.49) or (4.50) represent a system of four nonlinear constraint equations. These equations, when expressed in canonical coordinates, reveal constraints on the canonical variables.

In Eqs. (4.50), the diagonal equations, in canonical coordinates for two modes are

$$\frac{1}{2}\left(C_1^2 + (U_x - U_y)\right) = \frac{\hbar^2}{4}, \tag{4.51}$$

$$\frac{1}{2}\left(C_1^2 - (U_x - U_y)\right) = \frac{\hbar^2}{4}. \tag{4.52}$$

From these follow the two conditions

$$C_1^2 = \frac{\hbar^2}{2}, \tag{4.53}$$

$$U_x - U_y = 0. \tag{4.54}$$

The first of these, because $C_1^2 = \nu_+^2 + \nu_-^2$ is the total uncertainty, says that Gaussian states have minimum uncertainty. Moreover, because $\nu_\pm \geq \hbar/2$, the equality (4.53) implies $\nu_+ = \nu_- = \hbar/2$ and consequently, also that $C_2 = 0$ for a pure Gaussian state.

Using these constraints, the second condition (4.54) can be expressed as

$$4p_\alpha p_\beta + \sqrt{(4p_\alpha)^2\left(p_\alpha^2 - \frac{C_1^2}{2}\right)}\frac{\cos(\alpha)}{\sin(\beta)} = 0. \tag{4.55}$$

This can be solved by either of

$$p_\alpha = 0 \tag{4.56a}$$

$$p_\beta = \pm\sqrt{p_\alpha^2 - \frac{C_1^2}{2}}\frac{\cos(\alpha)}{\sin(\beta)}. \tag{4.56b}$$

The remaining off-diagonal equations in Eqs. (4.50) are also solved by $p_\alpha = 0$ in which case they do not present additional constraints. However, if we assume $p_\alpha \neq 0$ and instead use the constraint (4.56b), the off-diagonal equations give the two additional constraints

$$s_x p_{s_x} + s_y p_{s_y} = 0 \tag{4.57}$$

and

$$p_\alpha = \frac{1}{2}\frac{\pm\sin(\alpha)\sqrt{\frac{\hbar^2}{4}(\sin^2(\alpha) - \cos^2(\beta)) + s_x^2 p_{s_x}^2 \sin^2(\beta)} - s_x p_{s_x}\sin(2\beta)}{\cos(2\alpha) + \cos(2\beta)}. \tag{4.58}$$

The later condition allows $p_\alpha < C_1^2/2$ and, by (4.56b), would correspond to an imaginary solution for p_β.

If we require all of the momenta solving the equations (4.50) to be real, then we must rule out the solutions (4.56b), (B8), and (4.58). Then the matrix equality (4.50) imposes only the three independent conditions

$$C_1^2 = \frac{\hbar^2}{2}, \tag{4.59}$$

$$C_2 = 0, \tag{4.60}$$

$$p_\alpha = 0. \tag{4.61}$$

Mapping backward, these three conditions imply that only seven of the ten second-order moments for two modes are independent. In the moment parametrization, these are usually the three Σ_x and the four Σ_{xp}.

When Eqs. (4.59)–(4.61) are satisfied (or so long as C_2 and p_α are much smaller than C_1 and p_β), then the quartic part in the Hamiltonian (4.17) is negligible. In this case, we can approximate from Eqs. (2.64) and (2.65),

$$U_x \approx U_y \approx p_\beta^2 + \frac{C_1^2}{2\sin^2\beta} \tag{4.62}$$

and the quantum contributions to p_x^2 and p_y^2 from momentum variances are

$$\Delta(p_x^2) = p_{s_x}^2 + \frac{p_\beta^2}{s_x^2} + \frac{C_1^2}{2s_x^2\sin^2(\beta)}, \tag{4.63}$$

$$\Delta(p_y^2) = p_{s_y}^2 + \frac{p_\beta}{s_y^2} + \frac{C_1^2}{2s_y^2\sin^2(\beta)}, \tag{4.64}$$

and

$$\begin{aligned}\Delta(p_x p_y) \;=\; & \left(p_{s_x}p_{s_y} - \frac{p_\beta^2}{s_x s_y} - \frac{C_1^2}{2\sin^2(\beta)s_x s_y}\right)\cos(\beta) \\ & -\sin(\beta)p_\beta\left(\frac{p_{s_y}}{s_x} + \frac{p_{s_x}}{s_y}\right).\end{aligned} \tag{4.65}$$

These expressions indicate that centered two-mode pure Gaussian states are fully characterized on the six-dimensional subphase space coordinatized by $(s_x, p_{s_x}; s_y, p_{s_y}; \beta, p_\beta)$. This subspace arises from reducing the full ten-dimensional space of second moments

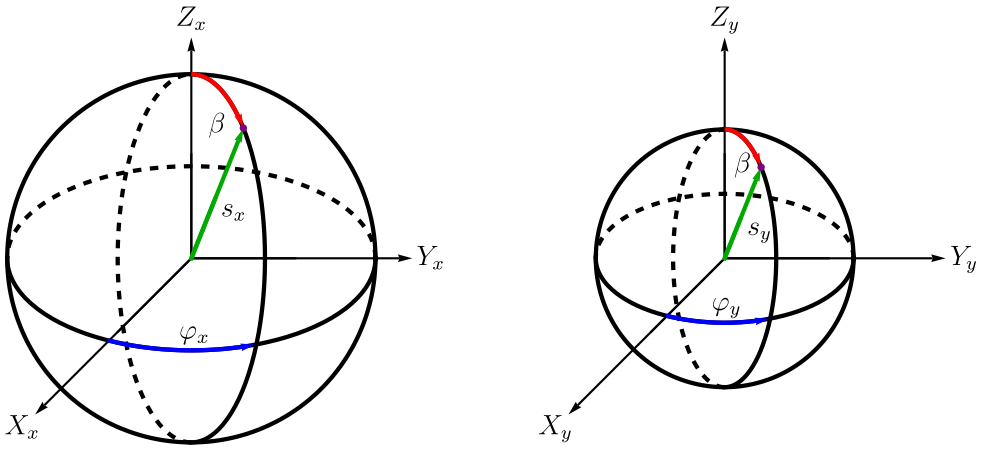

Figure 4.1: Auxiliary spherical and Cartesian coordinate systems used to describe pure two-mode Gaussian states. Each mode is associated with a three-dimensional auxiliary space in which the radial coordinate s_x or s_y corresponds to the single-mode spatial uncertainty. The polar angles, constrained by purity with $\vartheta_x = \vartheta_y = \beta$, capture the spatial correlation between modes, while the azimuthal angles φ_x and φ_y have conjugate momenta set by the global invariants of the state.

by the purity constraints Eqs. (4.49), which fix the values of the Casimirs C_1 and C_2, and eliminate the degree of freedom associated with the conjugate pair (α, p_α). The remaining variables describe both the local properties of each mode and their nonlocal coupling through the correlation angle β.

The moment expressions (4.63)–(4.65) for pure two-mode Gaussian states can be interpreted as centrifugal kinetic energies in two auxiliary three-dimensional configuration spaces. The variables s_x and s_y play the role of radial coordinates, while the angular structure encodes internal constraints of the state; see Figure 4.1. The polar angles ϑ_x and ϑ_y are constrained to a common angle β, capturing mode correlation, while the azimuthal angles φ_x and φ_y are gauge-like degrees of freedom. The conjugate momenta are fixed by purity constraints to be $p_{\varphi_x} = p_{\varphi_y} = C_1/\sqrt{2} = \hbar/2$ and $p_{\vartheta_x} = p_{\vartheta_y} = p_\beta$.[4]

This structure provides a geometric decomposition of the pure-state submanifold into two angular sectors with locked dynamics and a shared angular orientation β, which captures the entanglement-induced coupling between modes. While Gaussian states are often analyzed through symplectic invariants and covariance matrices, this spherical model offers a complementary mechanical perspective, where the internal structure of

[4]Because $C_1/\sqrt{2}$ is the momentum conjugate to φ_x and φ_y it would be consistent to identify these spurious angles with the cyclic coordinate φ, up to scaling; see paragraph before Eq. (2.59).

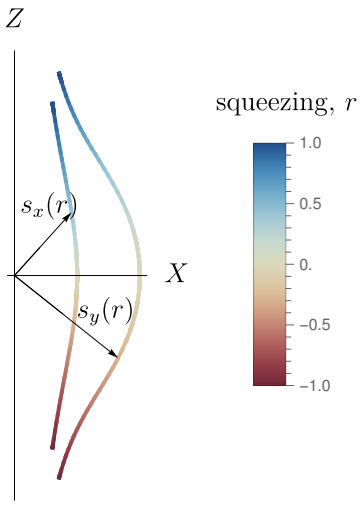

Figure 4.2: Representation of two-mode squeezing as a trajectory in the auxiliary configuration space. The initial unsqueezed Gaussian state is localized in the $X - Z$ plane, with position uncertainty s_y twice that of s_x. As the squeezing parameter increases in magnitude, the state evolves along a fixed azimuth toward the north or south pole of the sphere, depending on the sign. The polar limit corresponds to an idealized EPR state $\psi(x, y) \propto \delta(x - y)$, exhibiting perfect position correlations.

the state corresponds to constrained motion in auxiliary spaces.

As an illustrative example, we visualize the flow of two-mode squeezing within the auxiliary configuration space. The two-mode squeezing transformation acts on the covariance matrix by congruence as $\sigma_{\rm sq} = S_{\rm sq}(r)\sigma S_{\rm sq}^{\top}(r)$ where the symplectic squeezing matrix is given by

$$S_{\rm sq}(r) = \begin{pmatrix} \cosh(r)\mathbb{I}_2 & \sinh(r)\sigma_3 \\ \sinh(r)\sigma_3 & \cosh(r)\mathbb{I}_2 \end{pmatrix} . \tag{4.66}$$

Here, r is the real-valued squeezing parameter, $\mathbb{I}_2$ is the 2×2 identity matrix, and σ_3 is the third Pauli matrix. This transformation continuously deforms the state along a symplectic trajectory that preserves the Casimirs while modifying local and cross-mode correlations.

Figure 4.2 shows an example with an initial (unsqueezed) Gaussian state with a position uncertainty for the y mode that is twice that of the x mode. The initial, unsqueezed state is represented by a pair of points in each auxiliary configuration space. Since the azimuthal angles are spurious, we choose a representative configuration lying in the $X - Z$ plane. The squeezing transformation preserves these spurious angles, so the entire squeezing trajectory remains confined to this plane. For convenience, both mode configurations are depicted within the same three-dimensional auxiliary space.

In the auxiliary space representation, unsqueezed states lie in the $X - Y$ plane. As the squeezing parameter increases in magnitude, the state moves toward either the north or south pole of the sphere, depending on the sign of the squeezing. The limiting states along the polar axis correspond to idealized EPR states of the form $\psi(x, y) \propto \delta(x - y)$, in which the position difference is perfectly correlated.

4.4.2 Case 2

The pure Gaussian case represents a limiting configuration where the state is both pure and symplectically isotropic, with $\nu_+ = \nu_- = \hbar/2$ and $p_\alpha = 0$. In this case, the Finsler root $\sqrt{P}$ vanishes, reducing the two-mode geometry to a Riemannian structure.

Riemannian geometry can also emerge in more general, nonpure settings. Specifically, even when the symplectic eigenvalues take nonlimiting values, the geometry remains Riemannian if p_α can be chosen so that the Finsler discriminant vanishes. However, the momentum p_α is not free to vary arbitrarily. For given values of the Casimirs C_1 and C_2, reality conditions on the Finsler discriminant imposes a nontrivial constraint

$$P(p_\alpha, C_1, C_2) = (C_1^2 - 4p_\alpha^2)^2 - (C_1^4 - C_2^4) \geq 0. \tag{4.67}$$

This condition carves out a forbidden interval around $|p_\alpha| = C_1/2$. Specifically, if $|p_\alpha| < C_1/2$, then Eq. (4.67) requires

$$0 \leq |p_\alpha| \leq \sqrt{\frac{C_1^2 - \sqrt{C_1^4 - C_2^4}}{4}} = \frac{\nu_+ - \nu_-}{2}\,. \tag{4.68}$$

On the other hand, if $|p_\alpha| > C_1/2$, the inequality becomes

$$|p_\alpha| \geq \sqrt{\frac{C_1^2 + \sqrt{C_1^4 - C_2^4}}{4}} = \frac{\nu_+ + \nu_-}{2}\,. \tag{4.69}$$

Reality conditions thus imply that the allowed values of p_α lie outside the exclusion band defined by

$$I_{\text{exclusion}} = (p_-, p_+)\ . \tag{4.70}$$

with the minimal and maximal angular momenta

$$p_\pm = \frac{\nu_+ \pm \nu_-}{2}\,. \tag{4.71}$$

When p_α assumes one of the boundary values p_- or p_+, then $p_\alpha \neq 0$, yet the Finsler root still vanishes, signaling a return to a Riemannian form despite the presence of nontrivial correlations. These configurations generalize the pure-state limit and reveal a broader class of geometrically special states.

Explicitly, when p_α saturates the lower bound $p_\alpha = p_-$, we have the momentum variances

$$\Delta(p_x^2) = p_{s_x}^2 + \frac{(p_\alpha^{\min} - p_\beta)^2}{s_x^2} + \frac{\nu_+\nu_-}{s_x^2 \sin^2(\beta)}\,, \tag{4.72}$$

$$\Delta(p_y^2) = p_{s_y}^2 + \frac{(p_\alpha^{\min} + p_\beta)^2}{s_y^2} + \frac{\nu_+\nu_-}{s_y^2 \sin^2(\beta)}\,, \tag{4.73}$$

and

$$\begin{aligned}\Delta(p_x p_y) \;=\; & \left(p_{s_x} p_{s_y} + \frac{(p_\alpha^{\min})^2 - p_\beta^2}{s_x s_y} - \frac{\nu_+\nu_-}{s_x s_y \sin^2(\beta)}\right)\cos(\beta) \\ & + \left(\frac{p_{s_y}}{s_x}(p_\alpha^{\min} - p_\beta) - \frac{p_{s_x}}{s_y}(p_\beta + p_\alpha^{\min})\right)\sin(\beta)\,.\end{aligned} \tag{4.74}$$

When p_α saturates the upper bound, $p_\alpha = p_+$, the azimuthal terms become negative but otherwise retain the same structure.

The presence of a forbidden interval, (p_-, p_+), through which p_α cannot evolve under any Hamiltonian flow might be an artifact of our truncation. The variables p_α, C_1, and C_2 are of order $\hbar$, but the discriminant $P(p_\alpha, C_1, C_2)$ is quartic, contributing at quadratic order only due to its appearance under a square root. In a higher-order truncation, fourth order variables could plausibly modify the discriminant and the reality condition (4.67), potentially connecting the currently disjoint allowed regions or even removing one of them entirely. Since this remains uncertain, it is intriguing to consider the possibility that the forbidden interval is fundamental rather than an artifact. Such would indicate that the quantum state structure directly governs not only the qualitative nature of the geometry but also the accessible phase space itself. Transitions between disjoint p_α sectors would be dynamically forbidden—not by energetic barriers, but by deeper algebraic and geometric constraints.

The bounds on p_α show that its range is dictated by the symplectic eigenvalues ν_+ and ν_-, which encode the quantum uncertainty of the system. If the state is prepared in the outer region with $|p_\alpha| \geq p_+$, then its sign remains fixed under unitary evolution. This introduces a form of dynamical irreversibility, wherein the phase-space structure imposes global constraints on state evolution. In contrast, within the inner band, sign changes are allowed.

This result reveals a connection between information-theoretic bounds (such as uncertainty relations) and the topological structure of quantum phase space, suggesting that quantum information flow is fundamentally limited by the geometry it inhabits.

4.4.3 Case 3

Another quadratic case is obtained if $C_2 = C_1$ with arbitrary p_α, such that

$$U_x = (p_\alpha - p_\beta)^2 - \frac{1}{2}|C_1^2 - 4p_\alpha^2|\frac{\sin(\alpha+\beta)}{\sin\beta} \tag{4.75}$$

and a similar expression for U_y.

However, the two-mode uncertainty relation $\det(\sigma) \geq \hbar^4/16$ restricts physically realizable states. Comparing this to Eq. (2.79) reveals that the condition $C_1 = C_2$ is forbidden. This further highlights how information-theoretic constraints fundamentally shape the Finslerian geometry experienced by the system.

4.5 The role of purity and entropy in clock evolution

In this section, we explore how our canonical realization of second-order moments links fundamental quantum characteristics—such as uncertainty, entropy, and purity—to the geometry of the phase space.

When we restrict to Gaussian states, the two-mode covariance matrix σ provides a faithful parametrization. In this case, the invariants C_1 and C_2 not only parameterize the state of the system but also serve as direct measures of quantum correlations and entanglement. The von Neumann entropy of the quantum state with density matrix ρ is defined as

$$S_V(\rho) \coloneqq -\mathrm{Tr}\,(\rho \log_2 \rho) \tag{4.76}$$

This definition depends on the full spectrum of the density matrix. Alternatively, for Gaussian states the formula

$$S_V(\sigma) = s_V(2\nu_+/\hbar) + s_V(2\nu_-/\hbar) \tag{4.77}$$

holds, where ν_+ and ν_- are the symplectic eigenvalues of the covariance matrix σ and

$$s_V(\nu) \coloneqq \frac{\nu+1}{2}\log_2\left(\frac{\nu+1}{2}\right) - \frac{\nu-1}{2}\log_2\left(\frac{\nu-1}{2}\right). \tag{4.78}$$

An alternative indicator of a state's mixedness is the purity $\mu(\rho)$ defined as

$$\mu(\rho) \coloneqq \mathrm{Tr}(\rho^2). \tag{4.79}$$

For Gaussian states the purity has the special form

$$\mu(\sigma) = \frac{\hbar^2/4}{\sqrt{\det(\sigma)}}. \tag{4.80}$$

The statistics of σ provide one characterization of the state. However through these formulas, the Casimir variables C_1 and C_2 are explicitly linked to entanglement and purity as alternative characterizations of the quantum state. These important quantum concepts therefore determine the Finslerian nature of geometry.

Geometrical Finsler properties are then experienced in the direction of α, which is a correlation parameter with a more complicated relationship to moments than β. Our derivation of quantum-information variables as elements of canonical pairs on a phase space demonstrates their dynamical independence, defined as being subject to pairs of Hamilton's equations derived from partial derivatives of the Hamiltonian. Canonical variables are defined only up to the possibility of performing canonical transformations, and are therefore not unique without further conditions. Here, referring to the standard notions of quantum fluctuations s_x and s_y, correlations $\cos\beta$, as well as entropy and purity which are functions of C_1 and C_2, the only remaining non-momentum variable is given by α. Therefore, if we impose the condition that the standard notions should be represented as canonical coordinates, the pair (α, p_α) is distinguished as the remaining independent set. It is still possible to perform canonical transformations of (α, p_α) while keeping all the other variables fixed, but this would change the square-root expression $\sqrt{P}$ and the fact that it depends on p_α but not on α. Combining these conditions, the correlation parameter α is therefore distinguished in spite of its rather complicated expression in terms of second-order moments.

4.6 Geometric characterization of entanglement and its nonlocal phase space structure

Our formulation offers a geometric perspective on entanglement. According to the Peres–Horodecki criterion [38], a two-mode Gaussian state is entangled if and only if the smallest symplectic eigenvalue of the partially transposed covariance matrix satisfies

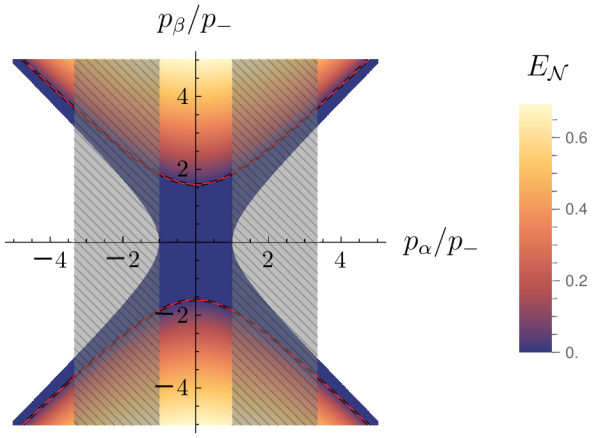

Figure 4.3: Logarithmic negativity ($\beta = \pi/2, C_1 = 2.7\hbar, C_2 = 2\hbar$) is a function of the Minkowski distance of (p_α, p_β). The colored region represents the physically allowed domain, excluding the vertical gray bars, which are forbidden by reality conditions on p_α (see main text). The blue region corresponds to separable (unentangled) states, while the areas outside the vertically opening hyperbolas (indicated by red and black dashed lines) are entangled. Warmer colors indicate higher logarithmic negativity, while cooler colors indicate lower entanglement.

$\nu_-^{\mathrm{PT}} < \hbar/2$. In our canonical framework, this eigenvalue becomes a phase space function. Although the full phase space expression for ν_-^{PT} is lengthy, its functional dependence can be succinctly represented as

$$(\nu_-^{\mathrm{PT}})^2 = (\nu_-^{\mathrm{PT}})^2(\alpha, \beta, p_\alpha, p_\beta, C_1, C_2). \tag{4.81}$$

This reveals that entanglement is determined entirely by the inter-mode structure—specifically, the angular correlation variables (α, β), their conjugate moments (p_α, p_β), and the global Casimir invariants (C_1, C_2) parametrizing the entropy and purity of the global state. Notably, ν_-^{PT} does not depend on single-mode variables (s_i, p_{s_i}), underscoring the nonlocal character of entanglement.

The logarithmic negativity $E_\mathcal{N}$ is a widely used entanglement measure in quantum information theory. It is computed from the covariance matrix according to

$$E_\mathcal{N} = \max(0, -\ln \nu_-^{\mathrm{PT}})\,. \tag{4.82}$$

This entanglement measure serves as an upper bound on distillable entanglement [33].

For $\beta = \pi/2$ the logarithmic negativity takes the manageable form

$$e^{-2E_\mathcal{N}}|_{\beta=\frac{\pi}{2}} = C_1^2 - 4(p_\alpha^2 - p_\beta^2) - \sqrt{(C_1^2 - 4(p_\alpha^2 - p_\beta^2))^2 - (C_1^4 - C_2^4)}\,. \tag{4.83}$$

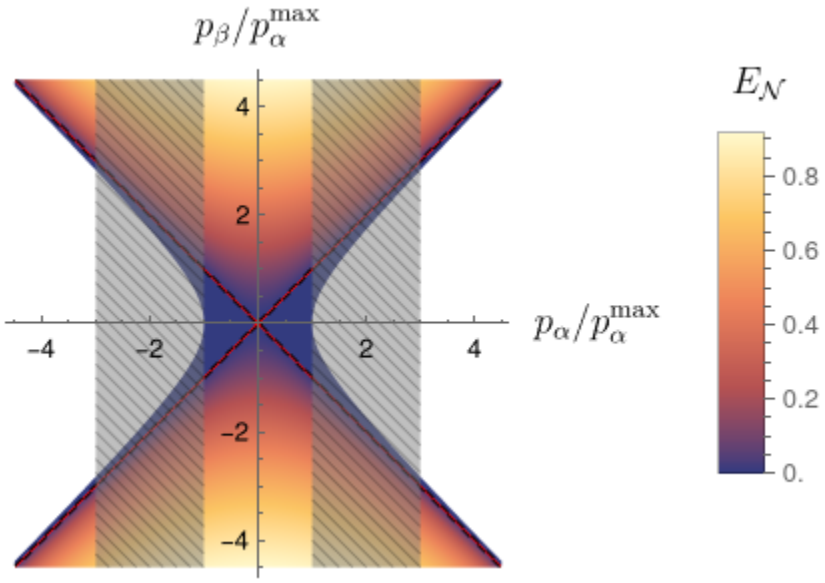

Figure 4.4: Unlike the nondegenerate case shown in Fig. 4.3, this plot corresponds to $\nu_+ = \hbar^2/2$ and $\nu_- = \hbar^2/4$, with ν_- saturating its minimal physical value. In this limiting case, the entanglement boundary hyperbolas described by Eq.(4.85) degenerate to 45-degree lines, creating two regions of separable states connected by the pure Gaussian state at the origin.

Fixing the Casimir invariants—or equivalently, the global entropy and purity—allows the logarithmic negativity to be expressed as a parametric function on the momentum space (p_α, p_β).

Reality conditions applied to expression (4.83) introduce a new boundary in angular momentum space, constraining the combination $p_\alpha^2 - p_\beta^2$

$$p_\alpha^2 - p_\beta^2 \leq \left(\frac{\nu_+ - \nu_-}{2}\right)^2 . \tag{4.84}$$

This inequality defines a pair of horizontally opening hyperbolas, shown in Figure 4.3, which bound the region describing allowed states.

The vertically opening hyperbolas in the same figure separate entangled and separable states. This boundary is given by

$$p_\beta^2 - p_\alpha^2 = \frac{(\nu_+^2 - 1)(\nu_-^2 - 1)}{(\nu_+ - \nu_-)^2} . \tag{4.85}$$

States lying above this curve are entangled. This curve is degenerate when at least one eigenvalue saturates its lower bound; c.f. Figure 4.4.

The entanglement structure identified here has direct implications for experimental scenarios involving entanglement generation and decoherence, offering intriguing opportunities for future investigation into the dynamics and controllability of quantum correlations in gravitational or relativistic settings.

Chapter 5
Quantum analysis of Schwarzschild radial geodesics

"I'm sorry. We're outside the light cone."

"What's that?"

"It's what physicists call the cone shape that light describes as it emanates along the time axis. It's impossible for people outside the cone to comprehend events taking place inside the cone. Think about it: Information about who-knows-how-many major events in the universe is flying toward us right now at the speed of light. Some of it has been traveling for hundreds of millions of years, but we're still outside the light cones of those events."

"Fate lies within the light cone."

Ringier considered this, then gave him an appreciative nod. "General, that's an excellent analogy! But sophons outside the light cone can see events on the inside."

"So the sophons have changed fate"

—Liu Cixin
The Dark Forest

This chapter applies the formalism developed in the previous chapters to a concrete physical setting: the behavior of a quantum clock freely falling into a Schwarzschild black hole. Specifically, we compute the proper time experienced by a semiclassical

quantum state as it undergoes radial infall from a finite initial radius. This serves as a demonstration of how the geometric formulation of quantum mechanics interacts with curved spacetime in realistic scenarios.

Chapter 4 established a simplified model by considering one-dimensional quantization in synchronous coordinates, valid in the nonrelativistic (low-velocity) limit. In that setting, the effective quantum spacetime retains a pseudo-Riemannian structure, enabling us to formulate geodesic motion via parallel transport using a modified Christoffel connection derived from the quantum-corrected metric. Section 5.1 presents quantum geodesics computed in a synchronous slicing of the Schwarzschild geometry.

A key result of this analysis is a quantum-corrected expression for gravitational time dilation. Since gravitational time dilation depends on the time component of the tangent vector along a clock's worldline, quantum corrections to the geodesic equations naturally lead to corrections in the accumulated proper time of the clock. These results are presented in Section 5.3.

More broadly, the quantum Hamiltonian constraint implies that both the trajectory of the state and the effective background spacetime are dynamically modified by quantum fluctuations. To study this interplay, we investigate several geometric structures: Section 5.4 examines possible coordinate singularities and signature changes in the quantum-corrected geometry; Section 5.5 computes the associated volume element; and these investigations culminate in Sec. 5.6, where we determine the slope of the lightcone implied by the perturbed metric and discuss under which conditions a quantum state might effectively "leak" outside its classical lightcone. Thus, we ask: Can quantum effects, like Liu Cixin's sophons, truly alter fate?

5.1 Schwarzschild quantum proper time

The standard (Schwarzschild-Droste) slicing of the Schwarzschild solution is expressed in coordinates (t_S, r) by the line element

$$\mathrm{d}s^2 = -\left(1 - \frac{r_s}{r}\right) c^2 \mathrm{d}t_S^2 + \frac{1}{1 - \frac{r_s}{r}} \mathrm{d}r^2 \,. \tag{5.1}$$

In this slicing, the ADM variables are

$$N(t_S, r) = \sqrt{1 - \frac{r_s}{r}} \,, \tag{5.2}$$

$$N^i(t_S, r) = 0 \,, \tag{5.3}$$

$$\gamma^{rr}(t_S, r) \;=\; 1 - \frac{r_s}{r}\,. \tag{5.4}$$

A transformation to Lemaître coordinates (t_L, ρ)

$$\mathrm{d}t_L \;=\; \mathrm{d}t_S + \frac{1}{c}\sqrt{\frac{r_s}{r}}\frac{\mathrm{d}r}{1-\frac{r_s}{r}}\,, \tag{5.5}$$

$$\mathrm{d}\rho \;=\; c\,\mathrm{d}t_S + \sqrt{\frac{r}{r_s}}\frac{\mathrm{d}r}{1-\frac{r_s}{r}}\,, \tag{5.6}$$

gives a synchronous slicing of the Schwarzschild solution with line element

$$\mathrm{d}s^2 = -c^2\mathrm{d}t_L^2 + \frac{r_s}{r}\mathrm{d}\rho^2\,, \tag{5.7}$$

where the r coordinate is implicitly defined in terms of ρ and t_L via

$$r = \left(\frac{3}{2}\frac{\rho - ct_L}{r_s}\right)^{2/3} r_s\,. \tag{5.8}$$

This expression is obtained by integrating the difference between Eqs. (5.6) and (5.5),

$$\mathrm{d}\rho - c\mathrm{d}t_L = \sqrt{\frac{r}{r_s}}\mathrm{d}r\,. \tag{5.9}$$

The inverse of Eq. (5.8) is

$$\rho = \frac{2}{3}\left(\frac{r}{r_s}\right)^{3/2} r_s + ct_L\,. \tag{5.10}$$

The metric in these coordinates is nonsingular at the Schwarzschild radius, corresponding to the surface $\frac{3}{2}(\rho - ct_L) = r_s$. The curvature singularity is located at $\rho - ct_L = 0$. In this synchronous slicing, the ADM variables are

$$N(t_L, \rho) \;=\; 1\,, \tag{5.11}$$

$$N^i(t_L, \rho) \;=\; 0\,, \tag{5.12}$$

$$\gamma^{\rho\rho}(t_L, \rho) \;=\; \left(\frac{3}{2}\frac{\rho - ct_L}{r_s}\right)^{2/3}\,. \tag{5.13}$$

The corresponding inverse metric coefficients are then

$$g^{ab} = \begin{pmatrix} -1 & 0 \\ 0 & \frac{r}{r_s} \end{pmatrix}\,. \tag{5.14}$$

The singular Lagrangian in proper-time gauge and the corresponding Hamiltonian constraint in Lemaître coordinates are given by

$$\mathrm{L}(t_L, \rho, \dot{t}_L, \dot{\rho}) = \frac{mc^2}{2}\left(\frac{\mathrm{d}t_L}{\mathrm{d}\tau}\right)^2 - \frac{m}{2}\frac{r_s}{r}\left(\frac{\mathrm{d}\rho}{\mathrm{d}\tau}\right)^2 + \frac{mc^2}{2} = mc^2\,, \tag{5.15}$$

and

$$\mathrm{H}(t_L, \rho, p_{t_L}, p_\rho) \;=\; \frac{p_{t_L}^2}{2m} - \left(\frac{3}{2}\frac{\rho - ct_L}{r_s}\right)^{2/3}\frac{p_\rho^2}{2m} - \frac{mc^2}{2} = 0\,. \tag{5.16}$$

The associated geodesic equations are

$$\ddot{t}_L + \frac{1}{2}\frac{\dot{\rho}^2}{cr_s}\left(\frac{2}{3}\frac{r_s}{\rho - ct_L}\right)^{5/3} \;=\; 0\,, \tag{5.17}$$

$$\ddot{\rho} - \frac{1}{3}\frac{\dot{\rho}^2 - 2c\dot{t}_L\dot{\rho}}{\rho - ct_L} \;=\; 0\,. \tag{5.18}$$

These equations admit an exact solution describing the worldline of an idealized pointlike clock with the initial conditions

$$(t_L, \rho, \dot{t}_L, \dot{\rho})(0) = (0, \rho_0, 1, 0)\,. \tag{5.19}$$

The resulting solution is

$$t_L(\tau) \;=\; \tau\,, \tag{5.20}$$

$$\rho(\tau) \;=\; \rho_0\,. \tag{5.21}$$

Thus, the clock and the observer are comoving in these coordinates, and the proper time along the observer's worldline coincides with the Lemaître coordinate time t_L.

Integrating Eq. (5.9) along the worldline with $\mathrm{d}\rho = 0$ gives the coordinate time elapsed as the clock falls radially inward between radii r_0 and r

$$t_L(r; r_0) = -\frac{1}{c}\int_{r_0}^{r}\sqrt{\frac{x}{r_s}}\,\mathrm{d}x = \frac{1}{c\sqrt{r_s}}\left(r_0^{3/2} - r^{3/2}\right)\,, \tag{5.22}$$

In particular, the coordinate time to reach the Schwarzschild horizon at $r = r_s$ is

$$t_{L\,\mathrm{horizon}} = \frac{1}{c}\left(\rho_0 - \frac{2}{3}r_s\right)\,. \tag{5.23}$$

Because the Lemaître slicing is synchronous, the proper time along the clock's worldline

coincides with the coordinate time t_L. Thus, Eq. (5.20) implies that the proper time to reach the horizon is also given by $t_{L\,\mathrm{horizon}}$.

Finally, the total proper time to reach the curvature singularity at $r = 0$ (or equivalently, the surface $\rho = ct_L$) is

$$\tau_{\mathrm{singularity}} = \frac{\rho_0}{c}\,. \tag{5.24}$$

If the clock is not an ideal point object, but has quantum features, then the formalism developed here permits us to compute leading-order corrections to the classical proper time. The spacetime Hamiltonian constraint (defined in Eq. (4.2) and specialized to the Lemaître slicing) is given by

$$\begin{aligned}\mathrm{H}_{\mathcal{Q}}(t_L,\rho,s,q,p_{t_L},p_\rho,p_s,p_q) &= \frac{p_{t_L}^2}{2m} - \gamma^{\rho\rho}\frac{p_\rho^2}{2m} - \frac{mc^2}{2} \\ &\quad - \frac{s^2}{2}\frac{\partial^2}{\partial\rho^2}\left(\gamma^{\rho\rho}\right)\frac{p_\rho^2}{2m} - \frac{\partial\gamma^{\rho\rho}}{\partial\rho}s\frac{p_\rho p_s}{m} - \gamma^{\rho\rho}\left(\frac{p_s^2}{2m} + \frac{\hbar^2}{4s^2}\frac{p_q^2}{2m}\right).\end{aligned} \tag{5.25}$$

The first two derivatives of $\gamma^{\rho\rho}$ are

$$\frac{\partial\gamma^{\rho\rho}}{\partial\rho} = \frac{1}{r_s}\left(\frac{2}{3}\frac{r_s}{\rho - ct_L}\right)^{1/3} = \frac{1}{r_s}\sqrt{\frac{r_s}{r}}\,, \tag{5.26}$$

$$\frac{\partial^2\gamma^{\rho\rho}}{\partial\rho^2} = -\frac{1}{2}\frac{1}{r_s^2}\left(\frac{2}{3}\frac{r_s}{\rho - ct_L}\right)^{4/3} = -\frac{1}{r^2}\,. \tag{5.27}$$

In the one-dimensional, synchronous gauge considered here, the quantum Hamiltonian constraint remains quadratic in momenta. The effective inverse metric $g_{\mathcal{Q}}^{\bar{a}\bar{b}}$, introduced in Eq. (4.3), takes the following form in this coordinate system

$$g_{\mathcal{Q}}^{\bar{a}\bar{b}} := \begin{pmatrix} -1 & 0 & 0 & 0 \\ 0 & \dfrac{r}{r_s} - \dfrac{1}{4}\dfrac{s^2}{r^2} & \dfrac{s}{r_s}\sqrt{\dfrac{r_s}{r}} & 0 \\ 0 & \dfrac{s}{r_s}\sqrt{\dfrac{r_s}{r}} & \dfrac{r}{r_s} & 0 \\ 0 & 0 & 0 & \dfrac{\hbar^2}{4s^2}\dfrac{r}{r_s} \end{pmatrix}. \tag{5.28}$$

This effective metric both corrects the classical metric coefficients at order $O(\hbar)$ and extends the geometry to include the additional quantum degrees of freedom s, representing spatial spread, and q, the conjugate variable to the Casimir invariant of the second-moment algebra which provides a measure of the purity of the state.

The resulting geodesic equations generalize the classical case and now include quantum

backreaction terms

$$\ddot{t}_L + \frac{1}{2}\frac{\dot{\rho}^2}{cr_s}\left(\frac{2}{3}\frac{r_s}{\rho - ct_L}\right)^{5/3} + f_t(t_L, \rho, s, q, \dot{t}_L, \dot{\rho}, \dot{s}, \dot{q}) = 0\,, \tag{5.29}$$

$$\ddot{\rho} - \frac{1}{3}\frac{\dot{\rho}^2 - 2c\dot{t}_L\dot{\rho}}{\rho - ct_L} + f_\rho(t_L, \rho, s, q, \dot{t}_L, \dot{\rho}, \dot{s}, \dot{q}) = 0\,, \tag{5.30}$$

$$\ddot{s} + f_s(t_L, \rho, s, q, \dot{t}_L, \dot{\rho}, \dot{s}, \dot{q}) = 0\,, \tag{5.31}$$

$$\ddot{q} + 2\dot{q}\left(\frac{\dot{s}}{s} - \frac{1}{3}\frac{\dot{\rho} - c\dot{t}}{\rho - ct}\right) = 0\,. \tag{5.32}$$

Here, the functions f_t, f_ρ, and f_S, represent the leading-order quantum corrections and are of order $O(\hbar)$. Although their full expressions are lengthy, they can be derived explicitly either from the Hamiltonian equations of motion of the quantum Hamiltonian (5.37), or by computing the Christoffel symbols associated with the quantum-corrected inverse metric $g_{\mathcal{Q}}^{\bar{a}\bar{b}}$.

We now specify semiclassical initial data for numerically solving the geodesic equations of a quantum clock undergoing radial infall. We consider a minimally squeezed quantum state that is initially stationary in the Lemaître frame. The momenta–velocity relations derived from the quantum Hamiltonian $\mathrm{H}_{\mathcal{Q}}$ are

$$\dot{t} = \frac{1}{c}\frac{\partial \mathrm{H}_{\mathcal{Q}}}{\partial p_t} = \frac{p_t}{mc}\,, \tag{5.33}$$

$$\dot{\rho} = \frac{\partial \mathrm{H}_{\mathcal{Q}}}{\partial p_\rho} = -\left(\frac{r}{r_s} - \frac{1}{4}\frac{s^2}{r^2}\right)\frac{p_\rho}{m} - \frac{s}{r_s}\sqrt{\frac{r_s}{r}}\frac{p_s}{m}\,, \tag{5.34}$$

$$\dot{s} = \frac{\partial \mathrm{H}_{\mathcal{Q}}}{\partial p_s} = -\frac{s}{r_s}\sqrt{\frac{r_s}{r}}\frac{p_\rho}{m} - \frac{r}{r_s}\frac{p_s}{m}\,, \tag{5.35}$$

$$\dot{q} = \frac{\partial \mathrm{H}_{\mathcal{Q}}}{\partial p_q} = -\frac{r}{r_s}\frac{p_q\hbar^2}{4ms^2}\,. \tag{5.36}$$

The uncertainty relation (Eq. (2.49)) requires $p_q \geq 1$, implying from Eq. (5.36) that $\dot{q} \neq 0$. Physically, this reflects the fact that one cannot simultaneously localize both position and momentum arbitrarily precisely. If we may impose $\dot{\rho}_0 = \dot{s}_0 = 0$, corresponding to an initially stationary clock with minimal spatial squeezing, then a direct consequence of $\dot{q} \neq 0$ is that the classical condition $\dot{t}_L(0) = 1$ is inconsistent the proper time normalization enforced by the quantum Hamiltonian constraint.

Setting $p_q = 1$, the minimum value allowed by the uncertainty principle, fixes the initial value of $\dot{q}$ via Eq. (5.36). Imposing the constraint $\mathrm{H}_{\mathcal{Q}}$ at the initial point determines

the required value of p_{t_L}, and hence $\dot{t}_L(0)$. Explicitly, we evaluate

$$\mathrm{H}_{\mathcal{Q}}(0,\rho_0,s_0,0,p_{t_L0},0,0,1) = \frac{p_{t_L0}^2}{2m} - \frac{mc^2}{2} - \frac{r_0}{r_s}\frac{\hbar^2}{8ms^2} = 0 \tag{5.37}$$

$$\Rightarrow \quad p_{t_L0} = \sqrt{m^2c^2 + \frac{r_0}{r_s}\frac{\hbar^2}{4s^2}}\,. \tag{5.38}$$

The full initial conditions for the quantum trajectory are therefore

$$(t_L,\rho,s,q)(0) = (0,\rho_0,s_0,0) \tag{5.39}$$

$$(\dot{t}_L,\dot{\rho},\dot{s},\dot{q})(0) = \left(\sqrt{1+\frac{r_0}{r_s}\left(\frac{\hbar/2}{mcs}\right)^2},0,0,\frac{r_0}{r_s}\frac{\hbar^2}{4ms_0^2}\right) \tag{5.40}$$

where the initial radial coordinate r_0 is determined from ρ_0 via Eq. (5.8)

$$r_0 = \left(\frac{3}{2}\frac{\rho_0}{r_s}\right)^{2/3} r_s\,. \tag{5.41}$$

Motion outside of the Schwarzschild horizon requires $p_0 > \frac{2}{3}r_s$.

In contrast to the classical case—where a comoving clock remains synchronized with the proper time of a synchronous observer, as expressed in Eq. (5.20)—the quantum initial condition in Eq. (5.40) shows that $\dot{t}_L \neq 1$. While the observer's clock can be treated as a perfect classical timekeeper, the quantum clock exhibits differential gravitational time dilation across the spatial extent of its wave packet. As a result, the two clocks gradually desynchronize. If the quantum clock maintains coherence over a sufficiently long timescale, this desynchronization may become experimentally measurable.

It is important to emphasize that Eq. (5.40) specifies only initial conditions. In the adiabatic limit where the clock's spatial spread s is frozen ($\dot{s} = 0$), the geodesic equations (5.29)–(5.32) admit a trivial solution with $\dot{t}_L = \dot{\rho} = \dot{q} = 0$, consistent with the initial configuration. This implies that a finite-time extension of the initial conditions is possible in the frozen-spread regime.

To investigate dynamical effects and uncover nonlinear deviations from classical evolution, one may go beyond this limit. Because the equations are derived perturbatively, higher-order adiabatic corrections can be computed systematically. Alternatively, one can integrate the full quantum geodesic equations numerically. Such numerical solutions are shown in Figure 5.1.

The four panels display the dynamical evolution of: (top left) the differential time

dilation $\frac{\mathrm{d}t_L}{\mathrm{d}\tau} - 1$; (top right) anomalous tidal motion $\frac{\rho}{\rho_0} - 1$; (bottom left) tidal stretching $s = \sqrt{\Delta(\rho^2)}$; (bottom right) and uncertainty coordinate q.

Classically, the proper time of the in-falling clock matches the coordinate time ($\frac{\mathrm{d}t_L}{\mathrm{d}\tau} = 1$). In the quantum case, however, the initial velocity $\dot{q} \neq 0$ causes the clock to initially run slightly slower than its classical counterpart. As the clock falls inward, the quantum time dilation factor $\frac{\mathrm{d}t_L}{\mathrm{d}\tau}$ decreases and eventually drops below unity, indicating that proper time accumulates faster than coordinate time.

The geodesic equations in this section were derived under the assumption of non-relativistic motion. For the numerical solution shown in Figure 5.1, we have explicitly verified that the kinetic term $\gamma^{\rho\rho} p_\rho^2$ remains much smaller than m^2c^2 throughout the entire trajectory.

Quantum backreaction effects cause the clock to drift from its initial radial position, ρ_0, as shown by the small but growing deviation in $\rho(\tau)$. Meanwhile, the spatial fluctuation s increases monotonically throughout the evolution, consistent with the assumption of sustained coherence. This growth corresponds to a monotonic decrease in the conjugate coordinate q, as dictated by conservation of p_q.

By the time the quantum clock approaches the classical horizon, the magnitude of its spread s becomes comparable to the remaining distance to the singularity, emphasizing the breakdown of point-particle intuition. For comparison, Figure 5.2 presents the trajectory in the Schwarzschild–Droste radial coordinate $r(\tau)$. In the classical case, where $\rho(\tau) = \rho_0$, the function $r(\tau)$ reduces to $r(\tau) = \left(\frac{3}{2}\frac{\rho_0 - c\tau}{r_s}\right)^{2/3}$, which terminates with a cusp at the curvature singularity. The quantum clock's trajectory $\rho(\tau)$ and coordinate time $t_L(\tau)$ both differ from the classical case, resulting in a delayed arrival at the singularity.

5.1.1 General slicings

In our original work [12], we computed proper-time evolution for radial geodesics in nonsynchronous slicings of the Schwarzschild geometry. Building on that analysis, we now generalize the quantum Hamiltonian constraint to arbitrary observer frames while preserving the nonrelativistic (slow-speed) limit. This generalization reflects the coordinate freedom inherent in general relativity and allows us to investigate how quantum geodesic motion depends on the slicing—that is, on the frame of the observer making the measurement. The result is a more general expression for the quantum constraint than the one used in the previous discussion, as it incorporates arbitrary lapse N, shift N^r, and spatial metric component γ^{rr}, allowing the formalism to accommodate a wider class of spacetime slicings beyond the synchronous case.

$$\begin{aligned}
\mathrm{H}_{\mathcal{Q}}(x^0,\vec{x},p_0,\vec{p},\Delta^2()) &= \left(-\frac{1}{N^2}+\frac{s^2}{N^3}\frac{\partial^2 N}{\partial r^2}\right)p_0^2 \\
&+2\left[\frac{N^r}{N^2}+\frac{s^2}{N^2}\left(\frac{1}{2}\frac{\partial^2 N^r}{\partial r^2}-\frac{\partial^2 N}{\partial r^2}\frac{N^r}{N}\right)\right]p_r p_0 \\
&+\left[\gamma^{rr}-\frac{(N^r)^2}{N^2}+\frac{s^2}{N}\left(\frac{\partial^2 N}{\partial r^2}\frac{(N^r)^2}{N^2}-\frac{\partial^2 N^r}{\partial r\partial r}\frac{N^r}{N}+\frac{\partial N}{\partial r}\frac{\partial\gamma^{rr}}{\partial r}+\frac{N}{2}\frac{\partial^2\gamma^{rr}}{\partial r^2}\right)\right]p_r^2 \\
&+\frac{2}{N^2}\frac{\partial N^r}{\partial r}sp_s p_0+\frac{2}{N}\left(\frac{\partial}{\partial r}\left(N\gamma^{rr}\right)-\frac{\partial N^r}{\partial r}\frac{N^r}{N}\right)sp_s p_r \\
&+\frac{\gamma^{rr}}{N}\left(p_s^2+\frac{p_q^2\hbar^2}{4s^2}\right)+m^2c^2\,.
\end{aligned} \tag{5.42}$$

From this expression, the quantum inverse metric $g^{\bar{a}\bar{b}}_{\mathcal{Q}}$ can be read off

$$g^{\bar{a}\bar{b}}_{\mathcal{Q}}=\begin{pmatrix}
-\frac{1}{N^2}+\frac{s^2}{N^3}\frac{\partial^2 N}{\partial r^2} & \frac{N^r}{N^2}+\frac{s^2}{N^2}\left(\frac{1}{2}\frac{\partial^2 N^r}{\partial r^2}-\frac{\partial^2 N}{\partial r^2}\frac{N^r}{N}\right) & \frac{s}{N^2}\frac{\partial N^r}{\partial r} & 0 \\
\frac{N^r}{N^2}+\frac{s^2}{N^2}\left(\frac{1}{2}\frac{\partial^2 N^r}{\partial r^2}-\frac{\partial^2 N}{\partial r^2}\frac{N^r}{N}\right) & \gamma^{rr}_{\mathcal{Q}} & \frac{s}{N}\left(\frac{\partial}{\partial r}\left(N\gamma^{rr}\right)-\frac{\partial N^r}{\partial r}\frac{N^r}{N}\right) & 0 \\
\frac{s}{N^2}\frac{\partial N^r}{\partial r} & \frac{s}{N}\left(\frac{\partial}{\partial r}\left(N\gamma^{rr}\right)-\frac{\partial N^r}{\partial r}\frac{N^r}{N}\right) & \frac{\gamma^{rr}}{N} & 0 \\
0 & 0 & 0 & \frac{\gamma^{rr}}{N}\frac{\hbar^2}{4s^2}
\end{pmatrix} \tag{5.43}$$

where the quantum-corrected spatial component $\gamma^{rr}_{\mathcal{Q}}$ is given by

$$\gamma^{rr}_{\mathcal{Q}}=\gamma^{rr}-\frac{(N^r)^2}{N^2}+\frac{s^2}{N}\left(\frac{\partial^2 N}{\partial r^2}\frac{(N^r)^2}{N^2}-\frac{\partial^2 N^r}{\partial r\partial r}\frac{N^r}{N}+\frac{\partial N}{\partial r}\frac{\partial\gamma^{rr}}{\partial r}+\frac{N}{2}\frac{\partial^2\gamma^{rr}}{\partial r^2}\right)\,. \tag{5.44}$$

These expressions define the quantum extension of the ADM inverse metric, valid in any foliation of a $1+1$ spacetime. The quantum correction terms arise from second-order

spatial moments of the wave packet (s) and are of order $\hbar$. The structure remains pseudo-Riemannian but depends on quantum degrees of freedom, forming a geometric precursor to full quantum gravity.

5.1.2 Note on the use of published material

The remainder of this chapter reproduces content from Ref. [12] without modification. While this material remains relevant, its presentation does not fully reflect the insights and refinements developed in the earlier sections of this dissertation. Future work could revisit and revise these discussions to integrate them more fully into the framework established in Chapters 1–4.

5.2 Schwarzschild–Droste slicing

In the case of the standard Schwarzschild–Droste slicing of Eq. (5.1), the shift vector vanishes and this expression simplifies further

$$g_{\mathcal{Q}}^{\bar{a}\bar{b}} = \begin{pmatrix} -\frac{1}{N^2} + \frac{s^2}{N^3}\frac{\partial^2 N}{\partial r^2} & 0 & 0 & 0 \\ 0 & \gamma^{rr} + \frac{s^2}{2N}\left(N\frac{\partial^2\gamma^{rr}}{\partial r^2} + 2\frac{\partial N}{\partial r}\frac{\partial\gamma^{rr}}{\partial r}\right) & \frac{s}{N}\frac{\partial}{\partial r}\left(N\gamma^{rr}\right) & 0 \\ 0 & \frac{s}{N}\frac{\partial}{\partial r}\left(N\gamma^{rr}\right) & \frac{\gamma^{rr}}{N} & 0 \\ 0 & 0 & 0 & \frac{\gamma^{rr}}{N}\frac{\hbar^2}{4s^2} \end{pmatrix}. \quad (5.45)$$

An in-falling clock which was originally stationary at r_0 measures proper time at some $r < r_0$ given by

$$\tau_{\text{classical}}(r; r_0) = \frac{r_0}{c}\left[\sqrt{\frac{r_0}{r_s}}\arctan\left(\sqrt{\frac{r_0}{r} - 1}\right) + \frac{r}{r_s}\sqrt{\frac{r_s}{r} - \frac{r_s}{r_0}}\right]. \quad (5.46)$$

In the quantum-adiabatic limit, $\dot{s} = 0$, the solution to the geodesic equation gives nonclassical contributions to the elapsed proper time of

$$\begin{aligned}\tau_{\text{nonclassical}}(r; r_0) = \left(\frac{p_q\hbar}{2mcs}\right)^2 &\left(\left(1 - \frac{3}{2}\frac{r_s}{r_0}\right)\tau_{\text{classical}} + \frac{r}{c}\sqrt{\frac{r_s}{r} - \frac{r_s}{r_0}}\right) \\ &- \frac{1}{2}\frac{r_s}{c}\frac{s^2}{r_0^2}\left(\frac{1}{\sqrt{r_s/r - r_s/r_0}} + 3\frac{\sqrt{r_0/r}\arctan\left(\sqrt{r_0/r - 1}\right)}{1 - r_s/r_0} + \frac{2\text{arctanh}\left(\sqrt{\frac{r_0/r-1}{r_0/r_s-1}}\right)}{(1 - r_s/r_0)^{3/2}}\right)\end{aligned} \quad (5.47)$$

(compare with Eq. (4.12)). The terms in this expression are determined by partial derivatives of the classical metric that appear in (4.3), evaluated at the classical $r(\sigma)$ and then integrated over σ. In this quantum adiabatic approximation, s as well as p_q are determined by moments of the initial state (details in Appendix D).

This result highlights the general geometrical nature of the separation of proper time into classical and quantum contributions, found earlier for specific wave functions in [58], and it generalizes this property to any semiclassical state. Our parameterization in terms of p_q and s further shows that there are two separate contributions to the quantum term since leading order corrections scale with two competing effects. One, an effect that originates in the U-term and enforces the uncertainty principle (see [29]), is proportional to p_q^2 as well as the squared Compton wavelength of the state and tends to increase the proper time read by the clock. The second is a spatial delocalization effect proportional to the state's position variance s^2 and tends to decrease the time read by the clock. Notice the mass dependence of the first term, which is a sign of quantum violations of the equivalence principle as in [14].

This quantum effect on proper time of a clock depends on geometric properties of a single clock's (extended) worldline. For infinitesimal trajectories, one clock's proper time can be related to the time read by any other clock by time dilation formulas. We obtain these in our next discussion.

5.3 Corrections to gravitational time dilation from quantum geometry

The absence of a preferred time coordinate is a feature of general relativity, highlighting the theory's principle that the measurement of time is relative to the observer's frame of reference. Consequently, in the classical theory, two clocks, A and B, measure proper times τ_A and τ_B which disagree depending on their relative position and motion (but independently of other properties such as their masses or compositions).

We quantify the first-order difference in the rates of two clocks by a Lorentz factor

$$\frac{\mathrm{d}\tau_A}{\mathrm{d}\tau_B} = \gamma(x_A, x_B, v_A, v_B). \tag{5.48}$$

To write a coordinate expression giving the functional form of γ, it is necessary to choose a slicing of spacetime. Time dilation formulas therefore require three choices: the worldline of each of the two clocks and also a choice of coordinate slicing.

In relativity, it is common to align the slicing of spacetime with the reference frame

of one of the two clocks, reducing the complexity of the problem. This choice introduces an asymmetry: the motion and position of the clocks are no longer on equal footing. One clock becomes anchored in the coordinate system, while the other is defined relative to it. This asymmetry implies that, in general, there is no straightforward relationship between the coordinate expressions for $\mathrm{d}\tau_A/\mathrm{d}\tau_B$ and $\mathrm{d}\tau_B/\mathrm{d}\tau_A$.

By treating one of the clocks implicitly as the coordinate observer (or a global frame), the expression (5.48) represents the 0-component of the tangent 4-vector to the worldline of the other clock. If the second clock is freely-falling, then its tangent vector components are determined by the geodesic equation. In the classical theory, the geodesic Hamilton function, Eq. (3.15), produces two equations for the tangent vector components of radial geodesics:

$$\dot{t} = c\sqrt{|\det(g^{ab})|\frac{p_r^2}{m^2c^2} - g^{tt}} \tag{5.49}$$

$$\dot{r} = \frac{|\det(g^{ab})|p_r + g^{tr}\sqrt{|\det(g^{ab})|p_r^2 - m^2c^2g^{tt}}}{mg^{tt}}. \tag{5.50}$$

Equation (5.49) gives the time dilation factor as a phase space function. We can instead write it as a function on the tangent bundle (using velocity components) by solving the equation (5.50) for p_r and substituting. The solution for the classical time dilation factor obtained in this way has a surprising form which depends on the deparametrized velocity of the noncoordinate clock, denoted in two spacetime dimensions as

$$\frac{\dot{x}^a}{\dot{t}} = \frac{\mathrm{d}x^a}{\mathrm{d}t} = \left(c, \frac{\mathrm{d}r}{\mathrm{d}t}\right). \tag{5.51}$$

With this definition, solving the Hamiltonian geodesic equation yields

$$\gamma_{\text{classical}} = \frac{1}{\sqrt{-g_{ab}\frac{\mathrm{d}x^a}{\mathrm{d}t}\frac{\mathrm{d}x^b}{\mathrm{d}t}/c^2}}. \tag{5.52}$$

In the quantum-perturbed case, Hamilton's equations involve two additional tangent vector components:

$$\dot{s} = \frac{\partial H_{\mathcal{Q}}}{\partial p_s} \tag{5.53}$$

$$\dot{q} = \frac{\partial H_{\mathcal{Q}}}{\partial p_q}. \tag{5.54}$$

Still, an analogous result to (5.52) holds in the quantum theory if we make the substitution

$g_{ab} \to g^{\mathcal{Q}}_{\bar{a}\bar{b}}$ and use the deparametrized tangent-vector velocities

$$\frac{\dot{x}^{\bar{a}}}{\dot{t}} = \frac{\mathrm{d}x^{\bar{a}}}{\mathrm{d}t} = \left(c, \frac{\mathrm{d}r}{\mathrm{d}t}, \frac{\mathrm{d}s}{\mathrm{d}t}, \frac{\mathrm{d}q}{\mathrm{d}t}\right). \tag{5.55}$$

Indeed, the form of the result, Eq. (5.52), is determined directly from the constraint

$$L = -\frac{m}{2} g_{ab} \dot{x}^a \dot{x}^b + \frac{mc^2}{2} = mc^2. \tag{5.56}$$

The quantum dynamics are determined by a Lagrangian with the same form obeying the same constraint. Dividing both sides of the constraint by $\dot{t}$ and rearranging yields immediately the deparametrized time dilation formula

$$\frac{\mathrm{d}t}{\mathrm{d}\tau} \equiv \gamma = \frac{1}{\sqrt{-g^{\mathcal{Q}}_{\bar{a}\bar{b}} \frac{\mathrm{d}x^{\bar{a}}}{\mathrm{d}t} \frac{\mathrm{d}x^{\bar{b}}}{\mathrm{d}t}/c^2}}. \tag{5.57}$$

In the quantum-adiabatic limit when $\dot{s} = 0$ and neglecting the classical Doppler effect by setting $\dot{r} = 0$ produces the special case

$$\gamma = \gamma_{\text{classical}} + \gamma_{\text{nonclassical}} \tag{5.58}$$

where $\gamma_{\text{classical}}$ is the classical factor, Eq. (5.52), and the nonclassical contribution is

$$\gamma_{\text{nonclassical}} = \gamma^3_{\text{classical}} \left(\frac{g_{tt} g''_{tt} - 2(g'_{tt})^2}{g_{tt}} \right) \frac{s^2}{4} + \gamma^3_{\text{classical}} \left(\frac{\hbar}{2mcs} \right)^2 \frac{p_q^2}{2} \frac{g_{tt}}{\det g_{ab}} \tag{5.59}$$

Using the standard Schwarzschild slicing in which the line element takes the form:

$$g_{ab} \mathrm{d}x^a \mathrm{d}x^b = -\left(1 - \frac{r_s}{r}\right) c^2 \mathrm{d}t^2 + \frac{1}{1 - r_s/r} \mathrm{d}r^2 \tag{5.60}$$

gives

$$\gamma_{\text{classical}} = \frac{1}{\sqrt{1 - r_s/r_0}} \tag{5.61}$$

and

$$\gamma_{\text{nonclassical}} = \frac{1}{2} \frac{s^2}{r^2} \frac{r_s/r}{(1 - r_s/r)^{5/2}} + \frac{p_q^2}{2} \left(\frac{\hbar}{2mcs} \right)^2 \left(1 - \frac{r_s}{r}\right)^{1/2}. \tag{5.62}$$

The time dilation factor has quantum corrections which scale in the same way as the proper time corrections, Eq. (5.47). The first correction predicts that in a curved

spacetime a poorly localized clock experience greater dilation than a clock in a more localized state. This tidal effect can be realized classically by a finite-size oscillator clock. The second, proportional to $\hbar^2$, is strictly quantum mechanical and expected even in flat spacetime. It scales according to the ratio of the particle's Compton wavelength to the spatial extent of its wavefunction, as noted independently in [58].

The reference [58] obtained this quantum time-dilation effect from the Page-Wootters formalism applied to two clocks, A and B, in a superposition of momentum states. In [58] the dilation effect appears when one considers the probability that the first clock reads time τ_A conditioned on the clock B reading time τ_B. Our formalism produces a similar result: the coordinate τ measures the proper time of an in-falling clock, while t represents the proper time of the coordinate clock.

Time dilation depends on the choice of clocks, and nominally the Painleve-Gullstrand slicing in which the line element takes the form

$$g_{ab}\mathrm{d}x^a\mathrm{d}x^b = -\left(1-\frac{r_s}{r}\right)c^2\mathrm{d}t^2 + 2c\sqrt{\frac{r_s}{r}}\mathrm{d}t\mathrm{d}r + \mathrm{d}r^2. \tag{5.63}$$

implies a separate class of coordinate clocks. However, (5.63) gives the same form for the 00-component of the metric. Therefore the time-dilation prediction in the adiabatic, static case $\dot{r} = \dot{s} = 0$, given by (5.59) is identical to the Schwarzschild-slicing prediction.

The two slicings differ most near the classical horizon, where the metric functions exhibit significantly distinct behaviors. This suggests that nonclassical reference frame effects between these two cases will be most apparent in that regime.

5.4 Signature change

The spectrum of the metric tensor is denoted $\lambda(g_{ab}) = \{\lambda_0, \ldots, \lambda_n\}$. Proper orthochronous basis changes can rescale the eigenvalues but not alter their signs. Therefore, the metric signature, defined by the signs of the eigenvalues, is invariant. In general relativity, the metric tensor has a Lorentzian signature, represented in two spacetime dimensions by the tuple $(-,+)$. Such a Lorentzian-signature metric distinguishes between time-like, space-like, and light-like intervals.

The result (4.3) for the quantum effective metric predicts that quantum effects will shift the locations of the zeros and singularities of the metric functions. This has implications for the causal structure of spacetime experienced by a quantum object. We demonstrate these notions in the standard slicing of the Schwarzschild metric where the

eigenvalues of the inverse metric are:

$$\lambda_t = -\frac{1}{1 - r_s/r}, \tag{5.64}$$

$$\lambda_r = 1 - r_s/r. \tag{5.65}$$

For $r > r_s$, the eigenvalue corresponding to the first eigenvector is negative, while the eigenvalue for the second eigenvector is positive. Although the standard slicing leads to poorly defined coordinates at the Schwarzschild radius, continuing the coordinates beyond this point results in a flip in the signs of the eigenvalues. Because the eigenvalues flip signs at the same point, the signature of the metric is preserved, while the causal nature of the basis vectors is reversed.

Computing eigenvalues for the quantum-effective inverse metric in the standard slicing yields

$$\lambda_t^{\mathcal{Q}} = -\frac{1}{1 - r_s/r} - \frac{r_s/r}{(1 - r_s/r)^3}\frac{s^2}{r^2}, \tag{5.66}$$

$$\lambda_{r-s}^{\mathcal{Q}} = 1 - \frac{r_s}{r} - \frac{r_s s}{r^2} - \frac{r_s s^2}{2r^3}, \tag{5.67}$$

$$\lambda_{r+s}^{\mathcal{Q}} = 1 - \frac{r_s}{r} + \frac{r_s s}{r^2} - \frac{r_s s^2}{2r^3}, \tag{5.68}$$

$$\lambda_q = \frac{\hbar^2}{4s^2}\left(1 - \frac{r_s}{r}\right). \tag{5.69}$$

Positivity of the eigenvalue λ_q indicates that the quantum coordinate q is spacelike for $r > r_s$. However, due to the block diagonal form of $g_{\mathcal{Q}}^{\bar{a}\bar{b}}$, it plays no further role in the current discussion.

The remaining three eigenvalues collapse to the classical ones, (5.64) and (5.65), in the classical limit. For any s, the sign of the first eigenvalue flips from negative to positive at $r = r_s$, as in the classical case. The new quantum coordinate s splits the classical eigenvalue (5.65) into two distinct values, $\lambda_{r-s}^{\mathcal{Q}}$ and $\lambda_{r+s}^{\mathcal{Q}}$, which change signs at $r \approx r_s + s$ and $r \approx r_s - s$, respectively. Table 5.1 summarizes the global structure of signature change.

For states within their correlation distance of the classical horizon, the effective metric governing their geodesic motion has two time-like directions. Precise causal implications for states both far from the horizon and near the horizon can be captured by the local light-cone structure. We compute this light-cone structure in Section 5.6.

Before then we address the matter of signature change when the quantization is

	I	II	III	IV
$\lambda_t^{\mathcal{Q}}$	+	+	−	−
$\lambda_{r-s}^{\mathcal{Q}}$	−	−	−	+
$\lambda_{r+s}^{\mathcal{Q}}$	−	+	+	+
$\lambda_q^{\mathcal{Q}}$	−	−	+	+

Table 5.1: Eigenvalue signs of the inverse quantum metric $g_{\mathcal{Q}}^{\bar{a}\bar{b}}$ in the standard slicing of Schwarzschild metric, across four regions: Region I ($r \in (0, r_s - s)$), Region II ($r \in (r_s - s, r_s)$), Region III ($r \in (r_s, r_s + s)$), and Region IV ($r \in (r_s + s, \infty)$).

computed in a slicing adapted to the region near the horizon. The Painleve-Gullstrand slicing of the Schwarschild metric, Eq. (5.63), produces the eigenvalues

$$\lambda_t = -\frac{1}{2}\frac{r_s}{r}\left(\sqrt{1+4\frac{r^2}{r_s^2}}+1\right), \tag{5.70}$$

$$\lambda_r = +\frac{1}{2}\frac{r_s}{r}\left(\sqrt{1+4\frac{r^2}{r_s^2}}-1\right). \tag{5.71}$$

The signs of these eigenvalues remain unchanged across the classical horizon, with (5.70) staying timelike and (5.71) staying spacelike.

Quantization in these coordinates leads to an effective metric with eigenvalues

$$\lambda_t^{\mathcal{Q}} = \lambda_t + \left(\frac{\lambda_t(\lambda_t-1)}{\lambda_r + (r/r_s)(\lambda_t - \lambda_r - 2)}\right)\frac{s^2}{r^2}, \tag{5.72}$$

$$\lambda_r^{\mathcal{Q}} = \lambda_r + \left(\frac{\lambda_r(\lambda_r-1)}{\lambda_t + (r/r_s)(\lambda_r - \lambda_t - 2)}\right)\frac{s^2}{r^2}, \tag{5.73}$$

$$\lambda_0^{\mathcal{Q}} = 1 - \frac{r_s}{r} - \frac{r_s}{r}\left(1-\frac{r_s}{r}\right)\frac{s^2}{r^2}, \tag{5.74}$$

$$\lambda_q = \frac{\hbar^2}{4s^2}\left(1-\frac{r_s}{r}\right) \tag{5.75}$$

with λ_t and λ_r in these expressions given by (5.70) and (5.71). Corrections to the classical eigenvalues computed in this slicing do not cause sign changes in $\lambda_t^{\mathcal{Q}}$ and $\lambda_r^{\mathcal{Q}}$. The horizon structure therefore appears different in the two slicings considered here.

5.5 Volume element

The determinant of the metric, computed as the product of the eigenvalues, is a coordinate-dependent construction which plays an important role in the geometric theory. The

volume element in curved spacetime is given in terms of the metric determinant as

$$\mathrm{d}V = \sqrt{-\det g_{ab}}\,\mathrm{d}^4x \tag{5.76}$$

where the dimension four refers to the four classical spacetime coordinates, integrating over t, r, ϑ and φ in a spherically symmetric geometry.

The determinant of the inverse quantum metric (4.3) extends the classical metric determinant. Computing directly we find

$$\begin{aligned}\det\left(g^{\bar{a}\bar{b}}_{\mathcal{Q}}\right) = \Bigg[&\det\left(g^{ab}\right) + \frac{s^2}{2}\left(g^{rr}\det\left(g^{ab}\right)'' - 2g^{rr\prime}\det\left(g^{ab}\right)'\right)\\ &+ \frac{s^4}{4}\Big(g^{rr}\det\left(g^{ab\prime\prime}\right)4g^{rr\prime}g^{tr\prime}g^{tr\prime\prime}\\ &\quad - 2(g^{tr\prime})^2g^{rr\prime\prime} - 2(g^{rr\prime})^2g^{tt\prime\prime}\Big)\Bigg]\cdot\frac{\hbar^2 g^{rr}}{4s^2}.\end{aligned} \tag{5.77}$$

This expression introduces series corrections associated with quantum fluctuations and an overall scaling associated with the quantum uncertainty coordinate q.

The inverse of this determinant provides the volume element in four dimensions but only for radial motion, integrating over t, r, s and q. This manifold may be extended to include angular coordinates ϑ and φ as well as their canonical moment coordinates analogous to s and q for each degree of freedom. If all these values are included, we obtain a 10-dimensional volume element.

5.6 Lightcone slope

Causal structure is locally determined by the slope of light cones. Material objects, including clocks, follow time-like worldlines whose tangent vectors always remain within the lightcone at each point, indicating that they experience the passage of time. In Section 5.3, we argued that a freely falling clock's tangent vector is altered by its quantum state, and in Section 5.4, we demonstrated that quantum effects modify the lightcone structure. Here, we check if these predictions are consistent,leading to a generalized, state-dependent causal structure.

In the classical theory, the tangent vector components to a radial null curve, $V^a = (\dot{t}, \dot{r})$, satisfy

$$g_{ab}V^aV^b = 0. \tag{5.78}$$

This quadratic equation can be solved for the lightcone slope

$$\left(\frac{\mathrm{d}t}{\mathrm{d}r}\right)_{\text{lightcone}} := \frac{\dot{t}}{\dot{r}} = \frac{-g_{tr} \pm \sqrt{-\det\left(g_{ab}\right)}}{g_{tt}}. \tag{5.79}$$

In the Schwarzschild slicing, Eq. (5.60), the lightcone slope of in-falling and out-going lightrays is given by

$$\left(\frac{\mathrm{d}t}{\mathrm{d}r}\right)_{\text{lightcone}} = \pm\frac{1}{c}\frac{1}{1-r_s/r}. \tag{5.80}$$

In the same coordinates, a classical point particle in-falling from finite position r_0 has tangent vector components

$$\begin{aligned} \frac{\mathrm{d}t}{\mathrm{d}\tau} &= \frac{1}{1-r_s/r}\sqrt{1-\frac{r_s}{r_0}} \\ \frac{\mathrm{d}r}{\mathrm{d}\tau} &= -c\sqrt{\frac{r_s}{r}-\frac{r_s}{r_0}}. \end{aligned} \tag{5.81}$$

These tangent vector components determine the slope of the massive particle's worldline:

$$\left(\frac{\mathrm{d}t}{\mathrm{d}r}\right)_{\text{massive particle}} = \frac{\mathrm{d}t/\mathrm{d}\tau}{\mathrm{d}r/\mathrm{d}\tau} = -\frac{1}{c}\frac{1}{1-r_s/r}\sqrt{\frac{r}{r_s}}\sqrt{\frac{1-r_s/r_0}{1-r/r_0}}. \tag{5.82}$$

When $r > r_s$ the trajectory of a massive particle remains always within the lightcone:

$$\left|\frac{(\mathrm{d}t/\mathrm{d}r)_{\text{massive particle}}}{(\mathrm{d}t/\mathrm{d}r)_{\text{lightcone}}}\right| = \sqrt{\frac{r}{r_s}}\sqrt{\frac{1-r_s/r_0}{1-r/r_0}} > 1. \tag{5.83}$$

In the quantum-perturbed case, the particle's tangent vector components are modified by tidal and quantum uncertainty effects. For a massive clock with quantum fluctuation $s = \sqrt{\Delta(r^2)}$ freely falling from finite position r_0, the tangent vector components now satisfy

$$\frac{\mathrm{d}t}{\mathrm{d}\tau} = \frac{\sqrt{1-r_s/r_0}}{1-r_s/r}\frac{1+\frac{s^2}{r^2}\frac{r_s/r}{(1-r_s/r)^2}}{\sqrt{1+\frac{s^2}{r_0^2}\frac{r_s/r_0}{(1-r_s/r_0)^2}}}\left(1+\left(\frac{p_q\hbar}{2mcs}\right)^2\left(1-\frac{r_s}{r_0}\right)\right)^{1/2} \tag{5.84}$$

and

$$\frac{\mathrm{d}r}{\mathrm{d}\tau} = -c\sqrt{\frac{r_s}{r}-\frac{r_s}{r_0}} - \frac{c}{2}\Bigg[\sqrt{\frac{r_s}{r}-\frac{r_s}{r_0}}\times \left(\frac{s^2}{r^2(1-r_s/r)}+\frac{s^2}{r_0^2(1-r_s/r_0)}+\frac{s^2}{rr_0(1-r_s/r)(1-r_s/r_0)}\right) + \left(\frac{p_q\hbar}{2mcs}\right)^2\left(2-\frac{r_s}{r}-\frac{r_s}{r_0}\right)\sqrt{\frac{r_s}{r}-\frac{r_s}{r_0}} + 2\frac{r_s/r}{1-rs/r}\frac{s}{r}\frac{\dot{s}}{c} + \frac{1}{\sqrt{r_s/r-r_s/r_0}}\frac{\dot{s}^2}{c^2}\Bigg]. \tag{5.85}$$

In the adiabatic limit we assume that the motion occurs in the $t-r$ plane and set $\dot{s}=0$. Then these tangent vector components determine the slope of the massive particle's worldline as

$$\left(\frac{\mathrm{d}t}{\mathrm{d}r}\right)_{\text{massive particle}} = -\frac{1}{c}\frac{1}{1-r_s/r}\sqrt{\frac{r}{r_s}}\sqrt{\frac{1-r_s/r_0}{1-r/r_0}} \times\left[1-\frac{1}{2}\left(1-\frac{r_s}{r}\right)\left(\left(\frac{1}{(r_0-r_s)^2}+\frac{1}{(r-r_s)^2} + \frac{1}{(r_0-r_s)(r-r_s)}+\frac{(r-r_0)(r+2r_0-3r_s)r_s}{(r-r_s)^3(r_0-r_s)^2}\right)s^2+\left(\frac{p_q\hbar}{2mcs}\right)^2\right)\right]. \tag{5.86}$$

The lightcone slope in the $t-r$ plane is also modified by the perturbed metric functions. In the quantum-adiabatic limit where $ds=0$,

$$\left(\frac{\mathrm{d}t}{\mathrm{d}r}\right)_{\text{lightcone}} = \pm\frac{1}{c}\frac{1}{1-r_s/r}\pm\frac{r_s s^2}{cr^3\left(1-r_s/r\right)^3}. \tag{5.87}$$

The ratio of (5.86) to (5.87) yields the quantum generalization of the classical lightcone condition (5.83) as

$$\left|\frac{(\mathrm{d}t/\mathrm{d}r)_{\text{massive particle}}}{(\mathrm{d}t/\mathrm{d}r)_{\text{lightcone}}}\right| = \sqrt{\frac{r}{r_s}}\sqrt{\frac{1-r_s/r_0}{1-r/r_0}}\times \left(1-\frac{(r^2+r(r_0-2r_s)+(r_0-r_s)^2)}{r(r-r_s)(r_0-r_s)^2}\frac{s^2}{2}-\frac{1}{2}\left(\frac{p_q\hbar}{2mcs}\right)^2\left(1-\frac{r_s}{r}\right)\right). \tag{5.88}$$

When the massive particle state is localized well away from the horizon, the ratio of velocities is greater than one, indicating that quantum effects are consistent with an appropriately generalized notion of causal structure implied by the extended geometry. However, as the state approaches to within its correlation distance of the Schwarzschild radius, the particle velocity can exceed the limit set by the local lightcone. This anomolous behavior was suggested by the metric signature analysis in Section 5.4.

In this region, a closer analysis including higher adiabatic orders may shed more light on the dynamics, but a deeper understanding of space-time structure will likely be required too. The signature effects observed when r is close to r_s are caused by quantum fluctuations of a wave function that, heuristically, is spread out over a region that crosses the horizon. Even if the radial position is still greater than the Schwarzschild radius and we may be tempted to consider the Schwarzschild slicing valid, the support of a wave function includes radii less than the Schwarzschild radius as well as at this radius itself, where the coordinate system and the slicing break down. The varying signatures according to Table 5.1 are then seen as an implication of a wave function that simultaneously experiences a spacelike r (outside of the Schwarzschild radius) and a timelike r (inside). As derived, these effects become relevant when $r \approx r_s \pm s$, just when the main support of the wave function reaches the classical position of the horizon. The horizon structure and, as seen in (5.88), the causal structure then become unsharp or, from the perspective of Riemannian geometry, ill-defined.

These observations have an important implication for quantum reference frames in spacetime. From the formal perspective of reference frames, it would be allowed to use t as a reference variable for relational evolution if t is timelike (outside of the horizon) or when t is spacelike (inside), in both cases a mathematical relationship $r(t)$ is strictly determined by initial conditions. However, our example demonstrates that quantization of such a function is not guaranteed to be compatible with causal properties of spacetime. From the perspective of physical observables, a key problem is that only the outside t can be related to an observer (an asymptotic one at large fixed radius) while this observer does not have access to the inside t, and there is no stationary observer in the interior that could measure t there. It is therefore important to develop a systematic role of spacetime structure in the general theory of quantum reference frames, at least in cases in which they are applied to gravitational systems. In this context, it is important to note perhaps related obstructions to covariance in models of time as a quantum reference frame with position-dependent momentum terms in the Hamiltonian constraint [15, 26, 59].

A breakdown of covariance does not necessarily constitute an inconsistency in quantum

reference frames. More likely, it would just mean that different choices of quantum reference frames (such as a stationary clock some distance from the horizon, compared with a freely falling clock) constitute physically distinct setups of experiments, and therefore may well predict different measurement outcomes. The main question is how much of the resulting physics can still be described geometrically within a meaningful setting of spacetime.

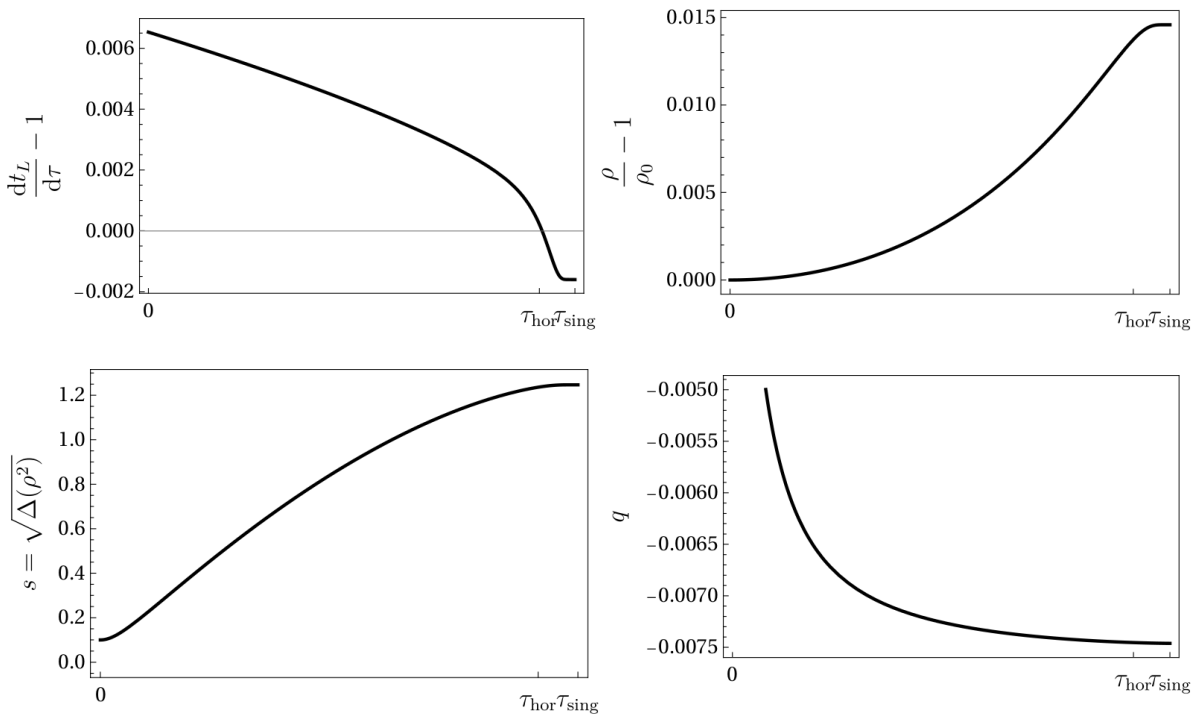

Figure 5.1: Geodesic motion of a radially in-falling quantum clock in the Lemaître slicing of Schwarzschild spacetime. A classical Lemaître observer records the spacetime location of a clock by noting the time t_L and radial coordinate ρ. In order to specify the state of a quantum clock, the observer must in addition specify the fluctuation coordinate $s = \sqrt{\Delta(\rho^2)}$ and the entropy of the clock, parametrized by q. The formalism developed in the main text allows these variables to be treated on equal footing within an extended quantum spacetime geometry. The clock is initialized in a minimally squeezed Gaussian state with no center-of-mass velocity at finite radius. It evolves according to the quantum geodesic equations (5.29)–(5.32), which govern motion on the quantum-corrected geometry. Initial conditions for the numerical integration are: $\rho_0 = 8r_s$, $\dot{\rho}_0 = 0$, $s_0 = 0.1r_s$, and $\dot{s}_0 = 0$. The initial value of $\dot{q}$ is determined from Eq. (5.36) with $p_q = 1$, and $\dot{t}_L(0)$ is fixed by enforcing the Hamiltonian constraint $\mathrm{H}_{\mathcal{Q}} = 0$. Units are defined so that $r_s = 1$, $c = 1$, and $\hbar = 0.01$. Because the quantum equations violate the weak equivalence principle, we fix the clock mass to $m = 1$. The horizontal axes indicate the classical proper time of horizon crossing and the time of arrival at the curvature singularity.

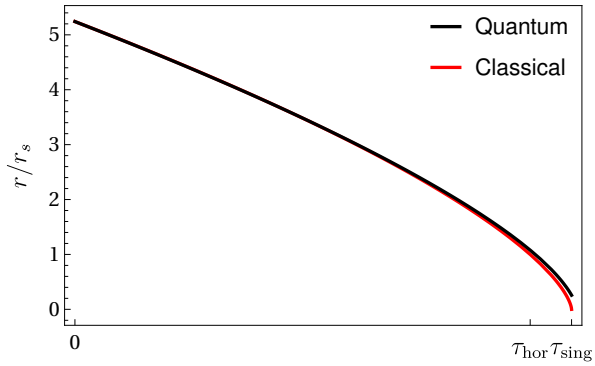

Figure 5.2: Radial coordinate evolution $r(\tau)$ of a quantum clock undergoing geodesic infall, plotted using the Schwarzschild–Droste radial coordinate defined in Eq. (5.8). This curve is obtained by applying the coordinate transformation to the quantum trajectory shown in Figure 5.1. Although the clock's motion was originally computed in Lemaître coordinates, this plot presents the corresponding trajectory in the more familiar Schwarzschild radial coordinate for comparison. The classical solution in these coordinates terminates in a cusp at the singularity; the quantum trajectory, by contrast, arrives slightly later due to quantum backreaction.

Chapter 6
Experimental outlook and testable predictions

. . . The numerical interpretation . . . is however necessary. . . . So long as it is not obtained, the solutions may be said to remain incomplete and useless, and the truth which it is proposed to discover is no less hidden in the formulae of analysis than it was in the physical problem itself.

—Joseph Fourier
The Analytic Theory of Heat

In this chapter, we collect the most promising predictions of the formalism for validation in near-term experiments. Although experimental physics has achieved remarkable precision in both gravitational and quantum domains independently, the longstanding goal of probing systems that simultaneously exhibit quantum and gravitational features remains largely unrealized.

Naturalness arguments, reviewed in [60], suggest that direct experimental access to quantum features of the spacetime metric is unlikely in the near future—though indirect signatures may be accessible through high-precision cosmological observations, such as those of the cosmic microwave background [61, 62]. An alternative and more tractable program involves generating and controlling quantum matter states that evolve within, or even source, gravitational fields [63]. Within this framework, feasible experimental tests include: modifications to particle dispersion relations (Sec. 6.1), violations of the universality of free fall (Sec. 6.2), anomalies in gravitational scattering return times (Sec. 6.3), and phase shifts in atom interferometry from quantum propagation effects (Sec. 6.4).

6.1 Modified dispersion relations

Most observable consequences of the quantum-gravitational effects discussed in this work arise from quantum-induced modifications to the kinematical properties of matter and radiation. These kinematical properties are governed by dispersion relations, which describe how energy and momentum are related for a given particle species. Quantum corrections to these relations can lead to measurable deviations from classical behavior, particularly in high-precision or long-baseline experiments. In this section, we derive modified dispersion relations for both nonrelativistic quantum matter and ultrarelativistic particles, including radiation, by analyzing quantum fluctuations in the Hamiltonian constraint.

In the nonrelativistic (slow-speed) limit, quantum fluctuations in the constraint $\mathrm{H}_{\mathcal{Q}}$, given in Eq. (4.1), lead to the modified dispersion relation

$$\left(g^{ab}+\frac{1}{2}\Delta(x^k x^l)\frac{\partial^2 g^{ab}}{\partial x^k \partial x^l}\right)p_a p_b + g^{ij}\Delta(p_i p_j) + \frac{\partial g^{aj}}{\partial x^k}p_a \Delta(x^k p_j) + m^2c^2 = 0. \tag{6.1}$$

In a region of weak gravitational field, where $g_{ab} \approx \eta_{ab}$ is close to the Minkowski metric, corrections containing the metric derivative become negligible and the mass-shell condition simplifies to

$$p_0^2 = |\vec{p}|^2 + \delta^{ij}\Delta(p_i p_j) + m^2c^2. \tag{6.2}$$

This expression indicates that quantum fluctuations contribute additively to the energy. As a result, even a particle that is classically at rest acquires a "zero-point" energy due to the momentum dispersion $\Delta(p_i p_j)$.

This motivates the interpretation of the fluctuation term as a quantum correction to the rest mass, through the definition of an effective mass

$$m_{\mathrm{eff}}^2 c^2 \coloneqq m^2c^2 + \delta^{ij}\Delta(p_i p_j), \tag{6.3}$$

For massless particles, the nonrelativistic approximation breaks down. In this case, one must refer to the full relativistic Hamiltonian constraint in Eq. (3.85) to identify corrections to the dispersion relation. In the weak-field limit, the dispersion relation becomes

$$p_0^2 = \delta^{ij}p_i p_j + \delta^{ij}\Delta(p_i p_j) + m^2c^2 - \frac{\delta^{il}\delta^{jk}p_i p_j \Delta(p_k p_l)}{\delta^{uv}p_u p_v + m^2c^2}\,. \tag{6.4}$$

The massless limit of this relation is

$$\omega^2 = \delta^{ij}\left(k_i k_j + \Delta(k_i k_j)\right) - \frac{\delta^{il}\delta^{jk}k_i k_j \Delta(k_k k_l)}{\delta^{uv}k_u k_v}\,. \tag{6.5}$$

which implies that even for classically massless fields (such as photons or gravitational waves) quantum fluctuations in momentum induce effective mass-like behavior. This opens the possibility of experimentally probing quantum corrections to dispersion in systems traditionally modeled as massless.

These modified dispersion relations have important implications for experimental tests of fundamental physics. While no deviation from the standard relativistic dispersion relation has yet been observed, several upcoming experiments are approaching the sensitivity required to detect such effects. The fluctuation term $\delta^{ij}\Delta(p_i p_j)$ scales as $\hbar^2/\sigma^2$, where σ characterizes the spatial spread of the wave packet. This implies that systems prepared in squeezed or engineered quantum states—where fluctuations can be enhanced—offer promising platforms for amplifying the predicted deviations.

High-precision atomic clocks based on alkaline-earth-like atoms, such as ^{24}Mg, are currently being developed with the goal of detecting fluctuation- or mass-dependent frequency shifts. As demonstrated in [13], such systems could offer a test of the fluctuation-induced time dilation effects derived in Chapter 5.

For freely propagating quantum particles—such as ultra-cold atoms in time-of-flight measurements or photons in long-baseline interferometers—the effective dispersion relation modifies the arrival time as a function of the initial wave packet profile. In particular, experiments that systematically vary the wave packet width, squeezing, or correlations can probe these effects. Several such experimental programs are underway globally. A prominent example is the Matter-wave Atomic Gradiometer Interferometric Sensor (MAGIS-100), currently under construction at Fermilab. Designed as a 100-meter atom interferometer, MAGIS-100 will test quantum coherence over macroscopic scales in the presence of gravity and is explicitly aimed at probing new physics at the intersection of quantum mechanics and general relativity [64].

At astrophysical scales, even minuscule modifications to the dispersion relation may accumulate into measurable effects for photons or gravitational waves traveling cosmological distances. Deviations could manifest as frequency-dependent time delays or distortions in pulse profiles. Although many of these studies are presently focused on constraining Lorentz invariance violations, fluctuation-induced dispersion relations may contribute subleading effects, potentially distinguishable in high-resolution multi-

messenger astrophysical observations. In particular, Finslerian modifications of spacetime geometry have been explored in the context of ultra-high-energy cosmic rays and the Greisen–Zatsepin–Kuzmin (GZK) cutoff [52], highlighting a concrete observational avenue for testing such geometric generalizations.

6.2 Eötvös parameter

Gravitational fields arising from matter sources exhibit inhomogeneity. In the Newtonian framework, inhomogeneity corresponds to nonlinear potentials. Quantum effects backreact on the classical degrees of freedom only when the second derivative $d^2\Phi/dx^2$ becomes dependent on x. However, accurately characterizing the source mass distribution with sufficient resolution to resolve the field structure to this order it is challenging. (A recent experiment by Overstreet et al. in [65] presents an intriguing counterexample, where deliberate efforts were made to precisely characterize the source mass distribution.) A simpler test, albeit with less far reaching implications, emerges from the consequence that the weak-field geodesic equation predicts a universal acceleration for all objects regardless of the specific geometry. This observation leads to a class of experiments known as Eötvös experiments. These experiments are designed to constrain the normalized differential acceleration between two objects, expressed as:

$$\eta(1,2) = \frac{a_1 - a_2}{\bar{a}}. \tag{6.6}$$

In this definition $\bar{a} = \frac{a_1+a_2}{2}$ represents the average acceleration, and the quantity η is referred to as the Eötvös parameter.

In general relativity, the geodesic equation, or its weak-field limit

$$\frac{d^2x^i}{dt^2} = \frac{1}{2}\frac{\partial h_{00}}{\partial x_i}\,, \tag{6.7}$$

predicts $\eta(1,2) = 0$ identically for any two objects even when their masses differ, $m_1 \neq m_2$. In a sense, general relativity is constructed as a geometric theory of gravity with the explicit aim reach of arriving at this conclusion. Modern extensions to the standard model and general relativity typically anticipate some deviation from this classical prediction. Consequently, the parameter η serves as a valuable model-independent framework for quantifying violations of the weak equivalence principle. We are particularly interested in whether quantum effects lead to $\eta \neq 0$ and, if so, at what level these effects become significant.

Our canonical effective methods provide direct predictions for quantum corrections to the acceleration of a quantum state in a nonuniform gravitational field. The dynamics are determined via the Hamilton function

$$H\left(x,p,s,p_s\right)=\frac{p^2}{2m}+\frac{p_s^2}{2m}+m\Phi_{\text{eff}}(x,s) \tag{6.8}$$

with the quantum-gravitational potential

$$\Phi_{\text{eff}}(x,s)=\Phi(x)+\frac{1}{2}\frac{d^2\Phi}{dx^2}s^2+\frac{1}{8}\left(\frac{\hbar}{m}\right)^2\frac{1}{s^2}. \tag{6.9}$$

The equations of motion for x and s in terms of the gravitational field strength $g(x)\equiv\Phi'$ are

$$\ddot{x}=-g-\frac{1}{2}\partial_x^2 g\, s^2 \tag{6.10}$$

$$\ddot{s}=-\partial_x g\, s+\left(\frac{\hbar}{m}\right)^2\frac{1}{4s^3}. \tag{6.11}$$

We read off the anomalous center of mass acceleration

$$\left|\frac{d^2}{dt^2}\langle\hat{x}\rangle-(-g(\langle\hat{x}\rangle))\right|=\frac{1}{2}\partial_x^2 g\,\Delta(x^2). \tag{6.12}$$

The center of mass acceleration deviates from the local gravitational field acceleration when both the width of the state and the gravitational field strength curvature are non-vanishing. Although this is the outcome expected from classical tidal forces acting on extended objects in an inhomogeneous field, our canonical formulation is more general because it provides also the dynamics of $s=\sqrt{\Delta(x^2)}$. In particular, the final value of the anomalous acceleration depends on the value of s which is plainly mass-dependent because m appears explicitly in $\ddot{s}$. The origin of the mass-dependence lies ultimately in the quantum requirement to preserve the uncertainty product, which is defined for moments of x together with p, rather than $\dot{x}$.

We estimate the Eötvös parameter for a delocalized quantum particle as compared to a more localized particle as

$$\eta\approx g^{-1}\left|\frac{d^2}{dt^2}\langle\hat{x}\rangle-(-g(x))\right|=\frac{1}{2}g^{-1}\partial_x^2 g\,\Delta(x^2) \tag{6.13}$$

Parameter values suitable for terrestrial experiments are $g\approx 10\,\text{m/s}^2$ and $\partial_x^2 g\approx$

$10^{-12}/\text{ms}^2$ however the wave packet width $\Delta(x^2)$ is not independently well constrained by experiment. Equation (6.13) indicates a range of values for η from $\eta \approx 0.5 \times 10^{-33}$ when the wave packet width is atomic scale ($s \approx 10^{-10}$ m) to $\eta \approx 0.5 \times 10^{-13}$ when the wave packet width approaches the arm-length of typical interferometers ($s \approx 1$ m). This latter value is within the sensitivity range of proposed atom-interferometers [66–69] and it is possible that proposed future experiments including km-scale underground tests, and space based atom interferometers could reach these dimensions.

Inverting the above reasoning with the experimental constraints of state-of-the-art atom interferometers which have resolutions of nearly $10^{-11}g$ [70] requires the wave packet width to remain bounded

$$s = \sqrt{\Delta(x^2)} \lesssim 10\,\text{m}. \tag{6.14}$$

6.3 Gravitational scattering return time

In [71, 72] Davies considered the possibility that the quantum dynamics of a particle may allow its time of flight to differ systematically from the classical prediction by travelling beyond the classical turning point into the forbidden region of the gravitational potential. Perhaps surprisingly, Davies found no evidence for tunneling delay. Instead, the particle return time adheres to the classical prediction in gravitational fields which are at most quadratic in position and provided that the particle is measured far from the classical turning point. This result does not challenge the status of the weak equivalence principle for quantum phenomena. However, stationary state analysis of quantum objects tunneling into the classically forbidden region of a potential gives only limited insight into the dynamical problems encountered, particularly in the context of interferometer experiments.

The equations of motion (6.10) and (6.11) indicate that for low order gravitational potentials where $\partial_x^2 g$ vanishes, the classical degrees of freedom decouple from the quantum degrees of freedom. It follows directly then that the measured return time for a wave packet in linear or quadratic potentials is identical to that of a classical point particle in agreement with the stationary state calculations of [71, 72]. For higher order potentials $\partial_x^2 g$ does not vanish and instead couples the spreading motion of the wave packet to the motion of its center of mass. This outcome was anticipated by [30] and [73], but neither provided quantitative calculations, which would be quite challenging if based on wave functions.

Estimating an out-and-back time of flight prediction requires integrating the equations

of motion. To do so, we specialize to the case of a Newtonian potential where the effective Hamilton function is

$$H(r,p,s,p_s) = \frac{p^2}{2m} + \frac{p_s^2}{2m} + \frac{U}{2ms^2} - \frac{GMm}{r} - \frac{GMm}{r^3}s^2. \tag{6.15}$$

It can be seen here that the classical Newtonian potential energy has a power law correction of the form

$$V(r) = -\frac{GMm}{r}\left[1 + \alpha_N \left(\frac{r_0}{r}\right)^{N-1}\right] \tag{6.16}$$

with $N = 3$, $\alpha_3 = 1$, and $r_0 = s$. Power law modifications of this form have previously been studied. In the context of extensions to the standard model, the case $N = 3$ can be considered as arising from the simultaneous exchange of two massless pseudoscalar particles [74]. A powerlaw correction with $N = 3$ also arises from the model of Randall and Sundrum [75] where non-compact warped extra dimensions with warping scale r_0 are considered. If there are indeed Yukawa-style couplings present, then the finite-width effects that we discuss here could confound their detection.

Choosing an arbitrary length scale equal for example to the earth radius, $r_c = r_e$ and corresponding time, energy, and momentum scales as

$$t_c = \sqrt{\frac{r_e^3}{GM}} \tag{6.17}$$

$$E_c = p_c\frac{r_c}{t_c} = \frac{GMm}{r_e} \tag{6.18}$$

gives the non-dimensional Hamilton function and equations of motion

$$H(r,p,s,p_s) = \frac{p^2}{2} + \frac{p_s^2}{2} + \frac{u}{2s^2} - \frac{1}{r} - \frac{s^2}{r^3} \tag{6.19}$$

$$\begin{aligned} \ddot{r} &= -\frac{1}{r^2}\left(1 + \frac{3s^2}{r^2}\right) \\ \ddot{s} &= \frac{u}{s^2} + \frac{2s}{r^3} \end{aligned} \tag{6.20}$$

Unlike the classical case where all free parameters may be scaled out, here a free parameter remains which depends on the particle mass

$$u = \frac{\hbar^2/4}{r_c^2 p_c^2} = \frac{\hbar^2/4}{GMm^2 r_e}. \tag{6.21}$$

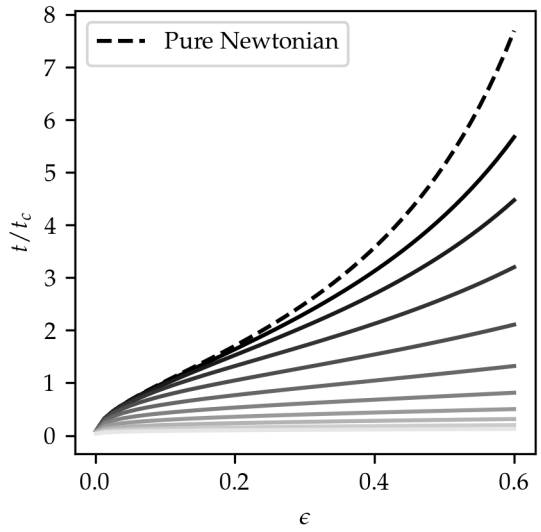

Figure 6.1: Particle return time. The dashed line plots the out-and-back return time for a classical point particle in Newtonian $1/r$ gravity. The behavior for small energy is quadratic as predicted from the linear potential result $t = \sqrt{\epsilon}$. At higher energy the return time grows until it diverges at the classical escape energy $\epsilon = 1$. The solid lines represent the return time for a particle obeying the perturbed equations of motion (6.20) for $u \in (10^{-5}, 1)$. These are generically lower than the unperturbed result and approach the classical result as $u \to 0$.

This parameter reflects the minimal uncertainty product compared to the scale of the problem. The same effect could be had in identifying characteristic length (r_c) and momentum (p_c) scales and rescaling $\frac{1}{2}\hbar \to \frac{1}{2}\hbar/(r_c p_c) = \frac{1}{2}\tilde{\hbar}$ such that the canonical commutation relation is dimensionless. Such a phrasing, however useful, tends to obscure the mass-dependence of the relation because it implies an m-dependent, non-fundamental $\tilde{\hbar}$.

The uncertainty-product enforcing term becomes important when the wave packet is very narrow compared to $\sqrt{u}$ in which case the wave packet is forced to expand but for terrestrial experiments, u is entirely negligible. For a neutron moving in the earth's gravitational field near the mean earth radius the numerical value is $u \approx 10^{-36}$ while for a 10 gram mass in the same conditions $u \approx 10^{-86}$. Without this term the resulting trajectory is the one predicted from classical tidal effects only and is not mass-dependent. This aligns with the thinking that existing atom interferometers are essentially classical in their operation. The main perturbation to the center of mass trajectory of a wave packet will come from tidal effects and not quantum effects owing to the uncertainty principle.

Figure 6.1 presents typical return time curves from numerical integration of the equations of motion for particles whose classical component of the energy is

$$\epsilon = \frac{p^2}{2} - \frac{1}{r}. \tag{6.22}$$

The total energy of the particle is still given by equation (6.19). In an experiment, the choice of initial conditions depends on the preparation of the state. The ability to discriminate the total energy of the particle from its classical initial conditions may complicate the return time–energy dependence. Here it is evident that a wave packet prepared at a given height and velocity returns quicker than an identically prepared point particle. The effect is most pronounced in the non-linear regime, a result in agreement with our earlier discussion.

6.4 Propagation phase in interferometry

In 1924, Louis de Broglie introduced a groundbreaking concept through his work [76], suggesting that massive particles possess wave-like characteristics. These wave properties can be understood within the framework of wave functions, where they stem from the polar decomposition described by equation (B1). A consequence of this description is interference of wave components. A simple example is the interference of two wave function components of equal magnitude where the resulting probability of measuring a particle depends on the relative phase of the two components via

$$|\exp(i\theta_1) + \exp(i\theta_2)|^2 = 2 + 2\cos(\theta_1 - \theta_2). \tag{6.23}$$

Equation (6.23) and its dependence on the phase difference $\delta\theta = \theta_1 - \theta_2$ is an example of an interference effect typically ascribed to wave phenomena.

The field of matter wave interference has matured significantly over time and atom interferometer experiments now play a crucial role in a variety of fundamental research endeavors. In this section, we describe how we can gain insights into interference by examining quantum moments. This goal begins with relating quantum moments to the phase difference between spacetime points, denoted $\theta(x_f, t_f) - \theta(x_i, t_i)$. This quantity is known as the propagation phase of a single wave function component. It is defined rigorously only in the wave function formalism. Nonetheless, we previously described how to determine a position-dependent phase from moments and separately explained the time dependence of these moments. In this section, we bring these concepts together

to describe the evolution of the phase along a spacetime trajectory.

As a point of comparison, we first review the approach for calculating the propagation phase presented in [77] based on Feynman path-integral techniques. Other approaches, based on evolving plane waves ([30]) and Gaussian wave packets ([78]) have also been described. These however produce predictions for the phase shift which agree with the semiclassical approach at the level of experiment; see [79].

6.4.1 Path integral method

In an approach based on the path integral, we consider a state prepared in the wave function state $\psi(x_i, t_i)$. The quantum evolution of this state is given by the propagator formula

$$\psi(x_f, t_f) = \int dx_i K(x_f, t_f, x_i, t_i)\psi(x_i, t_i). \tag{6.24}$$

The path integral method uses Feynman's expression for the quantum propagator, in which the propagator is represented as a sum over paths Γ connecting the spacetime points (x_f, t_f) and (x_i, t_i) according to

$$K(x_f, t_f, x_i, t_i) = \mathcal{N} \sum_{\Gamma} \mathrm{e}^{\frac{i}{\hbar} S_\Gamma}. \tag{6.25}$$

In this equation, S_Γ represents the action along the path Γ.

Storey and Cohen-Tannoudji [77] prove that when the system Lagrangian is quadratic, the quantum propagator (6.25) can be simplified as

$$K(x_f, t_f, x_i, t_i) = F(t_f, t_i) \exp\left(\frac{i}{\hbar} S_{\mathrm{cl}}(x_f, t_f, x_i, t_i)\right). \tag{6.26}$$

In this equation $S_{\mathrm{cl}}(x_f, t_f, x_i, t_i)$ represents the action along the classical path connecting (x_f, t_f) and (x_i, t_i). When we substitute this expression into equation (6.24), we obtain:

$$\psi(x_f, t_f) = F(t_f, t_i) \int dx_i \exp\left(\frac{i}{\hbar} S_{\mathrm{cl}}(x_f, t_f, x_i, t_i)\right) \psi(x_i, t_i). \tag{6.27}$$

In the quadratic case, the classical action is a quadratic function of x_f and x_i. Therefore, for certain initial states including plane wave and Gaussian states, this integral can be solved in closed form. For a plane wave initial state

$$\psi(x_i, t_i) = \frac{1}{\sqrt{2\pi\hbar}} \exp\left[\frac{i(p_0 x_i - E_0 t_i)}{\hbar}\right]. \tag{6.28}$$

In this case, the phase of the integrand is stationary when

$$\frac{\partial S_{\mathrm{cl}}}{\partial x_i} + p_0 = 0. \tag{6.29}$$

Since S_{cl} is quadratic, equation (6.29) is a linear equation for the stationary phase point $x_{i,\mathrm{stationary}} \equiv x_0$. The expansion of the classical action around this point is given by

$$S_{\mathrm{cl}}(x_f, t_f, x_0 + \zeta, t_i) = S_{\mathrm{cl}}(x_f, t_f, x_0, t_i) - p_0\zeta + C(t_f, t_i)\zeta^2. \tag{6.30}$$

In this expression, we used equation (6.29) to replace the first derivative of the action with the negative plane wave momentum. We also introduced the second derivative $\partial^2 S_{\mathrm{cl}}/\partial x_i^2 \equiv C(t_f, t_i)$, which is assumed to be independent of x_f and x_i. Following these adjustments, the integral (6.27) becomes straightforward to evaluate, yielding the result:

$$\psi(x_f, t_f) = F(t_f, t_i)\sqrt{\frac{i\pi\hbar}{C(t_f, t_i)}}\psi(x_0, t_i)\exp\left(\frac{i}{\hbar}S_{\mathrm{cl}}(x_f, t_f, x_0, t_i)\right). \tag{6.31}$$

From this expression we read off the propagation phase accumulated between spacetime points as

$$\theta(t_f, x(t_f)) - \theta(t_i, x(t_i)) = \frac{1}{\hbar}\int_{t_i}^{t_f} L_{\mathrm{classical}}(x, \dot{x})dt. \tag{6.32}$$

The classical Lagrangian $L_{\mathrm{classical}}(x, \dot{x})$ is treated as a function of time once we specify the classical trajectory $x(t)$.

6.4.2 Moment method

In the moment approach we obtained the reconstruction formula for the phase derivative $d\theta/dx$. Considering now the phase as a function of space and time, $\theta = \theta(x, t)$, it is appropriate to consider the reconstruction formula (B13) as providing the partial derivative with respect to position appearing in the differential

$$\mathrm{d}\theta = \frac{\partial\theta}{\partial x}\mathrm{d}x + \frac{\partial\theta}{\partial t}\mathrm{d}t. \tag{6.33}$$

Both of the partial derivatives may depend on the coordinates x and t. For example, the second order Hermite reconstruction depends explicitly on the position coordinate from equation (B20)

$$\frac{\partial\theta}{\partial x} = \frac{\langle\hat{p}\rangle}{\hbar} + (x - \langle\hat{x}\rangle)\frac{\Delta(xp)}{\hbar\Delta(x^2)}. \tag{6.34}$$

With this equations of motion for the moments supplied, this becomes also a function of time, $\partial\theta/\partial x = \partial\theta/\partial x(x,t)$. If the phase where genuinely a multivariate function, then to determine the phase difference between two spacetime points from differential data would require a line integral of the differential (6.33)

$$\theta(x_f,t_f) - \theta(x_i,t_i) = \int_\gamma \left(\frac{\partial\theta}{\partial x}\mathrm{d}x + \frac{\partial\theta}{\partial t}\mathrm{d}t\right) \tag{6.35}$$

where γ is a path connecting the spacetime points (x_f,t_f) and (x_i,t_i). We can define the path arbitrarily by a parametrization $\gamma : [\tau_i,\tau_f] \to \mathbb{R}^2, \gamma(\tau) = (x_\gamma(\tau), t_\gamma(\tau))$ where we require the coordinate functions satisfy $x_\gamma(\tau_{i/f}) = x_{i/f}$ and $t_\gamma(\tau_{i/f}) = t_{i/f}$. That is, we compute the parametrized line integral

$$\theta(x_f,t_f) - \theta(x_i,t_i) = \int_{\tau_i}^{\tau_f} \left(\frac{\partial\theta}{\partial x}\left(x_\gamma(\tau),t_\gamma(\tau)\right)\frac{\mathrm{d}x_\gamma}{\mathrm{d}\tau} + \frac{\partial\theta}{\partial t}\left(x_\gamma(\tau),t_\gamma(\tau)\right)\frac{\mathrm{d}t_\gamma}{\mathrm{d}\tau}\right)\mathrm{d}\tau \tag{6.36}$$

There are some difficulties in this approach. For one, the moment data does not directly constrain the partial derivative $\partial\theta/\partial t$. However, if we require that the result obtained be independent of the integration path, then the mixed partial condition

$$\frac{\partial}{\partial t}\frac{\partial\theta}{\partial x} = \frac{\partial}{\partial x}\frac{\partial\theta}{\partial t} \tag{6.37}$$

will allow us to reconstruct $\partial\theta/\partial t$ from integration of $\partial\theta/\partial x$ up to an overall time dependent function. For example, when we use the first order result for $\partial\theta/\partial x$ and substitute the time dependence of moments appropriate for a particle in a linear gravitational field we have

$$\frac{\partial\theta}{\partial x}(x,t) = \frac{\langle\hat{p}\rangle_0 - mg(t-t_0)}{\hbar} \tag{6.38}$$

which, being the plane wave approximation, is a trivial function of position. Partial differentiating with respect to time gives

$$\frac{\partial}{\partial t}\frac{\partial\theta}{\partial x} = -\frac{mg}{\hbar}. \tag{6.39}$$

Using the mixed partial condition (6.37) and integrating with respect to position gives the time partial in this case as

$$\frac{\partial\theta}{\partial t} = -\frac{mgx}{\hbar} + f(t) \tag{6.40}$$

where the arbitrary function of time $f(t)$ is added without affecting the mixed partial equality. This residual freedom of time-dependence cannot be eliminated using moment data alone and represents the non-physical arbitrary phase which may be included in any wave function under the scaling (2.20). Nonetheless, in this case we are free to choose this arbitrary function of time as

$$f(t) = -\frac{\langle\hat{p}\rangle(t)^2}{2m\hbar} \tag{6.41}$$

where $\langle\hat{p}\rangle(t)$ is the classical time-dependence of the momentum. Putting everything together, we have

$$\theta(x_f, t_f) - \theta(x_i, t_i) = \int_\gamma \left(\frac{\partial\theta}{\partial x}\mathrm{d}x + \frac{\partial\theta}{\partial t}\mathrm{d}t\right) \tag{6.42}$$

$$= \int_\gamma \left[\frac{\langle\hat{p}\rangle(t)}{\hbar}\mathrm{d}x - \left(\frac{\langle\hat{p}\rangle(t)^2}{2m\hbar} + \frac{mgx}{\hbar}\right)\mathrm{d}t\right] \tag{6.43}$$

This line integral was constructed to be independent of choice of integration path. It is convenient to choose the integration path parametrized by time, $\gamma = (\langle\hat{x}\rangle(t), t)$. Then the line integral is

$$\theta(x_f, t_f) - \theta(x_i, t_i) = \frac{1}{\hbar}\int_\gamma \left[\langle\hat{p}\rangle\frac{\mathrm{d}\langle\hat{x}\rangle}{\mathrm{d}t} - H\right]\mathrm{d}t \tag{6.44}$$

where H is the conserved energy

$$H = \frac{\langle\hat{p}\rangle^2}{2m} + mg\langle\hat{x}\rangle. \tag{6.45}$$

The integrand in (6.44) is numerically equal to the classical Lagrangian evaluated along the classical trajectory

$$\langle\hat{p}\rangle\frac{\mathrm{d}\langle\hat{x}\rangle}{\mathrm{d}t} - H\left(\langle\hat{x}\rangle, \langle\hat{p}\rangle\right) = L_{\text{classical}}(t) \tag{6.46}$$

This demonstrates equality between the moment approach and the result derived from the Feynman path integral, expressed in equation (6.32).

The plane wave approximation determines the propagation phase using only classically-defined quantities which respect the weak equivalence principle in the absence of quantum back-reaction. Quantum back-reaction occurs only if higher-order structure of the gravitational field can be resolved. Therefore, in low-order gravity-resolving atom

interferometer phase measurements, we anticipate no observed violation of the weak equivalence principle. This expectation is supported by experiments, including: (i) a series of simultaneous dual-species atom-interferometer Eötvös tests, presented in [70, 80, 81], which constrained $\eta(^{85}\mathrm{Rb},^{87}\,\mathrm{Rb}) < 10^{-12}$; (ii) the dual-species test conducted by [82], which placed constraints on the more significant mass gap, $\eta(^{39}\mathrm{K},^{87}\,\mathrm{Rb}) < 10^{-7}$; and (iii) the work of [83], which constrained the differential acceleration for atoms in a coherent superposition of metastable energy states at the 10^{-9} level.

These analyses highlight the importance of distinguishing between an atom interferometer's use of quantum properties in making a measurement and the absence of back-reaction of the quantum properties on the measurement. As discussed in [73] and revisited more recently in [79], the null results obtained so far indicate that quantum back-reaction on the center of mass dynamics either does not manifest, or itself conforms to the equivalence principle. Our analysis suggests that quantum effects do not conform to the equivalence principle. Therefore, it is reasonable to deduce that current instruments lack the detection sensitivity to resolve wave packet effects, i.e. the atoms used in these experiments mimic classical test particles, at least as far as their center of mass motion is concerned.

Our moment expansion, accommodates this conclusion through the moment hierarchy defined in equation (2.35). However, it also offers a new framework for performing calculations in the regime where quantum back-reactions become important. The challenge of incorporating the wave packet structure intrinsic to atomic test masses prepared for a local experiment has received comparatively little attention, with the work [78] being an exception.

6.4.3 Incorporating wave packet effects

The potential for quantum back-reaction onto the classical trajectory is highly interesting since it would signal a deviation from the geodesic motion predicted by general relativity, providing a unique regime for testing the compatibility of gravity and quantum mechanics. The effect of higher-order potentials on non-local wave packet structure is mass-dependent with the non-zero Eötvös parameter calculated in Section 6.2. This quantum effect may be incorporated into the phase determination with the second-order accurate result, equation (B20):

$$\frac{\partial\theta}{\partial x} = \frac{\langle\hat{p}\rangle}{\hbar} + (x - \langle\hat{x}\rangle)\frac{\Delta(xp)}{\hbar\Delta(x^2)}. \tag{6.47}$$

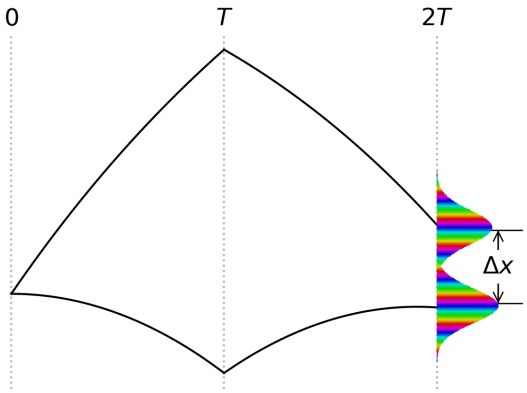

Figure 6.2: Mach-Zehnder interferometer spacetime geometry in an inhomogeneous gravitational field. The center of mass trajectories of the separated wave packet components do not intersect at the time of the third equally spaced pulse. Instead, spatial separation implies that wave packet structure will determine the interferometric phase difference. The phase of each component is most easily computed by integrating the differential phase along a piecewise path traveling first along the two center of mass trajectories, and then vertically at the fixed end time.

An example of the application of this formula could be to identify wave packet effects on the propagation phase.

We consider a simple Mach-Zehnder interferometer and imagine that the device operates based on light-pulses coherently splitting, redirecting, and recombining an atomic wave packet at equally spaced times. The spacetime geometry is sketched in Figure 6.2. In this sketch it is made evident that, in the presence of a linear gravity gradient, particle trajectories within a Mach-Zehnder interferometer do not close at the time of an equally spaced pulse after a single reflection. We can determine the phase of either wave packet component at the time of the recombining pulse, $t = 2T$, at any vertical displacement most easily if we choose an integration path which follows the component's center of mass trajectory until $t = 2T$, and then follows a vertical path at the fixed time $t = 2T$. This choice of integration path is convenient because for the first two segments of the piecewise path the path satisfies $x_\gamma = \langle \hat{x} \rangle$ and the second-order contributions to the phase vanish. Then in the last segment the moments are all time-independent yielding a simple integration.

Lastly, we comment on the structure of the second-order result. The first order phase difference, adequate for describing plane waves propagating in low-order potentials, was

determined by the classical Lagrangian action

$$\delta\theta = \frac{1}{\hbar}\int L_{\text{classical}} dt. \tag{6.48}$$

The moment approach with its canonical structure evaluates the same phase difference, but in phase space coordinates. At the lowest order this was expressed by the Legendre transform of the classical Lagrangian as

$$\delta\theta = \frac{1}{\hbar}\int \left(p\dot{x} - H_{\text{classical}}\right) dt. \tag{6.49}$$

The second-order formula for the phase derivative in canonical phase space coordinates was

$$\frac{\partial\theta}{\partial x} = \frac{p}{\hbar} + \frac{x - \langle\hat{x}\rangle}{s}\frac{p_s}{\hbar}. \tag{6.50}$$

Integrating over a physical trajectory and changing variables with the Jacobian

$$\frac{ds}{dx} = \frac{x - \langle\hat{x}\rangle}{s} \tag{6.51}$$

yields

$$\delta\theta = \frac{1}{\hbar}\int \left(pdx + p_s ds\right). \tag{6.52}$$

The integration is over the phase space trajectory $x(t)$, on which $s(t)$ depends through $s^2 = (x - \langle\hat{x}\rangle)^2 + \text{constant}$ according to (6.51). To this, we may incorporate the time-dependent contribution from the conserved energy, $H = \langle\hat{H}\rangle$, for free without leaving the same Hilbert space ray and finally obtain the propagation phase

$$\delta\theta = \frac{1}{\hbar}\int \left(p\dot{x} + p_s\dot{s} - H\right) dt \tag{6.53}$$

where $H = \langle\hat{H}\rangle$ is not equal to the classical Hamilton function but is the effective quantum energy including moments, for example as given by (6.8). This final result connects the phase contribution from second-order wave packet structure to the Lagrangian formulation. We expect that this result is obtainable also from the propagator method outlined in [77] because the integrals involved remain Gaussian. Nonetheless, it appears the quantum propagation phase is more naturally understood through its dependence on the quantum phase space structure.

6.5 Discussion

In curved spacetime, a particle's motion is typically described by geodesics of a quadratic metric. Corresponding observables—for instance based on particle dispersion relations—are tightly constrained by experimental data. However, quantum effects introduce deviations from these classical trajectories. Using the Hamiltonian formulation of the geodesic problem, applying canonical quantization, and parametrizing the state through moments of the canonical operators, this dissertation has shown that the quantum-corrected dynamics of a freely-falling particle retain a Hamiltonian structure. To fully utilize this structure, a faithful mapping of the second-order moments to canonical variables enabled us to distinguish quantum variables as either configuration variables or momentum variables and to establish the kinetic component of the Hamiltonian in a systematic way.

The identification of these canonical variables is further enriched by quantum information-theoretic considerations. Standard results for Gaussian states explicitly link entropy and purity to the covariance matrix of second-order statistics. Our methods, which are built on the semiclassical approximation (2.35) and which apply also for non-Gaussian or mixed states, encode these measures of quantum coherence and correlations into the Casimir's C_1 and C_2 of the canonical mapping previously derived in [21, 41]. Through this chain of mappings and their inversion analyzed here, these quantum information-theoretic quantities not only characterize the state but also influence the particle's interaction with the underlying geometry.

The classical theory of a free particle to which the quantum theory must reduce, is reparameterization-invariant as a consequence of the quadratic metric. This invariance is a cornerstone of any consistent physical theory. The four dimensions of the spacetime metric g_{ab} originate from the four-dimensional tangent space of the classical point particle. However, it has been argued that physical observables in canonical quantum gravity can only be defined by considering the quantum properties of the material bodies that form the reference systems [84–86]. Quantum reference frames therefore necessarily require a deeper understanding of spacetime structure, extending beyond the conventional four-dimensional tangent space.

When two classical degrees of freedom of a particle used as a reference frame are quantized, the classical tangent space is effectively extended to a 10-dimensional space. In this extended framework, the moments $\Delta(p_x^2), \Delta(p_y^2)$, and $\Delta(p_x p_y)$ are no longer quadratic functions of the tangent space, making it impossible to describe the quantum dynamics

within the standard spacetime setting provided by Riemannian geometry, even extended to additional dimensions. Nonetheless, these moments remain homogeneous functions of degree two in new momenta, making Finsler geometry a suitable broader framework that incorporates quantum degrees of freedom while preserving reparameterization-invariance.

The full Finsler Hamiltonian is exceptionally detailed and encodes an intricate interplay between quantum coherence, spacetime curvature, and higher-order corrections to classical geodesic motion, capturing both the anisotropy of quantum fluctuations and the non-quadratic nature of the effective metric in the presence of quantum effects. We expect that any physical reference system built on quantum continuous variables will experience spacetime through a geometry similar to those described here.

The quantum-corrected dispersion relation, expressed in terms of an effective mass, provides a simpler framework for bridging quantum mechanics and general relativity. By associating quantum corrections with an effective mass, the particle's trajectory is modified as if influenced by additional mass or energy linked to its quantum state. This effective mass directly connects quantum state properties, such as spread, to the particle's interaction with spacetime.

Our results also generalize concept of quantum-information theory independent of their connection to gravity or spacetime geometry. While most of the canonical parameters identified here—such as fluctuations, correlations, entropy and purity—have well-established interpretations, the canonical pair (α, p_α) appears to be new. The variable α, defined in (2.85) introduces a new correlation or uncertainty parameter. Its momentum p_α appears in the characteristic square root (2.69) in combination with $C_1^4 - C_2^4$, which is proportional to the determinant (2.79) of the covariance matrix. For pure gaussian states p_α is zero and the geometry is Riemannian. Two-mode thermal gaussian states which are nonetheless symmetric $\nu_+ = \nu_-$ need not have $p_\alpha = 0$. In this case the two canonical variables, α and p_α, are crucial for Finslerian properties of quantum geodesic motion.

If the symplectic eigenvalues are unequal—that is the two modes represent systems at different temperatures—then the nontrivial geometric structure requires p_α to have a fixed sign. The inability of p_α to change sign in this case implies directional irreversibility, making transitions between certain quantum states forbidden (or requiring non-Hamiltonian processes to occur).

The restriction on p_α may be understood in terms of quantum information flow. Since p_α is bounded by symplectic eigenvalues, which encode quantum uncertainty, it may be acting as a measure of how quantum correlations (or entanglement-like effects) distribute

in phase space. The sign-fixing condition could indicate a one-way transfer of information within the system, analogous to the way entropy increases in thermodynamics. This suggests that p_α behaves like an effective entropy-like quantity in phase space, encoding irreversible aspects of quantum state evolution.

The theory's predictions could be tested in several experimental settings, particularly in regimes where quantum coherence and spacetime curvature are both significant. Quantum coherence effects on massive particles, such as in cavity optomechanics using either silica nanospheres or cold atomic ensembles [87], could probe the effective mass corrections predicted by the theory. By subjecting ultracold atoms in coherent superpositions to gravitational potentials or artificial spacetime geometries created using optical lattices, deviations from classical trajectories predicted by the theory could be observed. If states can be controlled in such experiments, the influence of all the quantum parameters discussed here can be analyzed.

6.6 Conclusion and outlook

This dissertation has developed a geometric and physically transparent framework for analyzing relativistic quantum systems, with a particular focus on the role of quantum proper time and the structure of quantum phase space. By reformulating quantum theory in terms of expectation values and higher-order moments, and equipping the resulting space with a symplectic (and where appropriate, Kähler) structure, we have bridged the formalism of classical Hamiltonian mechanics with the statistical nature of quantum theory. This approach enables a unified description of quantum and classical dynamics and provides a powerful language for encoding semiclassical corrections in a systematically improvable way.

A central theme throughout this work has been the treatment of time in constrained relativistic systems. We explored both classical and quantum methods of gauge fixing, emphasizing the observer-dependence inherent in any operational definition of time. This led to the identification of evolution Hamiltonians adapted to specific spacetime slicings, and the construction of consistent quantum dynamics in terms of constrained Hamiltonian flows. In particular, we showed how the semiclassical dynamics of a quantum clock can be described by a Finsler geometry derived from entropy and purity—an extension of proper time that captures nonclassical features such as delocalization and entanglement.

The formalism developed here yields testable predictions. In particular, we derived modified dispersion relations and proposed measurable corrections to gravitational red-

shift, free-fall universality, return time in gravitational scattering, and phase shifts in atom interferometry. These results provide a roadmap for how quantum information features—such as coherence and state purity—can manifest in relativistic observables and how next-generation quantum sensors may probe the interface of general relativity and quantum theory.

Looking ahead, several avenues for further research emerge from this work. First, while the formalism allows for consistent truncation at second order in the moments, higher-order analyses remain challenging. This is due in part to the combinatorial growth in the number of terms and the absence of fully constructed canonical coordinate systems beyond second order. Nonetheless, the coordinate representation of the quantum Hamilton function, as defined in Eq. (2.41), preserves the homogeneity properties of the classical Hamiltonian at all orders in the moment expansion. This structure suggests that the full quantum dynamics retains a geometric character—specifically, a Finslerian one—even in curved spacetime.

The distinction often drawn between the geometry experienced by classical degrees of freedom and the geometry of quantum state space (such as that defined by entanglement structure in Sec. 4.6) is ultimately one of scale, not principle. In the complete theory, these descriptions should converge. This points toward an emergent picture of spacetime in which geometry is not an independent background but is instead shaped by—and arises from—the dynamical quantum degrees of freedom it governs.

Finally, a compelling direction for future research lies in incorporating backreaction: understanding how quantum clocks influence the geometry of spacetime itself. In a complete theory of quantum gravity, the spacetime metric would no longer be fixed, but a dynamical, entangled quantity subject to quantum fluctuations. The framework presented here offers a stepping stone toward that goal by treating matter in a geometric and constraint-consistent way, and by establishing tools that may be extended to coupled matter-geometry systems.

Taken together, the results and methods developed in this dissertation provide a conceptual and computational foundation for exploring the interface of quantum mechanics and general relativity, with promising implications for both foundational theory and experimental tests.

Appendix A
Symmetries

An essential feature of the classical theory is its covariance under spacetime transformations. However, the decision to gauge fix restricting moments involving the time coordinate is a frame-dependent condition, just as the choice of a classical time coordinate is a choice of frame. In the context of our quantum framework, we must consider how the dynamics generated by the quantum Hamilton function remain covariant under spacetime transformations, extending the classical notion of symmetry to the quantum regime.

In the classical theory, we describe a local change of coordinates by the Lorentz transformation

$$x^{a'} = \Lambda^{a'}_{a} x^{a}. \tag{A1}$$

This transformation gives in the quantum theory the corresponding unitary transformation of the operators

$$U(\Lambda)^{-1} \hat{x}^{a} U(\Lambda) = \Lambda^{a'}_{a} \hat{x}^{a} =: \hat{x}^{a'}. \tag{A2}$$

By appropriate insertions of the identity, the quantum statistics transform as tensor representations of the Lorentz group. For example, the second-order correlations have the transformation laws

$$\Delta\left(x^{a'} x^{b'}\right) = \Lambda^{a'}{}_{a} \Lambda^{b'}{}_{b'} \Delta\left(x^{a} x^{b}\right) \tag{A3}$$

$$\Delta\left(x^{a'} p_{b'}\right) = \Lambda^{a'}{}_{a} \Lambda_{b'}{}^{b} \Delta\left(x^{a} p_{b}\right) \tag{A4}$$

$$\Delta\left(p_{a'} p_{b'}\right) = \Lambda_{a'}{}^{a} \Lambda_{b'}{}^{b} \Delta\left(p_{a} p_{b}\right). \tag{A5}$$

With these transformation laws, the moment-based quantum theory is covariant under local changes of coordinates. The transformation laws, Eqs. (A3)–(A5), mix time and space statistics. Neglecting moments involving the time coordinate is a frame-dependent assumption on the quantum state.

Appendix B
Generation of wave function states from moments

Canonical effective methods work directly with the observable quantum statistics $\langle\hat{x}\rangle$, $\langle\hat{p}\rangle$, and $\Delta(x^\alpha p^\beta)$. These statistics can be measured and predicted without reference to a specific wave function state. Nonetheless, several important questions arise: Do these statistics fully encode the physical content of the quantum state? Is there redundancy in this set of variables? And how are these statistical descriptors related to the alternative representation of quantum states in terms of wave functions? In this section, we present a procedure for reconstructing a wave function $\psi(x)$ from a given set of moment data.

B.1 General considerations

Provided a Hilbert space equipped with an inner product, the extraction of moments from a wave function is straightforward. However, the inverse task—constructing a wave function representative compatible with specified moment data—is more challenging. In general, neither the existence nor the uniqueness of such a state is guaranteed. The mathematical literature refers to the task of determining a distribution that generates a given set of moments as the problem of moments. A historical perspective on the moment problem, along with its extension into complex function theory, is presented in [88].

The resolution of the moment problem depends on the choice of Hilbert space in which the reconstructed measure is expected to reside. The existence of a real-valued distribution corresponding to a given sequence of moments $\{m_j\}$ can be ensured by verifying that the associated Hankel matrices, defined by $(H_n)_{ij} = m_{i+j}$ for $i + j \leq n$, are positive definite for all $n \in \mathbb{N}$. An accessible proof of this criterion is provided in [89]. In our subsequent analysis, however, we will simply assume the existence of a wave function

based on physical reasoning, without explicitly checking the positivity of Hankel matrices constructed from moment data.

Non-uniqueness arises in two ways. First, a typical wave function encodes information for an infinite hierarchy of moments, whereas practical applications typically rely on a finite (truncated) set of low-order moments. Multiple nonidentical states may share the same low-order statistics. Consequently, any attempt to reconstruct a wave function from a truncated set of moments must arbitrarily specify the remaining, undetermined higher-order moments. This unavoidable choice introduces ambiguity into the reconstruction and reflects the inherent incompleteness of using only limited statistical data to fully characterize a quantum state. Second, even once a compatible wave function has been selected, there remains residual freedom due to complex rescaling as defined in Eq. (2.20).

To address these ambiguities, we present a procedure for selecting a specific representative from the space of states compatible with the given moment data. The method constructs a wave function in polar form

$$\psi(x,t) = \sqrt{\rho(x,t)}\exp(i\theta(x,t)) \tag{B1}$$

by first determining the probability density $\rho(x,t)$, followed by the phase $\theta(x,t)$, out of moment data. An extension of this procedure to states described by density matrices is discussed in [41].

Results obtained through moment evolution and this procedure should agree with experimental results, but may not agree with results obtained from the Schrödinger wave function theory. Such disagreements do not have physical implications because they merely correspond to different rescaling choices of the form (2.20). Examples of disagreement with the Schrödinger theory appear in the reference [14]. Application of this method to determine the interferometer phase identified by certain experiments is presented in Section 6.4.

B.2 Density reconstruction

If the unknown probability density ρ can be expressed as a polynomial in x, the reconstruction problem is linear and has a unique solution. However, due to normalization constraints, ρ typically is not polynomial. Nonetheless, the simplicity of reconstructing polynomials suggests a general approach: we decompose ρ into a polynomial basis that approximate it. We then reconstruct these approximations order-by-order to achieve the desired level of accuracy.

Following this idea, let $L_n(x)$ be a complete, orthogonal set of polynomials with weight function w on $L^2(w, \mathbb{R})$ and let $u_n(x)$ be the associated orthonormal basis such that

$$\int_{\mathbb{R}} u_n(x)u_k(x)dx = \delta_{nk}. \tag{B2}$$

with

$$u_n(x) = \frac{1}{\sqrt{N_n}}\sqrt{w(x)}L_n(x). \tag{B3}$$

Having assumed the basis property of the u_n, any function $f(x)$ in $L^2(w, \mathbb{R})$ can be expanded with coefficients in $\mathbb{R}$ as

$$f(x) = \sum_{n=0}^{\infty} c_n u_n(x) \tag{B4}$$

with coefficients

$$c_n = \int f(x)u_n(x)dx. \tag{B5}$$

In particular, we can reconstruct the density ρ from moment data if we choose $f(x) = \rho(x)/\sqrt{w(x)}$. In this case, the expansion coefficients reduce expectation values of polynomials:

$$c_n = \int \frac{\rho(x)}{\sqrt{w(x)}}\frac{1}{\sqrt{N_n}}\sqrt{w(x)}L_n(x)dx = \frac{1}{\sqrt{N_n}}\langle L_n(\hat{x})\rangle. \tag{B6}$$

Because $L_n(x)$ is a polynomial in x, $\langle L_n(\hat{x})\rangle$ can be reconstructed from moments

$$\langle L_n\rangle = \sum_{k=0}^{n} l_{n,k}\langle \hat{x}^k\rangle. \tag{B7}$$

Expressing the expectation value in coefficient form uses the so-called raw forms of the moments, not the centralized ones. The two are nonetheless related by the binomial theorem

$$\Delta(x^a) = \langle(\hat{x} - \langle\hat{x}\rangle)^a\rangle = \sum_{i=0}^{a}\binom{a}{i}(-1)^{a-i}\langle\hat{x}\rangle^{a-i}\langle\hat{x}^i\rangle \tag{B8}$$

which is a matrix equation that can be inverted to solve for the $\langle\hat{x}^i\rangle$ from the provided $\Delta(x^a)$.

Tracing these steps backwards gives finally the distribution reconstructed from its moments as

$$\rho(x) = w(x)\sum_{n=0}^{\infty}\frac{1}{N_n}\langle L_n(\hat{x})\rangle L_n(x) = w(x)\sum_{n=0}^{\infty}\sum_{j=0}^{n}\sum_{k=0}^{n}\frac{1}{N_n}l_{n,j}l_{n,k}\langle\hat{x}^j\rangle x^k. \tag{B9}$$

B.3 Phase reconstruction

Moments of the form $\langle \hat{x}^n \hat{p} \rangle$ can be used to reconstruct the phase. These non-symmetric moments can be obtained as linear combinations of symmetrically ordered ones. The real part of these moments are given from the definition as

$$\begin{aligned} \Re\left(\langle \hat{x}^n \hat{p} \rangle\right) &= \Re \int dx\, \psi^* \left(x^n \frac{\hbar}{i} \frac{d}{dx} \right) \psi && \text{(B10)} \\ &= \Re \int dx \sqrt{\rho} \exp(-i\theta) x^n \frac{\hbar}{i} \left[\frac{d\sqrt{\rho}}{dx} \exp(i\theta) + \sqrt{\rho} i \frac{d\theta}{dx} \exp(i\theta) \right] && \text{(B11)} \\ &= \hbar \int dx\, x^n \rho \frac{d\theta}{dx}. && \text{(B12)} \end{aligned}$$

The function that multiplies the monomial powers of x in this is $\hbar\rho d\theta/dx$. Consequently, we can apply the reconstruction procedure from before on this product with the outcome:

$$\frac{d\theta}{dx} = \frac{w(x)}{\hbar\rho(x)} \sum_{n=0}^{\infty} \sum_{j=0}^{n} \sum_{k=0}^{n} \frac{1}{N_n} l_{n,j} l_{n,k} \Re\left(\langle \hat{x}^j \hat{p} \rangle \right) x^k. \tag{B13}$$

This result determines the phase derivative from moment data because the density's dependence on moments is already established. Together with equation (B9), these results provide the link between moments and wave function states.

B.4 Propagation phase shift

The reconstruction procedure works by adapting a reference distribution—the selected weighting function $w(x)$—to nearby distributions such that the result matches the specified statistics. Here "nearby" means that only finitely many Taylor coefficients change. In a finite truncation of the procedure there are many nearby distributions having the same statistics depending on the arbitrary choice of orthogonal polynomial system. We focus our examples on the useful choice of generalized Hermite polynomials which are characterized by the shifted and rescaled Hermite weight function $\exp(-\frac{(x-m)^2}{2\alpha})$. This choice allows us to encompass not only Gaussian states but also provides a structured approach for handling states that go beyond the Gaussian approximation.

Explicitly substituting generalized Hermite polynomials into the reconstruction pro-

vides the first order in moments approximations

$$\rho(x;m,\alpha) = \frac{1}{\sqrt{\pi\alpha^2}} e^{-\frac{(x-m)^2}{\alpha^2}} \left(1 + 2\frac{m^2}{\alpha^2} - \frac{2m\langle\hat{x}\rangle}{\alpha^2} - 2\frac{mx}{\alpha^2} + 2\frac{\langle\hat{x}\rangle x}{\alpha^2}\right) \tag{B14}$$

$$\frac{d\theta}{dx}(x;m,\alpha) = \frac{\langle\hat{p}\rangle}{\hbar\left(1 + 2\frac{m^2}{\alpha^2} - \frac{2m\langle\hat{x}\rangle}{\alpha^2} - \frac{2mx}{\alpha^2} + \frac{2\langle\hat{x}\rangle x}{\alpha^2}\right)}. \tag{B15}$$

Centering the generalized Hermite functions about the center of mass with the choice $m = \langle\hat{x}\rangle$ simplifies these expressions to

$$\rho(x) = \frac{e^{-\frac{(x-\langle\hat{x}\rangle)^2}{\alpha^2}}}{\sqrt{\pi\alpha^2}} \tag{B16}$$

$$\frac{d\theta}{dx} = \frac{\langle\hat{p}\rangle}{\hbar} \tag{B17}$$

where α is still arbitrary because we have not assumed any second order statistics.

For fixed choices of the first order data at a time t, the phase derivative may be integrated with respect to x to give the phase profile of the instantaneous state as

$$\theta(x,t) = \theta(x_0) + \frac{\langle\hat{p}\rangle(t)(x - x_0)}{\hbar}. \tag{B18}$$

This linear phase profile matches that of a plane wave with momentum $\langle\hat{p}\rangle$ so we refer to the first order result as the plane wave approximation to the phase, see Figure B.1. In this approximation, the phase at any position is known if the phase at any other position and the (mean) momentum of the state are known.

In Section 6.4, this first-order reconstruction will be shown already to reproduce the interferometer phase identified for plane-wave states evolving in linear and quadratic potentials as presented in [77] and [90]. We extend those results by carrying the reconstruction to the next order (i.e. first non-trivial quantum order). Incorporating second order quantum fluctuations and choosing $\alpha^2 = \Delta(x^2)$ provides the reconstructions

$$\rho(x) = \frac{e^{-\frac{(x-\langle\hat{x}\rangle)^2}{2\Delta(x^2)}}}{\sqrt{2\pi\Delta(x^2)}} \tag{B19}$$

$$\frac{d\theta}{dx} = \frac{\langle\hat{p}\rangle}{\hbar} + (x - \langle\hat{x}\rangle)\frac{\Delta(xp)}{\hbar\Delta(x^2)}. \tag{B20}$$

The probability density obtained in this case reproduces the well-known formula for

Figure B.1: An abs-arg plot of a plane wave demonstrating its linear phase profile.

Figure B.2: A Gaussian state as defined in equation (B22). The parameters for this state were chosen to give a narrow momentum distribution about the same mean momentum as the plane wave in Fig. B.1.

a Gaussian probability density parametrized by its first two statistical moments. More interestingly, the phase derivative gains an additional term which is non-zero for $x \neq \langle \hat{x} \rangle$. When looked at nearby to the wave packet center, the phase of a Gaussian state resembles that of a plane wave with momentum $\langle \hat{p} \rangle$ and has a well-defined wavelength, see Figures B.2 and B.3. Corrections to the plane wave phase due to spatial localization become important when displacements from the wave packet center are significantly larger than the ratio of second-order moments $\Delta(xp)/\hbar\Delta(x^2)$.

The spatial dependence of corrections is better understood when the phase derivative

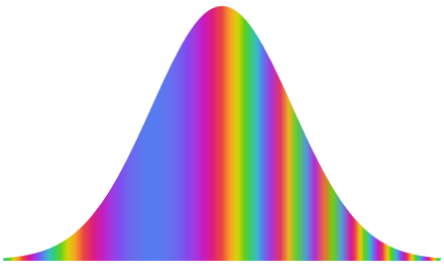

Figure B.3: A Gaussian state with the same mean momentum but with a wide momentum distribution compared with Fig. B.2.

formula is expressed in canonical coordinates. In this form, the phase derivative is given by:

$$\frac{d\theta}{dx} = \frac{p}{\hbar} + \frac{x - \langle\hat{x}\rangle}{s}\frac{p_s}{\hbar} \tag{B21}$$

with $s = \sqrt{\Delta(x^2)}$ giving the standard width of the packet. This result resembles that of a plane wave when either p_s is small, indicating narrow momentum spread, or when looking near the distribution center where $(x - \langle\hat{x}\rangle)/s < 1$.

Figure B.2 illustrates the case of a state with narrow momentum spread. Its phase closely matches that of a plane wave for most of its weight. Conversely, when the momentum distribution is wide (and $p_s > 0$), the phase increases more rapidly than a plane wave for $x > \langle\hat{x}\rangle$, resulting in wavelength compression, and more slowly for $x < \langle\hat{x}\rangle$, causing wavelength elongation. These corrections to the plane wave result are evident in Figure B.3 where parameters are chosen for a Gaussian wave packet with a broad momentum distribution.

For fixed choices of statistics, the equation (B20) (or its canonical form, equation (B21)) may be integrated and combined with the density reconstruction, equation (B19), to give the instantaneous pure state reconstruction

$$\psi(x) = \left(\frac{1}{2\pi\Delta(x^2)}\right)^{1/4} \exp\left[-\frac{(x - \langle\hat{x}\rangle)^2}{4\Delta(x^2)}\left(1 - i\frac{\Delta(xp)}{\hbar/2}\right) + i\frac{\langle\hat{p}\rangle x}{\hbar} + i\theta_0\right]. \tag{B22}$$

The overall phase $\exp(i\theta_0)$ incorporates both the arbitrary integration constant from equation (B20) as well as the unspecified choice of branch from the square root of ρ. It is interesting to compare this result with the general form for a Gaussian pure state.

In the position basis, a general Gaussian wave packet can be represented as

$$\psi(x; A, B, C) = \exp\left(Ax^2 + Bx + C\right) \tag{B23}$$

with $A, B, C \in \mathbb{C}$. We identify the real degrees of freedom as

$$A = -(a + i\alpha) \tag{B24}$$

$$B = b + i\beta \tag{B25}$$

$$C = c + i\gamma \tag{B26}$$

and require $a > 0$ so that the state is normalizable. A tedious, but straightforward process of evaluating expectation value integrals and solving systems of equations identifies these

parameters in terms of the state's statistical moments as

$$a = \frac{1}{4\Delta(x^2)} \tag{B27}$$

$$b = \frac{\langle \hat{x} \rangle}{2\Delta(x^2)} \tag{B28}$$

$$\alpha = -\frac{\Delta(xp)}{2\Delta(x^2)\hbar} \tag{B29}$$

$$\beta = \frac{\langle \hat{p} \rangle}{\hbar} - \frac{\Delta(xp)\langle \hat{x} \rangle}{\Delta(x^2)\hbar} \tag{B30}$$

$$c = -\frac{b^2}{4a} + \log\left[\left(\frac{2a}{\pi}\right)^{\frac{1}{4}}\right] \tag{B31}$$

with the overall phase γ undetermined. With this choice of parametrization, the general Gaussian wave packet written in (B23) is expressed in terms of its statistics as

$$\psi(x) = \left(\frac{1}{2\pi\Delta(x^2)}\right)^{1/4} \exp\left[-\frac{(x - \langle \hat{x} \rangle)^2}{4\Delta(x^2)}\left(1 - i\frac{2\Delta(xp)}{\hbar}\right) + i\frac{\langle \hat{p} \rangle x}{\hbar} + i\gamma\right]. \tag{B32}$$

Up to an overall (x-independent) phase, this result is identical to equation (B22). Agreement between these two results indicates that our reconstruction procedure with the choice of generalized Hermite polynomials contains Gaussian states. When higher-order fluctuations are provided, the general reconstruction equations (B9) and (B13) allow state approximations beyond the Gaussian form to be derived.

Appendix C
Efficient quantum state sampling by canonical realization

C.1 Efficient sampling of one-mode quantum states

An extensive investigation of the quantum free particle using the geometric point of view implied by our methods appears in [91]. The quantum Hamilton function for a nonrelativistic free particle is

$$H_{\mathcal{Q}} = \frac{p^2}{2m} + \frac{\Delta(p^2)}{2m}\,. \tag{C1}$$

The Hamiltonian equations of motion for a quantum free particle, derived from the Poisson structure with the brackets defined in Eq. (2.44), are given by

$$\frac{\mathrm{d}\langle\hat{x}\rangle}{\mathrm{d}t} = \frac{\langle\hat{p}\rangle}{m}\,, \tag{C2}$$

$$\frac{\mathrm{d}\langle\hat{p}\rangle}{\mathrm{d}t} = 0\,, \tag{C3}$$

$$\frac{\mathrm{d}\Delta(x^2)}{\mathrm{d}t} = \frac{2\Delta(xp)}{m}\,, \tag{C4}$$

$$\frac{\mathrm{d}\Delta(xp)}{\mathrm{d}t} = \frac{\Delta(p^2)}{m}\,, \tag{C5}$$

$$\frac{\mathrm{d}\Delta(p^2)}{\mathrm{d}t} = 0. \tag{C6}$$

These equations have solutions in terms of initial data as

$$\langle\hat{x}\rangle(t) = x_0 + \frac{p_0}{m}(t - t_0) \tag{C7}$$

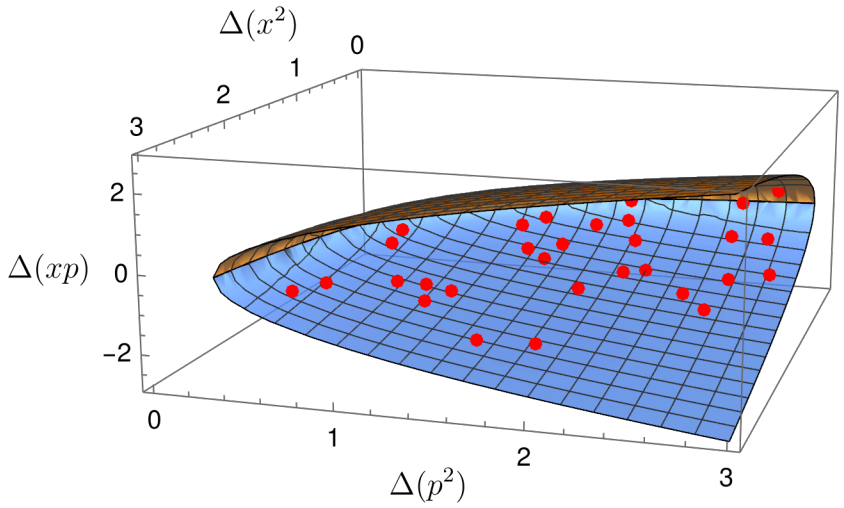

Figure C.1: Sampling of second-order moments for a single-mode quantum state. Points within the surface represent physically valid states. The boundary is defined by saturation of the uncertainty relation, Eq. (C12). Units are chosen with $\hbar = 1$.

$$\langle \hat{p} \rangle(t) = p_0 \tag{C8}$$

and

$$\Delta(x^2)(t) = \Delta(x^2)_0 + \frac{2\Delta(xp)_0}{m}(t - t_0) + \frac{\Delta(p^2)_0}{m^2}(t - t_0)^2 \tag{C9}$$

$$\Delta(xp)(t) = \Delta(xp)_0 + \frac{\Delta(p^2)_0}{m}(t - t_0) \tag{C10}$$

$$\Delta(p^2)(t) = \Delta(p^2)_0 \tag{C11}$$

An important question is how to sample valid initial data. Obviously, one must impose some constraints, for instance positivity of the variances $\Delta(x^2) > 0$ and $\Delta(p^2) > 0$. Additionally, the second-order moments must also respect the uncertainty relation

$$\Delta(x^2)\Delta(p^2) - \Delta(xp)^2 \geq \frac{\hbar^2}{4}\,. \tag{C12}$$

This inequality defines a nonlinear constraint surface in moment space, complicating direct sampling of valid states. The set of physically admissible states corresponds to the interior (and boundary) of a rotated elliptic paraboloid defined by Eq. (C12), as illustrated in Fig. C.1.

A more efficient sampling procedure leverages the canonical structure of the moments. One introduces a set of canonical variables (s, p_s, U) where $s > 0$, $U \geq \hbar^2/4$, and then

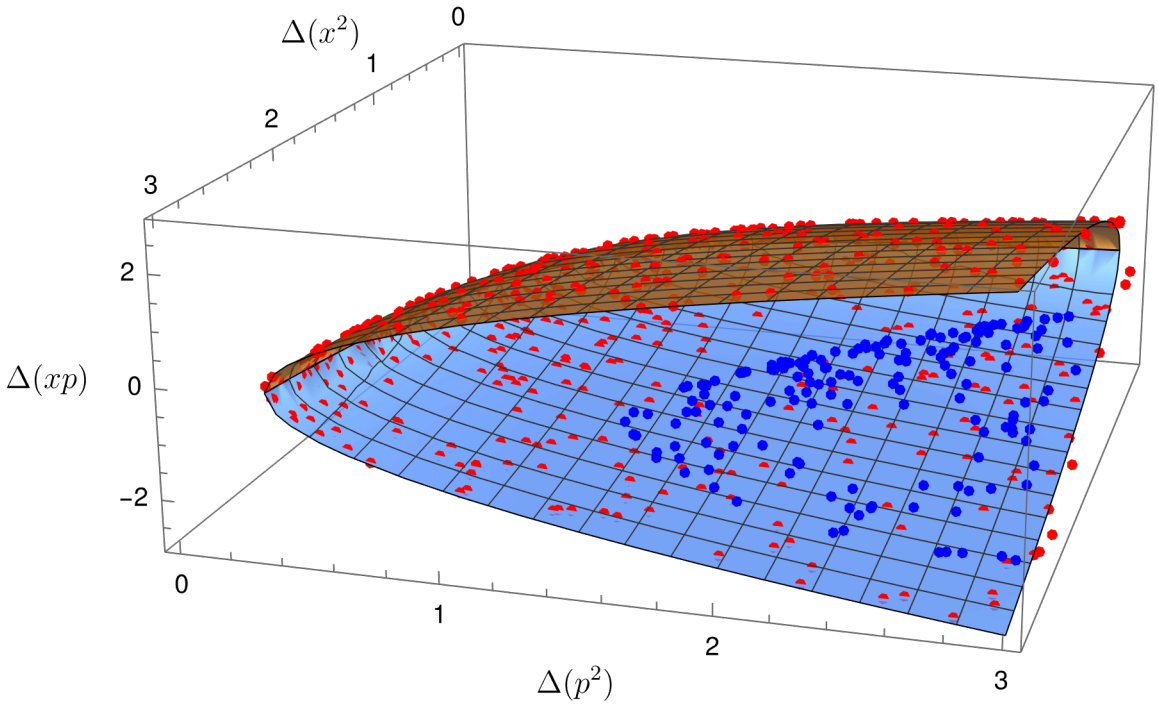

Figure C.2: Sampling of second-order moments for pure (red) and thermal (blue) single-mode quantum states. All samples are constructed from canonical variables (s, p_s) via Eq. (C13). The red points lie on the minimal uncertainty surface ($U = \hbar^2/4$), while the blue points correspond to mixed states with $U = 5\hbar^2/4$. Units are chosen with $\hbar = 1$.

computes the moments via

$$\Delta(x^2) = s^2, \qquad \Delta(xp) = sp_s, \qquad \Delta(p^2) = p_s^2 + \frac{U}{s^2}\,. \tag{C13}$$

This transformation allows uniform sampling of valid pure Gaussian and thermal states by fixing the Casimir invariant U and sampling over the symplectic subspace (s, p_s), Fig. C.2. The benefit of this method is demonstrated in Fig. C.2, which shows both pure states (with $U = \hbar^2/4$) and mixed states (with $U > \hbar^2/4$).

C.2 Efficient sampling of two-mode quantum states

The utility of canonical sampling becomes even more apparent when extended to higher-dimensional systems. For two-mode quantum states, the second-order moment space is already 10-dimensional, and valid states must satisfy the nontrivial requirement that both symplectic eigenvalues obey $\nu_+ \geq \hbar^2/4$ and $\nu_- \geq \hbar^2/4$, as defined in Sec. 2.5.2. The saturation of these inequalities defines a highly nonlinear surface within the 10-dimensional

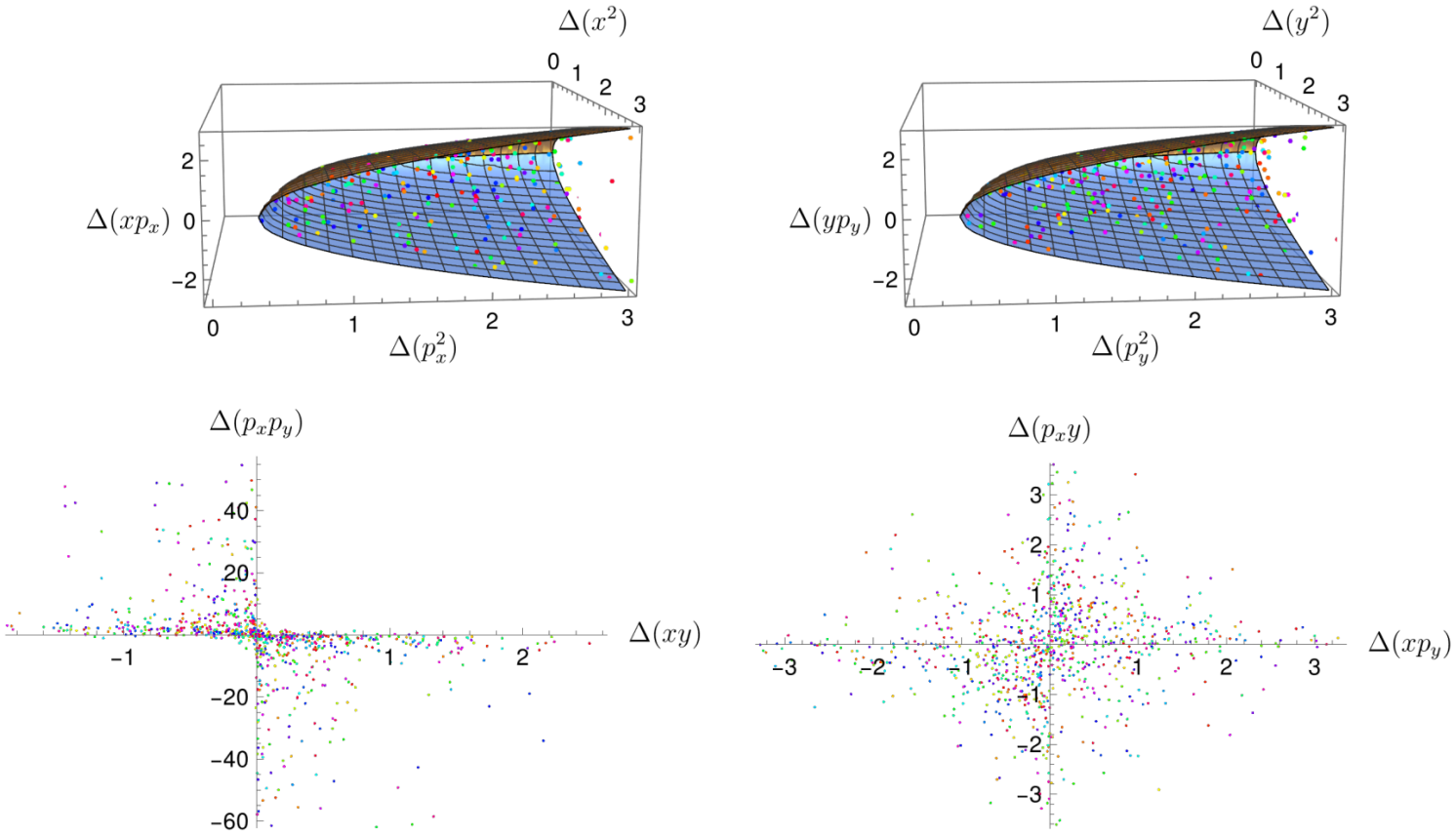

Figure C.3: Sampling of second-order moments for two-mode quantum states. Samples are efficiently generated by fixing the Casimir invariants C_1 and C_2, then uniformly sampling the canonical variables $(s_x, p_{s_x}, s_y, p_{s_y}, \alpha, p_\alpha, \beta, p_\beta)$, followed by reconstruction of the moments using the canonical transformations in Eqs. (2.59)–(2.68). Each sample represents a Gaussian state of fixed entropy and purity. The 10 moment components are visualized via projections: marginal statistics for the x- and y-modes are shown as 3D scatter plots, and cross-mode correlations are shown in 2D. Each tuple of points across the four panels corresponds to a single quantum state.

moment space.

As in the single-mode case, fixing the Casimir invariants C_1 and C_2—which correspond to the entropy and purity of the two-mode Gaussian state—ensures that uniformly sampled points in the symplectic subspace $(s_x, p_{s_x}, s_y, p_{s_y}, \alpha, p_\alpha, \beta, p_\beta)$ map to physically valid quantum states via the canonical transformations Eqs. (2.59)–(2.68).

This canonical parametrization provides a framework for exploring decoherence in quantum systems. By isolating physically meaningful quantities such as marginal fluctuations, inter-mode correlations, and Casimir invariants that encode purity and entropy, it enables a clear characterization of how coherence and entanglement degrade

under environmental interactions. The ability to efficiently sample physically valid initial conditions with fixed entropy or purity allows systematic exploration of decoherence dynamics across different regimes. In particular, the evolution of canonical variables under dissipative or stochastic dynamics directly reflects the structure and timescale of decoherence, making this approach especially suited to studies of open quantum systems and quantum-to-classical transition phenomena. This parametrization permits monitoring decoherence by observing how trajectories in phase space move away from minimal-uncertainty (pure) states.

Appendix D
Supplementary derivations for chapter 5

This Appendix collects a variety of calculations supporting the analyses of Chapter 5. The main results are derivations of quantum proper time computed in the standard Schwarzschild slicing, Eq. (5.47). Since the structure of spacetime remains Riemannian in the presence of quantum corrections for radial geodesics, the quantum derivations of follow the same scheme as the classical counterparts which we present first.

D.1 Classical proper time for radial free fall

The proper-time Lagrange function for radial free fall of a massive particle in the Schwarzschild-Droste slicing is

$$\mathrm{L}(t,r,\dot{t},\dot{r}) = -\frac{1}{2}mg_{ab}\frac{dx^a}{d\tau}\frac{dx^b}{d\tau} + \frac{mc^2}{2} = \frac{mc^2}{2}\left(1-\frac{r_s}{r}\right)\left(\frac{dt}{d\tau}\right)^2 - \frac{1}{1-\frac{r_s}{r}}\frac{m}{2}\left(\frac{dr}{d\tau}\right)^2 + \frac{mc^2}{2}. \tag{D1}$$

The classical Hamilton function in the same slicing is

$$\mathrm{H}(t,r,p_t,p_r) = -\frac{1}{2m}(g^{ab}p_a p_b + m^2c^2) = \frac{1}{1-\frac{r_s}{r}}\frac{p_t^2}{2mc^2} - \left(1-\frac{r_s}{r}\right)\frac{p_r^2}{2m} - \frac{mc^2}{2}. \tag{D2}$$

Conservation Laws:

1. The Lagrange equation of motion for t gives a conserved quantity

$$\frac{d}{d\tau}\frac{\partial L}{\partial \dot{t}} = 0 \quad \Longrightarrow \quad \frac{\partial L}{\partial \dot{t}} =: p_t = mc^2\left(1-\frac{r_s}{r}\right)\frac{dt}{d\tau} = \text{ constant}. \tag{D3}$$

2. Both L and H are quadratic and therefore equal to each other. In particular, both functions are conserved along the particle worldline. Setting initial conditions at

Mass	r_s	$\tau(r_s, 10r_s)$
$1.4M_\odot$	4150 meters	milliseconds
$10^3 M_\odot$	3 million meters	tenths of a second
$10^6 M_\odot$	3 billion meters	hundreds of seconds

Table D.1: Proper fall time to horizon order-of-magnitude examples.

$(t, r, p_t, p_r) = (0, r_0, p_t, 0)$, we have

$$\text{conservation of } H\text{:} \qquad \frac{1}{1-\frac{r_s}{r}}\frac{p_t^2}{2mc^2} - \left(1-\frac{r_s}{r}\right)\frac{p_r^2}{2m} = \frac{1}{1-\frac{r_s}{r_0}}\frac{p_t^2}{2mc^2}. \tag{D4}$$

The constraint $H = 0$ at the initial time gives an equation for the value of p_t for all time

$$\begin{aligned} H(0, r_0, p_t, 0) &= \frac{1}{1-\frac{r_s}{r_0}}\frac{p_t^2}{2mc^2} - \frac{mc^2}{2} \approx 0 \\ \implies \left(\frac{p_t}{mc}\right)^2 &= c^2\left(1-\frac{r_s}{r_0}\right). \end{aligned} \tag{D5}$$

Using this to substitute for p_t and using

$$p_r = \frac{m}{1-\frac{r_s}{r}}\dot{r} \tag{D6}$$

to reëxpress the Hamilton energy in terms of the radial velocity leads to the effective potential equation

$$\frac{1}{2}\left(\frac{dr}{d\tau}\right)^2 + \underbrace{\frac{c^2}{2}\left(1-\frac{r_s}{r}\right)}_{V(r)} = \underbrace{\frac{1}{2}\left(\frac{p_t}{mc}\right)^2}_{\mathcal{E}}. \tag{D7}$$

Solving this for the radial component of the velocity yields

$$\frac{dr}{d\tau} = \pm c\sqrt{\frac{r_s}{r} - \frac{r_s}{r_0}} = \pm\sqrt{2\left(\frac{GM}{r} - \frac{GM}{r_0}\right)} \tag{D8}$$

This actually is the Newtonian equation (although here the parameter is proper time). The integral of this equation (with minus sign) with initial condition is

$$\tau(r) = -\frac{1}{c}\int_{r_0}^{r} \frac{1}{\sqrt{\frac{r_s}{r'} - \frac{r_s}{r_0}}} dr' = \frac{1}{cr_s^{1/2}}\left[r_0^{3/2}\arcsin\left(\sqrt{1-\frac{r}{r_0}}\right) + rr_0\sqrt{\frac{1}{r}-\frac{1}{r_0}}\right] \tag{D9}$$

which is the main text Eq. (5.46). The fall time to the horizon is

$$c\tau(r_s; r_0) = \left(\frac{r_0}{r_s}\right)^{1/2} r_0 \arcsin\left(\sqrt{1-\frac{r_s}{r_0}}\right) + r_0\sqrt{1-\frac{r_s}{r_0}} \approx \frac{\pi r_0}{2}\sqrt{\frac{r_0}{r_s}} - \frac{2r_s}{3}. \tag{D10}$$

The latter expression is valid for $r_0 \gg r_s$. Examples are computed in Table D.1.

The expression for $\tau(r)$ is not directly invertible for $r(\tau)$. However, the function $\tau(r; r_0)$ is monotone on the domain $[r_0, r_s]$ as may be checked either graphically or by looking at the derivative formula. Locally therefore, the inverse function theorem applies. We can solve for $r(\tau; r_0)$ by solving the equation $\tau - \tau(r; r_0) = 0$. A numerical approach to solving this is Newton's method, detailed in Sec. D.1.1. Alternatively, in Sec. D.1.2 we develop a series expression for $r(\tau)$ from the derivative formula (D8).

D.1.1 Newton's method solution for $r(\tau)$

Newton's method solves nonlinear equations.

$$\begin{aligned} &\text{know:} \quad f(r) = \tau \qquad && r \in [r_0, r_s] \\ &\text{want:} \quad f^{-1}(\tau) = r \qquad && \tau \in [\underbrace{f(r_0)}_{0}, \underbrace{f(r_s)}_{\tau_f}] \end{aligned}$$

We make an initial guess for $r(\tau) \approx r_1(\tau)$ with $r_1(\tau)$ as

$$r_1(\tau) = r_0 - \frac{r_0 - r_s}{\tau_f}\tau. \tag{D11}$$

Each guess is improved according to

$$r_{n+1}(\tau) = r_n(\tau) - \frac{f(r_n) - \tau}{f'(r_n)}. \tag{D12}$$

This approach is challenging to pursue because: (i) Newton's method may converge to the incorrect root and (ii) the expression (D12) quickly becomes unweildy even for $r_2(\tau)$.

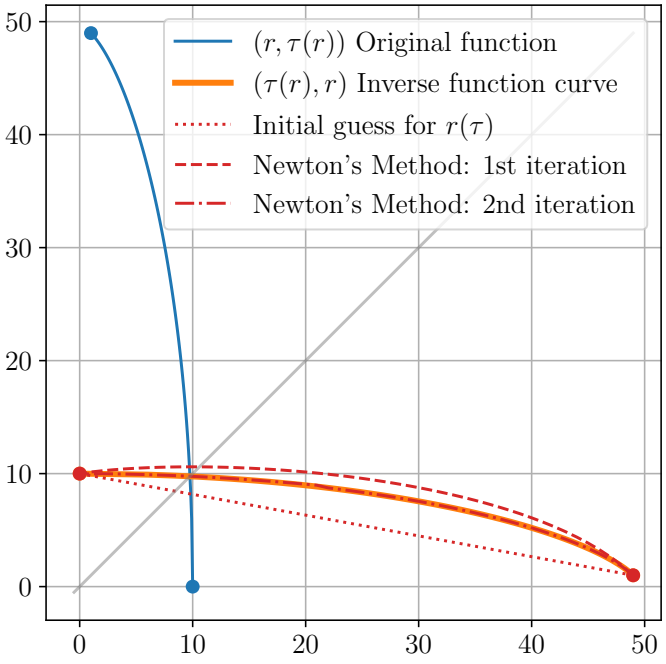

Figure D.1: Proper time $\tau(r)$ along a radial infall geodesic in Schwarzschild spacetime, plotted as $(r, \tau(r))$, along with Newton's method iterations to approximate its inverse $(\tau, r(\tau))$. The geodesic starts from rest at $r = 10r_s$ and terminates at the horizon $r = r_s$, with $\tau(r)$ given analytically in Eq. (D9). The plot shows the original geodesic, its parametrized inverse, an initial guess for the inverse, and the first and second Newton iterations. Care must be taken to ensure that Newton's method converges to the correct root due to the square root in the derivative $\frac{d\tau}{dr}$, but once properly initialized, convergence is rapid. Axes are in units where $c = r_s = 1$.

D.1.2 Series solution for $r(\tau)$

We assume that $r(\tau)$ is analytic on the interval $[r_0, r_s]$. Performing the expansion at the initial point produces the series

$$r(\tau) = r_0 + \left.\frac{dr}{d\tau}\right|_{\tau=0} \tau + \frac{1}{2} \left.\frac{d^2 r}{d\tau^2}\right|_{\tau=0} \tau^2 + \cdots . \tag{D13}$$

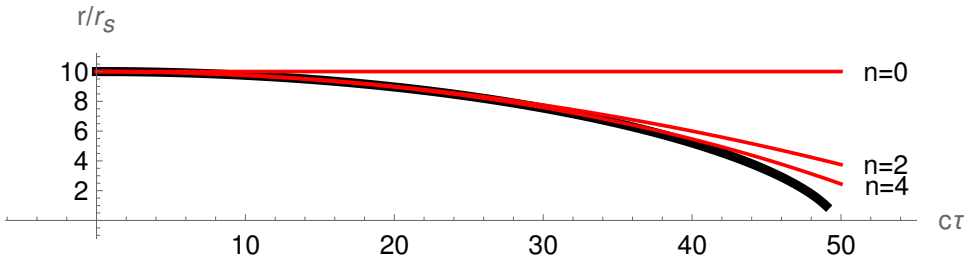

Figure D.2: Series approximations to the radial solution $r(\tau)$ in Schwarzschild for a massive particle initially at rest at $r = 10r_s$. The quadratic approximation $T_{r,2}(\tau) = r_0 - g/2\tau^2$ is the result from the Newtonian approximation in proper time.

The higher derivatives may be obtained from derivatives of expression (D8). For example, the second derivative is

$$\begin{aligned} \frac{d^2r}{d\tau^2} &= \frac{d}{d\tau}\frac{dr}{d\tau} \\ &= -c\frac{dr}{d\tau}\frac{d}{dr}\sqrt{\frac{r_s}{r} - \frac{r_s}{r_0}} = -\frac{c^2 r_s}{r^2}. \end{aligned} \tag{D14}$$

The odd-order derivatives all vanish at the initial position. The expansion to 4th-order reads

$$r(\tau) = r_0 - \frac{c^2 r_s}{4r_0^2}\tau^2 - \frac{c^4 r_s^2}{48 r_0^5}\tau^4 + \cdots \tag{D15}$$

$$= r_0 - \frac{1}{2}\frac{GM}{r_0^2}\tau^2 - \frac{G^2M^2}{12r_0^5}\tau^4 + \cdots \tag{D16}$$

$$\frac{r(\tau)}{r_s} = \frac{r_0}{r_s} - \frac{1}{4}\left(\frac{r_s}{r_0}\right)^2\left(\frac{c\tau}{r_s}\right)^2 - \frac{1}{48}\left(\frac{r_s}{r_0}\right)^5\left(\frac{c\tau}{r_s}\right)^4 + \cdots \tag{D17}$$

where the second expression substitutes the formula for the Schwarzschild radius. Figure D.2 plots the first few Taylor series approximations to $r(\tau)$ for $r_0 = 10r_s$. The second order approximation is nearly the parabolic result from Newtonian theory, except for its parametrization in proper time.

D.2 Classical time dilation

We obtain the remaining component of the tangent vector from the known momentum:

$$p_t = \frac{\partial L}{\partial \dot{t}} = -mg_{tt}\frac{dt}{d\tau} \quad \Longrightarrow \quad \frac{dt}{d\tau} = -g^{tt}\frac{p_t}{m} = \frac{1}{1 - \frac{r_s}{r}}\frac{p_t}{mc^2}. \tag{D18}$$

Substituting the constraint relation $p_t/mc = c\sqrt{1 - r_s/r_0}$ gives the useful form

$$\begin{aligned} \frac{dt}{d\tau} &= \frac{1}{1 - \frac{r_s}{r}}\sqrt{1 - \frac{r_s}{r_0}} \\ \frac{dr}{d\tau} &= -c\sqrt{\frac{r_s}{r} - \frac{r_s}{r_0}}. \end{aligned} \tag{D19}$$

The derivative $dt/d\tau$ can be used to obtain a series expansion for $t(\tau)$. Performing the expansion at the initial point produces the series

$$t(\tau) = t_0 + \left.\frac{dt}{d\tau}\right|_{\tau=0} \tau + \frac{1}{2}\left.\frac{d^2t}{d\tau^2}\right|_{\tau=0} \tau^2 + \cdots \tag{D20}$$

$$= t_0 + \frac{\tau}{\sqrt{1 - \frac{r_s}{r_0}}} + \frac{c^2 r_s^2}{12 r_0^4 \left(1 - \frac{r_s}{r_0}\right)^{3/2}} \tau^3 + \cdots . \tag{D21}$$

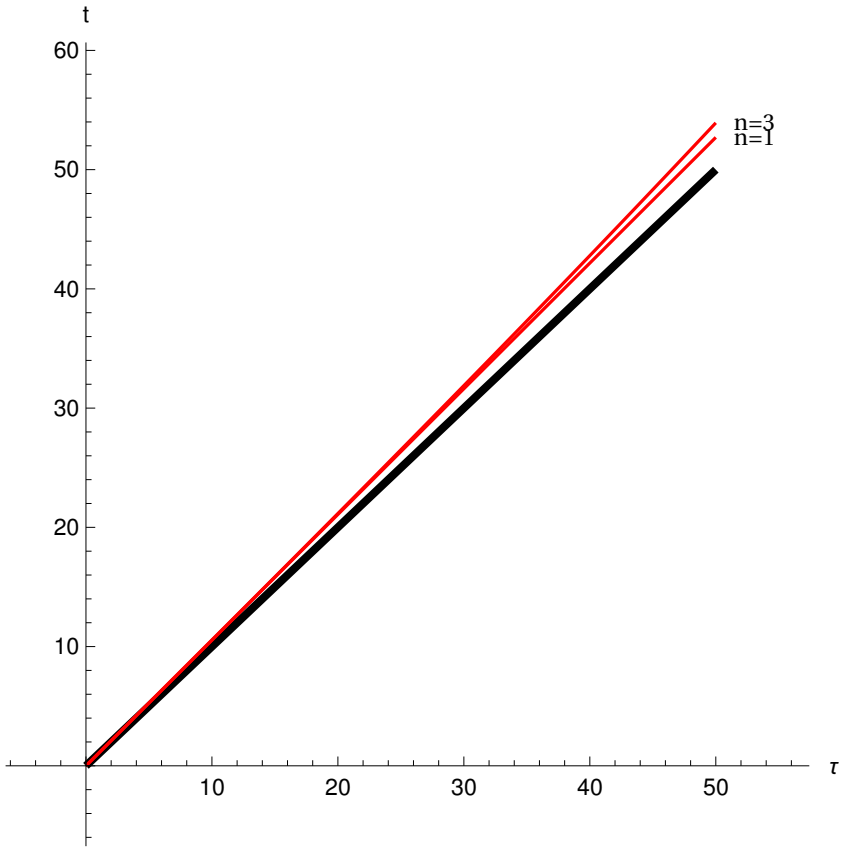

Figure D.3: Series approximations to the time coordinate $t(\tau)$ for a massive particle initially at rest at $r = 10r_s$ in Schwarzschild. The linear approximation is the standard gravitational time dilation result.

The dimensionless expression is

$$\frac{ct(\tau)}{r_s} = \frac{ct_0}{r_s} + \frac{1}{\sqrt{1-\frac{r_s}{r_0}}}\frac{c\tau}{r_s} + \frac{1}{12}\left(\frac{r_s}{r_0}\right)^4 \frac{1}{\left(1-\frac{r_s}{r_0}\right)^{3/2}}\left(\frac{c\tau}{r_s}\right)^3 + \cdots . \tag{D22}$$

For a particle at infinity $r_0 \to \infty$ we have $t = \tau$. Closer to the horizon the coordinate time loses track with the particle proper time and $t > \tau$, i.e., closer to the horizon time appears to pass more slowly.

D.3 Causality and light cone slope

The tangent vector components (D19) are used to identify the slope of a massive particle's worldline in Schwarzschild-Droste coordinates:

$$\left(\frac{dt}{dr}\right)_{\text{massive particle}} = \frac{\frac{dt}{d\tau}}{\frac{dr}{d\tau}} = \pm\frac{1}{c}\frac{1}{1-\frac{r_s}{r}}\sqrt{\frac{r}{r_s}}\sqrt{\frac{1-\frac{r_s}{r_0}}{1-\frac{r}{r_0}}}. \tag{D23}$$

One can compare this coordinate velocity to the light-cone slope

$$\left(\frac{dt}{dr}\right)_{\text{lightcone}} = \pm\frac{1}{c}\frac{1}{1-\frac{r_s}{r}}. \tag{D24}$$

When $r > r_s$ the trajectory of a massive particle remains always within the lightcone:

$$\frac{\left(\frac{dt}{dr}\right)_{\text{massive particle}}}{\left(\frac{dt}{dr}\right)_{\text{lightcone}}} = \sqrt{\frac{r}{r_s}}\sqrt{\frac{1-\frac{r_s}{r_0}}{1-\frac{r}{r_0}}} > 1. \tag{D25}$$

The coordinate velocity may be integrated to give the unparametrized trajectory of a radially falling massive particle in Schwarzschild-Droste coordinates. The Newtonian part of the trajectory is approached asymptotically for $r, r_0 \gg r_s$:

$$t(r) = \frac{1}{cr_s^{1/2}}\left[\underbrace{(2r_s+r_0)\sqrt{r_0-r_s}}_{\to r_0^{3/2}}\arcsin\left(\sqrt{1-\frac{r}{r_0}}\right) + \underbrace{\sqrt{r_0-r_s}\sqrt{r(r_0-r)}}_{\to\sqrt{rr_0(r_0-r)}} + 2r_s^{3/2}\underbrace{\operatorname{arcsinh}\sqrt{\frac{\frac{r_s}{r}-\frac{r_s}{r_0}}{1-\frac{r_s}{r}}}}_{\to 0}\right]. \tag{D26}$$

The non-Newtonian arcsinh term diverges as $r \to r_s$ (see Figure D.4). In order to address behavior near the horizon (and also to address coordinate-dependence as

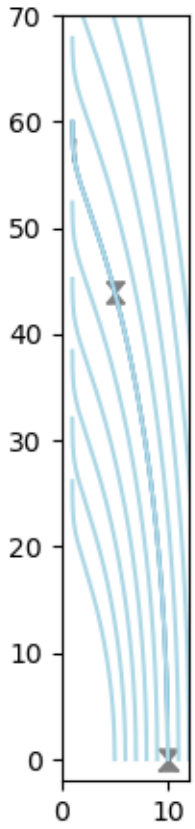

Figure D.4: Schwarzschild-Droste massive particle trajectories with lightcone.

a proxy for observer-dependence) it is necessary to choose new coordinates. Many coordinate systems exist for resolving the Schwarzschild horizon. In the quantization of the relativistic free particle, we will choose coordinates adapted to the particle.

Bibliography

[1] Gwinner, G. (2005) "Experimental tests of time dilation in special relativity," *Modern Physics Letters A*, **20**(11), pp. 791–805, publisher: World Scientific Publishing Co.
URL https://www.worldscientific.com/doi/abs/10.1142/S0217732305017202

[2] Bothwell, T., C. J. Kennedy, A. Aeppli, D. Kedar, J. M. Robinson, E. Oelker, A. Staron, and J. Ye (2022) "Resolving the gravitational redshift across a millimetre-scale atomic sample," *Nature*, **602**(7897), pp. 420–424, publisher: Nature Publishing Group.
URL https://www.nature.com/articles/s41586-021-04349-7

[3] Will, C. M. (2014) "The Confrontation between General Relativity and Experiment," *Living Reviews in Relativity*, **17**(1), p. 4.
URL https://doi.org/10.12942/lrr-2014-4

[4] Kuchař, K. V. (2011) "Time and interpretations of quantum gravity," *International Journal of Modern Physics D*, **20**(supp01), pp. 3–86, publisher: World Scientific Publishing Co.
URL https://www.worldscientific.com/doi/abs/10.1142/S0218271811019347

[5] Anderson, E. (2012) "Problem of time in quantum gravity," *Annalen der Physik*, **524**(12), pp. 757–786, _eprint: https://onlinelibrary.wiley.com/doi/pdf/10.1002/andp.201200147.
URL https://onlinelibrary.wiley.com/doi/abs/10.1002/andp.201200147

[6] Dirac, P. A. M. (1997) "The theory of gravitation in Hamiltonian form," *Proceedings of the Royal Society of London. Series A. Mathematical and Physical Sciences*, **246**(1246), pp. 333–343, publisher: Royal Society.
URL https://royalsocietypublishing.org/doi/10.1098/rspa.1958.0142

[7] Katz, J. (1962) "Les crochets de Poisson des contraintes du champ gravitationne," *Comptes Rendus Acad. Sci. Paris*, **254**, pp. 1386–1387.

[8] Arnowitt, R., S. Deser, and C. W. Misner (2008) "Republication of: The dynamics of general relativity," *General Relativity and Gravitation*, **40**(9), pp. 1997–2027.
URL https://doi.org/10.1007/s10714-008-0661-1

[9] Page, D. N. and W. K. Wootters (1983) "Evolution without evolution: Dynamics described by stationary observables," *Physical Review D*, **27**(12), pp. 2885–2892, publisher: American Physical Society.
URL https://link.aps.org/doi/10.1103/PhysRevD.27.2885

[10] Smith, A. R. H. and M. Ahmadi (2019) "Quantizing time: Interacting clocks and systems," *Quantum*, **3**, p. 160, publisher: Verein zur Förderung des Open Access Publizierens in den Quantenwissenschaften.
URL https://quantum-journal.org/papers/q-2019-07-08-160/

[11] Balsells, J. and M. Bojowald (2025), "Quantum proper time: A Finsler space from entropy and purity," ArXiv:2503.06667 [quant-ph].
URL http://arxiv.org/abs/2503.06667

[12] ——— (2024) "Geometry and proper time of a relativistic quantum clock," *Physical Review D*, **110**(12), p. 124061, publisher: American Physical Society.
URL https://link.aps.org/doi/10.1103/PhysRevD.110.124061

[13] Hu, Y., M. P. E. Lock, and M. P. Woods (2024) "On the feasibility of detecting quantum delocalization effects on relativistic time dilation in optical clocks," *Quantum Science and Technology*, **9**(4), p. 045052, publisher: IOP Publishing.
URL https://dx.doi.org/10.1088/2058-9565/ad752c

[14] Balsells, J. and M. Bojowald (2023) "Adherence and violation of the equivalence principle from classical to quantum mechanics," *Physical Review D*, **108**(8), p. 084030, publisher: American Physical Society.
URL https://link.aps.org/doi/10.1103/PhysRevD.108.084030

[15] Bojowald, M. and A. Tsobanjan (2023) "Algebraic Properties of Quantum Reference Frames: Does Time Fluctuate?" *Quantum Reports*, **5**(1), pp. 22–37, number: 1 Publisher: Multidisciplinary Digital Publishing Institute.
URL https://www.mdpi.com/2624-960X/5/1/3

[16] ——— (2009) "Effective constraints for relativistic quantum systems," *Physical Review D*, **80**(12), p. 125008, publisher: American Physical Society.
URL https://link.aps.org/doi/10.1103/PhysRevD.80.125008

[17] Bojowald, M., B. Sandhöfer, A. Skirzewski, and A. Tsobanjan (2009) "Effective constraints for quantum systems," *Reviews in Mathematical Physics*, **21**(01), pp. 111–154, publisher: World Scientific Publishing Co.
URL https://www.worldscientific.com/doi/abs/10.1142/S0129055X09003591

[18] Bojowald, M. and A. Skirzewski (2006) "Effective equations of motion for quantum systems," *Reviews in Mathematical Physics*, **18**(07), pp. 713–745, publisher: World Scientific Publishing Co.
URL https://www.worldscientific.com/doi/abs/10.1142/S0129055X06002772

[19] Bengtsson, I. and K. Zyczkowski (2006) *Geometry of Quantum States: An Introduction to Quantum Entanglement*, Cambridge University Press, Cambridge.
URL https://www.cambridge.org/core/books/geometry-of-quantum-states/4BA9DCEED5BB16B222A917EAAAD17028

[20] Ashtekar, A. and T. A. Schilling (1997), "Geometrical Formulation of Quantum Mechanics," ArXiv:gr-qc/9706069.
URL http://arxiv.org/abs/gr-qc/9706069

[21] Baytaş, B., M. Bojowald, and S. Crowe (2020) "Faithful realizations of semiclassical truncations," *Annals of Physics*, **420**, p. 168247.
URL https://www.sciencedirect.com/science/article/pii/S0003491620301810

[22] Bjelaković, I. and W. Stulpe (2005) "The Projective Hilbert Space as a Classical Phase Space for Nonrelativistic Quantum Dynamics," *International Journal of Theoretical Physics*, **44**(11), pp. 2041–2049.
URL https://doi.org/10.1007/s10773-005-8982-2

[23] Strocchi, F. (1966) "Complex Coordinates and Quantum Mechanics," *Reviews of Modern Physics*, **38**(1), pp. 36–40, publisher: American Physical Society.
URL https://link.aps.org/doi/10.1103/RevModPhys.38.36

[24] Kibble, T. W. B. (1979) "Geometrization of quantum mechanics," *Communications in Mathematical Physics*, **65**(2), pp. 189–201, publisher: Springer.
URL https://projecteuclid.org/journals/communications-in-mathematical-physics/volume-65/issue-2/Geometrization-of-quantum-mechanics/cmp/1103904831.full

[25] Bojowald, M., S. Brahma, and U. Büyükçam (2015) "Testing Nonassociative Quantum Mechanics," *Physical Review Letters*, **115**(22), p. 220402, publisher: American Physical Society.
URL https://link.aps.org/doi/10.1103/PhysRevLett.115.220402

[26] Bojowald, M. and A. Tsobanjan (2023) "Algebraic approach to the frozen formalism problem of time," *Physical Review D*, **107**(2), p. 024003, publisher: American Physical Society.
URL https://link.aps.org/doi/10.1103/PhysRevD.107.024003

[27] Reed, M. and B. Simon (1972) *Methods of Modern Mathematical Physics*, vol. 2, Academic Press, Boston.
URL https://doi.org/10.1016/B978-0-12-585001-8.X5001-6

[28] Brizuela, D. (2014) "Statistical moments for classical and quantum dynamics: Formalism and generalized uncertainty relations," *Physical Review D*, **90**(8), p. 085027, publisher: American Physical Society.
URL https://link.aps.org/doi/10.1103/PhysRevD.90.085027

[29] Bojowald, M. (2023) "Canonical description of quantum dynamics*," *Journal of Physics A: Mathematical and Theoretical*, **55**(50), p. 504006, publisher: IOP Publishing.
URL https://dx.doi.org/10.1088/1751-8121/acafb0

[30] Lämmerzahl, C. (1996) "On the equivalence principle in quantum theory," *General Relativity and Gravitation*, **28**(9), pp. 1043–1070.
URL https://doi.org/10.1007/BF02113157

[31] Aragón-Mu{\~n}oz, L., G. Chacón-Acosta, and H. Hernandez-Hernandez (2020) "Effective quantum tunneling from a semiclassical momentous approach," *International Journal of Modern Physics B*, **34**(29).
URL https://worldscientific.com/doi/abs/10.1142/S0217979220502719

[32] Cannas da Silva, A. and A. Weinstein (1999) *Geometric Models for Noncommutative Algebras*, vol. 10 of *Berkeley Mathematics Lectures*, Am. Math. Soc., Providence.
URL https://bookstore.ams.org/BMLN/10

[33] Serafini, A. (2023) *Quantum Continuous Variables: A Primer of Theoretical Methods*, 2 ed., CRC Press, Boca Raton.

[34] Jackiw, R. and A. Kerman (1979) "Time-dependent variational principle and the effective action," *Physics Letters A*, **71**(2), pp. 158–162.
URL https://www.sciencedirect.com/science/article/pii/0375960179901518

[35] Arickx, F., J. Broeckhove, W. Coene, and P. Van Leuven (1986) "Gaussian wave-packet dynamics," *International Journal of Quantum Chemistry*, **30**(S20), pp. 471–481, _eprint: https://onlinelibrary.wiley.com/doi/pdf/10.1002/qua.560300741.
URL https://onlinelibrary.wiley.com/doi/abs/10.1002/qua.560300741

[36] Prezhdo, O. V. (2006) "Quantized Hamilton Dynamics," *Theoretical Chemistry Accounts*, **116**(1), pp. 206–218.
URL https://doi.org/10.1007/s00214-005-0032-x

[37] Simon, R. (2000) "Peres-Horodecki Separability Criterion for Continuous Variable Systems," *Physical Review Letters*, **84**(12), pp. 2726–2729, publisher: American

Physical Society.
URL https://link.aps.org/doi/10.1103/PhysRevLett.84.2726

[38] Aurell, E., L. Hackl, P. Horodecki, R. H. Jonsson, and M. Kieburg (2024) "Random Pure Gaussian States and Hawking Radiation," *Physical Review Letters*, **133**(6), p. 060202, publisher: American Physical Society.
URL https://link.aps.org/doi/10.1103/PhysRevLett.133.060202

[39] Cariolaro, G., R. Corvaja, and F. Miatto (2022) "Gaussian States: Evaluation of the Covariance Matrix from the Implementation with Primitive Component," *Symmetry*, **14**(7), p. 1286, number: 7 Publisher: Multidisciplinary Digital Publishing Institute.
URL https://www.mdpi.com/2073-8994/14/7/1286

[40] Adesso, G. and F. Illuminati (2007) "Entanglement in continuous-variable systems: recent advances and current perspectives," *Journal of Physics A: Mathematical and Theoretical*, **40**(28), p. 7821.
URL https://dx.doi.org/10.1088/1751-8113/40/28/S01

[41] Baytaş, B., M. Bojowald, and S. Crowe (2019) "Effective potentials from semiclassical truncations," *Physical Review A*, **99**(4), p. 042114, publisher: American Physical Society.
URL https://link.aps.org/doi/10.1103/PhysRevA.99.042114

[42] Di Casola, E., S. Liberati, and S. Sonego (2015) "Nonequivalence of equivalence principles," *American Journal of Physics*, **83**(1), pp. 39–46.
URL https://doi.org/10.1119/1.4895342

[43] Gitman, D. M. and I. V. Tyutin (1990) "Quantization of Singular Theories with Higher Derivatives and Theories with Time-Dependent Constraints," in *Quantization of Fields with Constraints* (D. M. Gitman and I. V. Tyutin, eds.), Springer, Berlin, Heidelberg, pp. 217–253.
URL https://doi.org/10.1007/978-3-642-83938-2_7

[44] Khatsymovsky, V. M. (2021) "On the Kerr metric in a synchronous reference frame," *International Journal of Modern Physics D*, **30**(10), p. 2150071, publisher: World Scientific Publishing Co.
URL https://www.worldscientific.com/doi/abs/10.1142/S0218271821500711

[45] Peres, A. and D. R. Terno (2004) "Quantum information and relativity theory," *Reviews of Modern Physics*, **76**(1), pp. 93–123, publisher: American Physical Society.
URL https://link.aps.org/doi/10.1103/RevModPhys.76.93

[46] Pfeifer, C. and M. N. R. Wohlfarth (2012) "Finsler geometric extension of Einstein gravity," *Physical Review D*, **85**(6), p. 064009, publisher: American Physical

Society.
URL https://link.aps.org/doi/10.1103/PhysRevD.85.064009

[47] Hohmann, M., C. Pfeifer, and N. Voicu (2019) "Finsler gravity action from variational completion," *Physical Review D*, **100**(6), p. 064035, publisher: American Physical Society.
URL https://link.aps.org/doi/10.1103/PhysRevD.100.064035

[48] Shen, Y.-B. and Z. Shen (2016) *Introduction to Modern Finsler Geometry*, Higher Education Press, New Jersey.
URL https://doi.org/10.1142/9726

[49] Girelli, F., S. Liberati, and L. Sindoni (2007) "Planck-scale modified dispersion relations and Finsler geometry," *Physical Review D*, **75**(6), p. 064015, publisher: American Physical Society.
URL https://link.aps.org/doi/10.1103/PhysRevD.75.064015

[50] Rätzel, D., S. Rivera, and F. P. Schuller (2011) "Geometry of physical dispersion relations," *Physical Review D*, **83**(4), p. 044047, publisher: American Physical Society.
URL https://link.aps.org/doi/10.1103/PhysRevD.83.044047

[51] Randers, G. (1941) "On an Asymmetrical Metric in the Four-Space of General Relativity," *Physical Review*, **59**(2), pp. 195–199, publisher: American Physical Society.
URL https://link.aps.org/doi/10.1103/PhysRev.59.195

[52] Zhe, C. and L. Xin (2009) "Ultra-high energy cosmic rays threshold in Randers–Finsler space," *Chinese Physics C*, **33**(8), p. 626.
URL https://dx.doi.org/10.1088/1674-1137/33/8/005

[53] Kapsabelis, E., E. N. Saridakis, and P. C. Stavrinos (2024) "Finsler–Randers–Sasaki gravity and cosmology," *The European Physical Journal C*, **84**(5), p. 538.
URL https://doi.org/10.1140/epjc/s10052-024-12924-1

[54] Carvalho, P., C. Landri, R. Mistry, and A. Pinzul (2023) "Multimetric Finsler geometry," *International Journal of Modern Physics A*, **38**(03), p. 2350018, publisher: World Scientific Publishing Co.
URL https://www.worldscientific.com/doi/10.1142/S0217751X23500185

[55] Tayebi, A., M. Shahbazi Nia, and E. Peyghan (2012) "On generalized m-th root finsler metrics," *Linear Algebra and its Applications*, **437**(2), pp. 675–683.
URL https://www.sciencedirect.com/science/article/pii/S0024379512001802

[56] Tabatabaeifar, T. (2020) "On generalized 4-th root Finsler metrics," *Journal of Finsler Geometry and its Applications*, **1**(1), pp. 54–59, publisher: University of Mohaghegh Ardabili.
URL https://jfga.uma.ac.ir/article_1010.html

[57] Ohta, S.-i. (2014) "On the Curvature and Heat Flow on Hamiltonian Systems," *Analysis and Geometry in Metric Spaces*, **2**(1), publisher: De Gruyter Open Access Section: Analysis and Geometry in Metric Spaces.
URL https://www.degruyterbrill.com/document/doi/10.2478/agms-2014-0003/html?lang=en

[58] Smith, A. R. H. and M. Ahmadi (2020) "Quantum clocks observe classical and quantum time dilation," *Nature Communications*, **11**(1), p. 5360, publisher: Nature Publishing Group.
URL https://www.nature.com/articles/s41467-020-18264-4

[59] Bojowald, M. and A. Tsobanjan (2021) "Quantization of Dynamical Symplectic Reduction," *Communications in Mathematical Physics*, **382**(1), pp. 547–583.
URL https://doi.org/10.1007/s00220-020-03856-4

[60] Hossenfelder, S. (2013) "Minimal Length Scale Scenarios for Quantum Gravity," *Living Reviews in Relativity*, **16**(1), p. 2.
URL https://doi.org/10.12942/lrr-2013-2

[61] Bianchi, E. and M. Gamonal (2025), "Squeezed vacua and primordial features in effective theories of inflation at N2LO," ArXiv:2410.11812 [gr-qc].
URL http://arxiv.org/abs/2410.11812

[62] Starobinskiĭ, A. A. (1979) "Spectrum of relict gravitational radiation and the early state of the universe," *Soviet Journal of Experimental and Theoretical Physics Letters*, **30**, p. 682, publisher: Springer ADS Bibcode: 1979JETPL..30..682S.
URL https://ui.adsabs.harvard.edu/abs/1979JETPL..30..682S

[63] Overstreet, C., J. Curti, M. Kim, P. Asenbaum, M. A. Kasevich, and F. Giacomini (2023) "Inference of gravitational field superposition from quantum measurements," *Physical Review D*, **108**(8), p. 084038, publisher: American Physical Society.
URL https://link.aps.org/doi/10.1103/PhysRevD.108.084038

[64] Abe, M., P. Adamson, M. Borcean, D. Bortoletto, K. Bridges, S. P. Carman, S. Chattopadhyay, J. Coleman, N. M. Curfman, K. DeRose, T. Deshpande, S. Dimopoulos, C. J. Foot, J. C. Frisch, B. E. Garber, S. Geer, V. Gibson, J. Glick, P. W. Graham, S. R. Hahn, R. Harnik, L. Hawkins, S. Hindley, J. M. Hogan, Y. Jiang, M. A. Kasevich, R. J. Kellett, M. Kiburg, T. Kovachy, J. D. Lykken, J. March-Russell, J. Mitchell, M. Murphy, M. Nantel, L. E. Nobrega, R. K. Plunkett,

S. Rajendran, J. Rudolph, N. Sachdeva, M. Safdari, J. K. Santucci, A. G. Schwartzman, I. Shipsey, H. Swan, L. R. Valerio, A. Vasonis, Y. Wang, and T. Wilkason (2021) "Matter-wave Atomic Gradiometer Interferometric Sensor (MAGIS-100)," *Quantum Science and Technology*, **6**(4), p. 044003, publisher: IOP Publishing.
URL https://dx.doi.org/10.1088/2058-9565/abf719

[65] Overstreet, C., P. Asenbaum, J. Curti, M. Kim, and M. A. Kasevich (2022) "Observation of a gravitational Aharonov-Bohm effect," *Science*, **375**(6577), pp. 226–229, publisher: American Association for the Advancement of Science.
URL https://www.science.org/doi/10.1126/science.abl7152

[66] Tino, G. M., L. Cacciapuoti, K. Bongs, C. J. Bordé, P. Bouyer, H. Dittus, W. Ertmer, A. Görlitz, M. Inguscio, A. Landragin, P. Lemonde, C. Lammerzahl, A. Peters, E. Rasel, J. Reichel, C. Salomon, S. Schiller, W. Schleich, K. Sengstock, U. Sterr, and M. Wilkens (2007) "Atom interferometers and optical atomic clocks: New quantum sensors for fundamental physics experiments in space," *Nuclear Physics B - Proceedings Supplements*, **166**, pp. 159–165.
URL https://www.sciencedirect.com/science/article/pii/S0920563206010152

[67] Tino, G. M. (2021) "Testing gravity with cold atom interferometry: results and prospects," *Quantum Science and Technology*, **6**(2), p. 024014, publisher: IOP Publishing.
URL https://dx.doi.org/10.1088/2058-9565/abd83e

[68] Trimeche, A., B. Battelier, D. Becker, A. Bertoldi, P. Bouyer, C. Braxmaier, E. Charron, R. Corgier, M. Cornelius, K. Douch, N. Gaaloul, S. Herrmann, J. Müller, E. Rasel, C. Schubert, H. Wu, and F. Pereira dos Santos (2019) "Concept study and preliminary design of a cold atom interferometer for space gravity gradiometry," *Classical and Quantum Gravity*, **36**(21), p. 215004, publisher: IOP Publishing.
URL https://dx.doi.org/10.1088/1361-6382/ab4548

[69] Altschul, B., Q. G. Bailey, L. Blanchet, K. Bongs, P. Bouyer, L. Cacciapuoti, S. Capozziello, N. Gaaloul, D. Giulini, J. Hartwig, L. Iess, P. Jetzer, A. Landragin, E. Rasel, S. Reynaud, S. Schiller, C. Schubert, F. Sorrentino, U. Sterr, J. D. Tasson, G. M. Tino, P. Tuckey, and P. Wolf (2015) "Quantum tests of the Einstein Equivalence Principle with the STE–QUEST space mission," *Advances in Space Research*, **55**(1), pp. 501–524.
URL https://www.sciencedirect.com/science/article/pii/S0273117714004384

[70] Asenbaum, P., C. Overstreet, M. Kim, J. Curti, and M. A. Kasevich (2020) "Atom-Interferometric Test of the Equivalence Principle at the ${10}^{\ensuremath{-}12}$ Level," *Physical Review Letters*, **125**(19), p. 191101, publisher: American Physical Society.
URL https://link.aps.org/doi/10.1103/PhysRevLett.125.191101

[71] Davies, P. C. W. (2004) "Quantum mechanics and the equivalence principle," *Classical and Quantum Gravity*, **21**(11), p. 2761.
URL https://dx.doi.org/10.1088/0264-9381/21/11/017

[72] ——— (2004) "Transit time of a freely falling quantum particle in a background gravitational field," *Classical and Quantum Gravity*, **21**(24), p. 5677.
URL https://dx.doi.org/10.1088/0264-9381/21/24/001

[73] Hogan, J. M., D. M. S. Johnson, and M. A. Kasevich (2008), "Light-pulse atom interferometry," ArXiv:0806.3261 [physics].
URL http://arxiv.org/abs/0806.3261

[74] Fischbach, E. and D. E. Krause (1999) "Constraints on Light Pseudoscalars Implied by Tests of the Gravitational Inverse-Square Law," *Physical Review Letters*, **83**(18), pp. 3593–3596, publisher: American Physical Society.
URL https://link.aps.org/doi/10.1103/PhysRevLett.83.3593

[75] Randall, L. and R. Sundrum (1999) "An Alternative to Compactification," *Physical Review Letters*, **83**(23), pp. 4690–4693, publisher: American Physical Society.
URL https://link.aps.org/doi/10.1103/PhysRevLett.83.4690

[76] Broglie, L. d. (1924) "XXXV. A tentative theory of light quanta," *The London, Edinburgh, and Dublin Philosophical Magazine and Journal of Science*, **47**(278), pp. 446–458, publisher: Taylor & Francis _eprint: https://doi.org/10.1080/14786442408634378.
URL https://doi.org/10.1080/14786442408634378

[77] Storey, P. and C. Cohen-Tannoudji (1994) "The Feynman path integral approach to atomic interferometry. A tutorial," *Journal de Physique II*, **4**(11), pp. 1999–2027, publisher: EDP Sciences.
URL http://dx.doi.org/10.1051/jp2:1994103

[78] Bordé, C. J. (2004) "Quantum Theory of Atom-Wave Beam Splitters and Application to Multidimensional Atomic Gravito-Inertial Sensors," *General Relativity and Gravitation*, **36**(3), pp. 475–502.
URL https://doi.org/10.1023/B:GERG.0000010726.64769.6d

[79] Overstreet, C., P. Asenbaum, and M. Kasevich (2021) "Physically significant phase shifts in matter-wave interferometry," *Am. J. Phys.*, **89**(3), pp. 324–332.
URL https://doi.org/10.1119/10.0002638

[80] Bonnin, A., N. Zahzam, Y. Bidel, and A. Bresson (2013) "Simultaneous dual-species matter-wave accelerometer," *Physical Review A*, **88**(4), p. 043615, publisher: American Physical Society.
URL https://link.aps.org/doi/10.1103/PhysRevA.88.043615

[81] Zhou, L., S. Long, B. Tang, X. Chen, F. Gao, W. Peng, W. Duan, J. Zhong, Z. Xiong, J. Wang, Y. Zhang, and M. Zhan (2015) "Test of Equivalence Principle at $1{0}^{\ensuremath{-}8}$ Level by a Dual-Species Double-Diffraction Raman Atom Interferometer," *Physical Review Letters*, **115**(1), p. 013004, publisher: American Physical Society.
URL https://link.aps.org/doi/10.1103/PhysRevLett.115.013004

[82] Schlippert, D., J. Hartwig, H. Albers, L. Richardson, C. Schubert, A. Roura, W. Schleich, W. Ertmer, and E. Rasel (2014) "Quantum Test of the Universality of Free Fall," *Physical Review Letters*, **112**(20), p. 203002, publisher: American Physical Society.
URL https://link.aps.org/doi/10.1103/PhysRevLett.112.203002

[83] Rosi, G., G. D'Amico, L. Cacciapuoti, F. Sorrentino, M. Prevedelli, M. Zych, C. Brukner, and G. M. Tino (2017) "Quantum test of the equivalence principle for atoms in coherent superposition of internal energy states," *Nature Communications*, **8**(1), p. 15529, publisher: Nature Publishing Group.
URL https://www.nature.com/articles/ncomms15529

[84] Aharonov, Y. and T. Kaufherr (1984) "Quantum frames of reference," *Physical Review D*, **30**(2), pp. 368–385, publisher: American Physical Society.
URL https://link.aps.org/doi/10.1103/PhysRevD.30.368

[85] Rovelli, C. (1991) "Quantum reference systems," *Classical and Quantum Gravity*, **8**(2), p. 317.
URL https://dx.doi.org/10.1088/0264-9381/8/2/012

[86] Bartlett, S. D., T. Rudolph, and R. W. Spekkens (2007) "Reference frames, superselection rules, and quantum information," *Reviews of Modern Physics*, **79**(2), pp. 555–609, publisher: American Physical Society.
URL https://link.aps.org/doi/10.1103/RevModPhys.79.555

[87] Brandão, I., B. Suassuna, B. Melo, and T. Guerreiro (2020) "Entanglement dynamics in dispersive optomechanics: Nonclassicality and revival," *Physical Review Research*, **2**(4), p. 043421, publisher: American Physical Society.
URL https://link.aps.org/doi/10.1103/PhysRevResearch.2.043421

[88] Kjeldsen, T. H. (1993) "The Early History of the Moment Problem," *Historia Mathematica*, **20**(1), pp. 19–44.
URL https://www.sciencedirect.com/science/article/pii/S0315086083710049

[89] Schmüdgen, K. (2017) *The Moment Problem*, vol. 277 of *Graduate Texts in Mathematics*, Springer International Publishing, Cham.
URL http://link.springer.com/10.1007/978-3-319-64546-9

[90] Peters, A., K. Y. Chung, and S. Chu (2001) "High-precision gravity measurements using atom interferometry," *Metrologia*, **38**(1), p. 25.
URL https://dx.doi.org/10.1088/0026-1394/38/1/4

[91] Bojowald, M. (2022) "Canonical description of quantum dynamics*," *Journal of Physics A: Mathematical and Theoretical*, **55**(50), p. 504006.
URL https://iopscience.iop.org/article/10.1088/1751-8121/acafb0

Vita

Joseph A. Balsells

Joey was born in Boulder, Colorado. He attended public schools in Boulder where he was graduated from Fairview High School with an IB diploma in May 2014. The following August he matriculated at Yale and in 2018 was graduated with a Bachelor of Science degree in Physics. He spent the summers of 2015, 2016, and 2017 as a student researcher in the National Oceanic and Atmospheric Administration's Earth Sciences Division. He entered the doctoral program in physics at Penn State in August 2018. At present he is hired to work in the Cornell Laboratory for Accelerator-based ScienceS and Education (CLASSE) in Ithaca, New York.

He has two grandparents, a mother, a twin brother, a wife, two cats, and many friends.